2008

Reducing Eddy Currents In High Magnetic Field Environments

Russell Case
University of Central Florida

REDUCING EDDY CURRENTS IN HIGH MAGNETIC FIELD ENVIRONMENTS

by

RUSSELL L. CASE JR.
B.S. Eng. University of Central Florida, 1985

A thesis submitted in partial fulfillment of the requirements
for the degree of Master of Science in Electrical Engineering
in the School of Electrical Engineering and Computer Science
in the College of Engineering and Computer Science
at the University of Central Florida
Orlando, Florida

Spring Term
2008

ABSTRACT

When an electrical conducting volume is placed into the bore of an MRI undergoing an image scan, time varying magnetic gradients induce eddy currents in this conducting material. These eddy currents in turn produce a mechanical torque on this volume. It is the goal of this thesis to produce a computer simulation of eddy currents produced by placing conducting materials inside an MRI bore. The first part of the thesis establishes the physics and principles behind an MRI system along with several applications. Next, this thesis presents an analysis of eddy current effects produced on a conductor placed into an MRI bore. The design and construction of simulated MRI magnetic fields is then presented along with a study of simulated eddy currents in various test conducting volumes of selected materials. Finally, techniques are discussed for reducing eddy currents in these conducting volumes and materials, along with simulation results showing the reduction in the applied eddy current. The findings of this thesis are summarized in the conclusions and recommendations are made for modification and future applications of these techniques and simulations.

This thesis is dedicated to my father, Russell L. Case Sr., who introduced me to electricity at a very early age and encouraged me to explore the subject in all its wonderful intricacies.

ACKNOWLEDGMENTS

With almost any complex task, it is impossible to complete without the help of others. This thesis is no different.

I would like to thank Mr. Steven D. Fisher, Chief Engineer, Invivo Research, Inc. for his guidance and insights into the problems associated with eddy currents in MRI patient monitoring equipment. I hope that some small contribution to a solution can be found through my efforts.

Special thanks go to Dr. Arthur Weeks for his significant help with the planning, outline, assembly, and editing of this thesis. Without his "special" assistance at unusual hours, weekends, and holidays, as well as his constant encouragement, this effort would have probably dragged on for yet another semester.

Thanks to Dr. Thomas X. Wu for his support with the Ansoft Maxwell 3D software.

I am also grateful for Brandon White, Bob Helsby, and Mark Solveson, all of Ansoft Corporation, for providing me with hard to find documentation, providing me with expert technical advice for utilization of the Maxwell 3D tool, guidance for getting up to speed with Maxwell 3D quickly, and tips and tricks to getting the most out of Maxwell 3D.

Finally, my most sincere gratitude to Dr. Samuel M. Richie, a lifelong friend and mentor, for his incredible support, expert knowledge, and extreme patience working with me to achieve this and many other goals.

TABLE OF CONTENTS

LIST OF FIGURES

LIST OF TABLES

LIST OF ACRONYMS/ABBREVIATIONS

3D	Three Dimensional
AWG	American Wire Gauge
CAD	Computer Aided Design
CRT	Cathode Ray Tube
FEA	Finite Element Analysis
MRI	Magnetic Resonance Imager/Imaging
RF	Radio Frequency
SNR	Signal-to-noise ratio

CHAPTER ONE: INTRODUCTION

There are three major groups of problems associated with eddy currents related to the use of Magnetic Resonance Imaging (MRI). The first group includes the effects of eddy currents on the image quality. This includes effects caused by eddy currents in the gradient coils themselves[1,2,3,4] and the MRI structural components.[5] The second group includes physical effects inside the body of a patient (implants and the body itself) undergoing an MRI scan.[6] The third group includes the physical effects caused by eddy currents outside the body, and is the focus of this thesis.[i]

A typical medical MRI contains a large electromagnet capable of creating a static magnetic field in the range of 0.5 Tesla (T) to 3.0 T with a uniformity across the bore of 0.5 parts per million (ppm). The central volume, in which patients are placed, is called the bore. Research MRI bore magnets can create fields exceeding 14.0T. This static magnetic field within the bore is used to align the billions of atoms in the human body (or other object), which are primarily the hydrogen atoms of water molecules. Because hydrogen atoms have a single proton and single electron, these atoms have a large magnetic moment and thus are more easily measured than other atoms. Although the vast majority of the atoms will line up in one direction or the other along the lines of magnetic flux, canceling each other's bulk magnetic moment, there will be sufficient numbers of atoms that are not cancelled to give a sufficient "signal" to be detected.

---

[i] S. D. Fisher, Chief Engineer, Invivo Research, Inc. (personal communication, 6 June 2007)

In order to create a "signal" that can be detected from a hydrogen atom, it is excited by an external radio frequency (RF) pulse at a precise frequency called the Larmour frequency (42.57 MHz / Tesla for hydrogen).[7] The Larmour frequency is based on the hydrogen atom itself and the applied magnetic field strength. When the RF pulse is applied, it causes most of the hydrogen atoms to spin (precess) in a manner that causes the dipole moment of the hydrogen atoms to rotate 90 degrees to an unstable state (non-aligned) and store energy imparted by the RF pulse. When the RF pulse terminates, the hydrogen atoms naturally tend to re-align themselves with the static magnetic field and release the stored energy. During the time when the hydrogen atoms naturally tend to re-align themselves with the static magnetic field, this stored energy is re-radiated as RF energy at the Larmour frequency and is detected by receiving electronics. The amplitude of this signal is dependent on the density of the hydrogen atoms present.

The discussion in the previous paragraph produces a signal that has no dependence on spatial information. To spatially encode a signal, the static magnetic field within the MRI bore is spatially modulated. Coincidentally with the application of the RF pulse, there are a number of "gradient coils" in an MRI, typically aligned to create magnetic field variations in the x, y, and z-axes. These gradient coils alter the magnetic field created by the bore magnet on a specific and local level, typically less than one-eighth of a cubic millimeter. The main purpose of the gradient coils is to spatially modulate the magnetic field within the MRI bore. Since the different spatial positions within the MRI bore will have a different magnetic field strength, the Larmour frequency of the proton precession will be different at these spatial positions. Hence, the signal generated in the MRI bore will be dependent on the spatial position. Typically the x-axis is frequency encoded while the y-axis is phase encoded. An accumulation of the detected energy

along each of the three axes is then assembled to create a two-dimensional or a three-dimensional image of the subject.

In many cases, a patient undergoes MRI testing in conjunction with other tests. These additional tests may require RF receive and transmit coils, instrumentation, wires, sensors, and other devices attached to the patient or the MRI system. The current in the gradient coils of an MRI are changed rapidly, and this rapid change in magnetic field induces eddy currents in electrically conducting materials exposed to these time varying magnetic fields. The induced eddy currents in these materials induce a torque, causing discomfort and annoying effects to patients in the form of vibrations and acoustic noise. Additionally, and more importantly, electronics associated with the ancillary test equipment typically contain integrated circuits, resistors, capacitors, and other electronic components. These electronic components contain conductors that when placed in time varying magnetic fields produce eddy currents. This can lead to stress on these components. Furthermore, metal materials such as aluminum, copper, or other composite metals are typically used in the manufacturing of electronic enclosures or mechanical fasteners. It is this conducting material that contributes to the annoying vibration and acoustic effects. Also, the RF transmit and receive coils are composed of loops of copper wire. When the static magnetic gradient field is incident on these coils, these coils also undergo the same vibration and acoustic stresses from the eddy current effects.

It is the purpose of this thesis to develop a computer simulation model of the MRI bore and gradient fields. Next, the functional performance of the computer simulation is verified. Using a sine wave gradient signal, the eddy currents in several geometrical shaped objects are simulated. The torque of these objects is then measured from the computer simulation. A comparison is made between these geometrical objects to determine which object produces the

lowest eddy current or torque. Other experimental simulations are performed to determine if adding various types of holes in a material can reduce the eddy current in the object.

Chapter one (this chapter) introduces the concept of eddy currents in an MRI environment, an overview of the MRI system, and the plans for developing solutions for reducing eddy currents in an MRI environment. Chapter two lays the foundational physics behind induced currents and the creation of magnetic fields with some history of Faraday's Law, Lenz's Law, and Ampere's Law. Chapter three provides a brief discussion of eddy currents in a general sense and begins the process of establishing the coordinate spaces in which eddy currents exist. Chapter four describes the physics and concepts of the MRI system. Chapter five begins the connection of the concepts of chapter three and four with a discussion of eddy currents in the MRI system and establishes the coordinate system and geometry of an eddy current for the remainder of the thesis. Chapter six establishes the validity of the Maxwell 3D electromechanical analysis software with reference geometries and physics comparisons as well as modeling of the MRI components and system. Chapter seven describes the various test volumes used in this eddy current analysis and the results. Chapter eight continues with a presentation of test volumes with incorporated eddy current reduction features and simulation results. Chapter nine completes this thesis with a presentation of the overall concepts and comparison of the simulation results.

CHAPTER TWO: INDUCED CURRENTS

The MRI brings together a number of fundamental principles in physics and engineering. A brief reminder of the principles involved, and how they are used, will be sufficient to form the foundation upon which the principles of eddy current reduction techniques can be implemented.

Faraday's Law

Faraday's Law, which essentially states that a changing magnetic field produces a corresponding electric field, and thus a current in a conductor, is fundamental to understanding the effects of eddy currents. In the case of the MRI, the magnetic field is changing due to changes in current through the gradient coils. This changing magnetic field produces currents in conductive materials exposed to the MRI magnetic fields.[8]

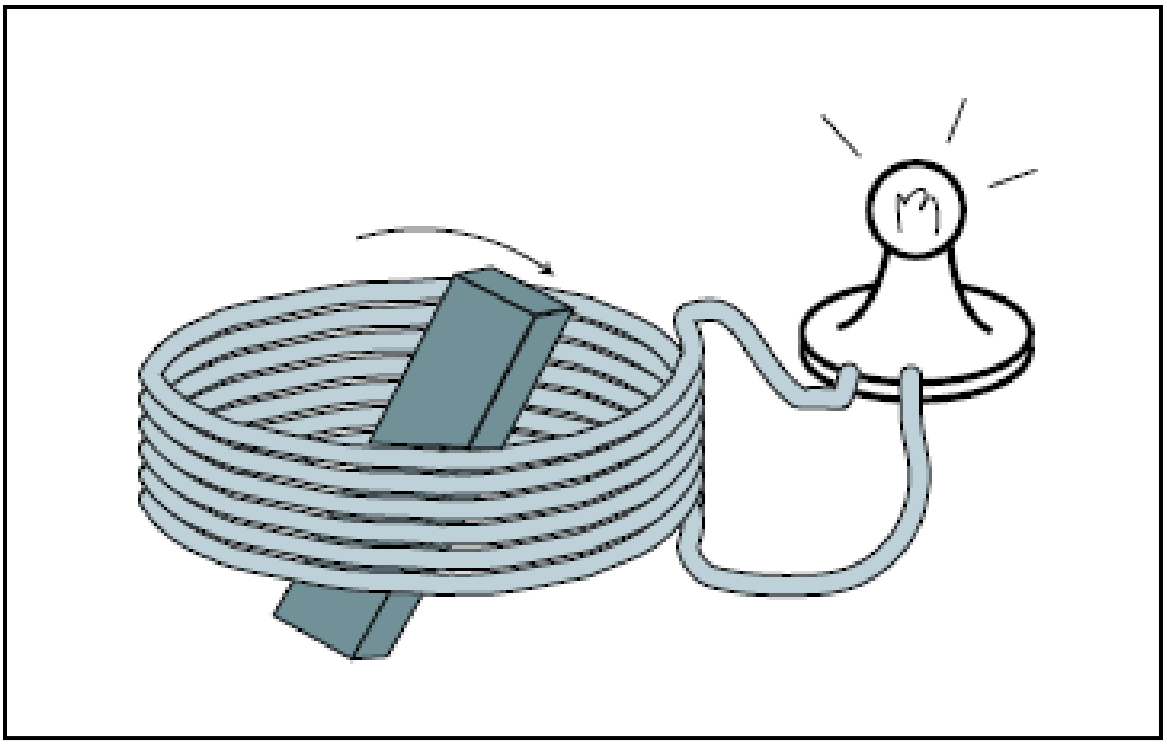

Figure 1. Induced Current

The graphic of Figure 1 demonstrates Faraday's Law showing a rotating magnetic field inducing a current in a conductor. Faraday's relationship is expressed as follows, where B is the magnetic field and E is the electric field:

$$\Gamma_E \propto -\partial B/\partial t \qquad (1)$$

This equation essentially states that the electric circulation is proportional to the change in the magnetic field over time. The negative sign indicates the "left handedness" of the effect. (If one uses the right hand rule, and curls the fingers in the direction of the electric field, the thumb will point in the "negative" direction of the magnetic field.)

Lenz's Law and the Lorentz Relation

Lenz's Law describes the directionality of forces upon conductors in motion relative to a magnetic field. In general, Lenz's law states that the induced current in a circuit tends to oppose the action that created it.[9] An induced current in a conductor will produce a magnetic field that opposes the inducing magnetic field. The magnitude and directionality of the forces on a conductor follow the Lorentz relation, where q_0 is the charge and **v** is the velocity vector:

$$\mathbf{F} = q_0\mathbf{E} + q_0\mathbf{v} \times \mathbf{B} \qquad (2)$$

In the MRI system there typically is no applied electric field, so the contribution of force due to charged bodies in an electric field can be eliminated and the equation reduced to:

$$\mathbf{F} = q_0\mathbf{v} \times \mathbf{B} \qquad (3)$$

Furthermore, since a current is an assembly of moving charges, the equation can be modified to replace the charge and its associated velocity vector with the current, i:

$$\mathbf{F} = i\mathbf{l} \times \mathbf{B} \qquad (4)$$

Equation 4 takes into account the volume of interest, the number of charges in the volume and the vector direction of the charge movement.

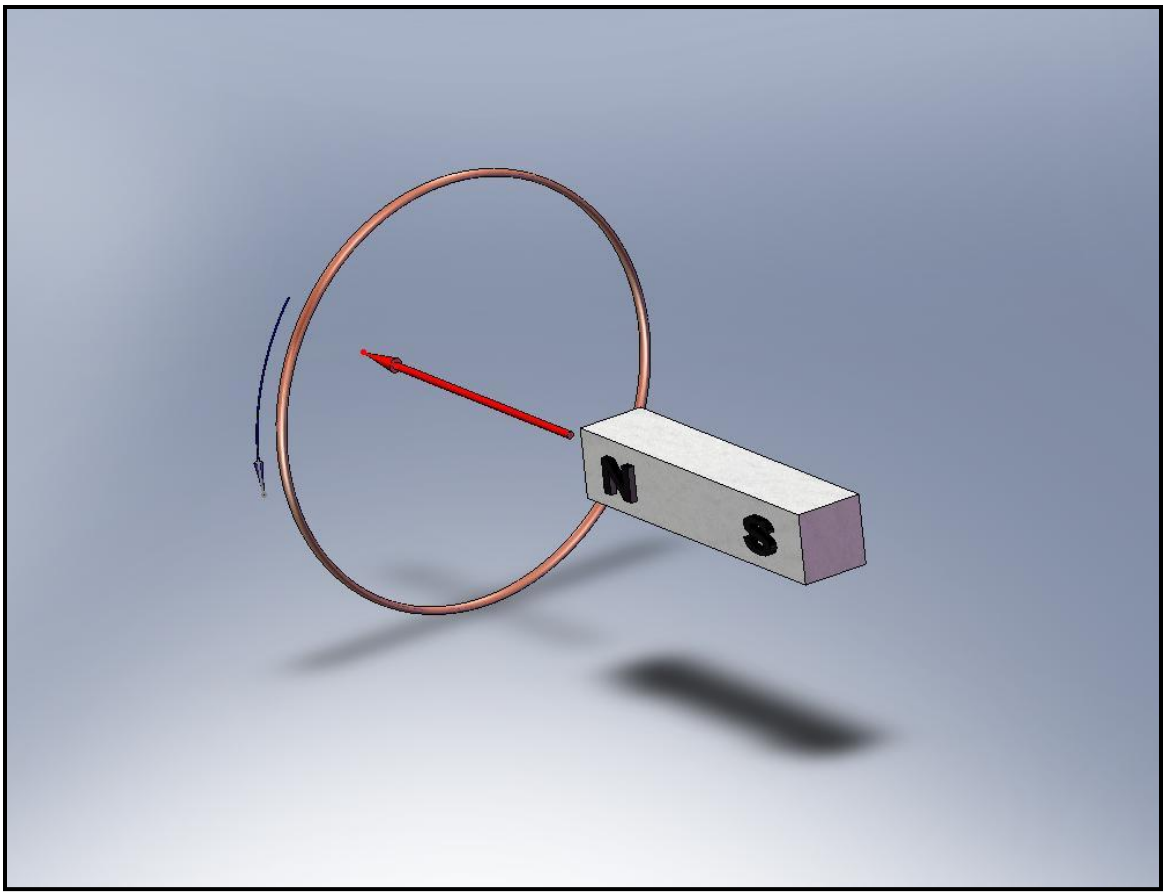

Figure 2. Current Flow

The picture shown in Figure 2 illustrates Lenz's Law. With the north pole of the magnet moving toward the conducting loop (straight red arrow), a current is induced in the loop (curved blue arrow), that will oppose the motion of the magnet. Using the right hand rule for current flow, the magnetic field of the current loop has a north pole pointing towards the magnet.

Ampere's Law

In contrast to Faraday's Law and Lenz's Law, which establish the foundation for induced currents and the forces acting on conductors, produced by external magnetic fields, Ampere's

Law establishes the foundation for understanding the magnetic field produced by a current-carrying conductor. Ampere's Law, which was later enhanced by Maxwell, establishes the quantitative relationship between the current in a conductor and the magnetic field produced as a result. Extending Ampere's Law to the special case of a solenoid, the magnitude of the magnetic field inside the solenoid can be calculated by:

$$B_0 = \mu_0 n i_0 \quad (5)$$

where B_0 is the magnitude of the magnetic field, μ_0 is the permeability constant $4\pi \times 10^{-7}$ Henries per meter, n is the turn per length ratio (n = N/L, where N is the number of turns and L is the length of the solenoid), and i_0 is the current through the solenoid. The permeability constant assumes that the solenoid encloses a vacuum. The permeability constant in the equation above can be replaced by:

$$\mu = \mu_0 k \quad (6)$$

where k is the relative permeability of the material enclosed by the solenoid. In the case of air, the relative permeability is 1.0000004.[10]

CHAPTER THREE: EDDY CURRENTS

A current is induced in a conductor and its direction and associated forces are established using Faraday's Law and Lenz's Law. These concepts are initially considered using a conductor that is dimensionally large in one axis only – a wire.

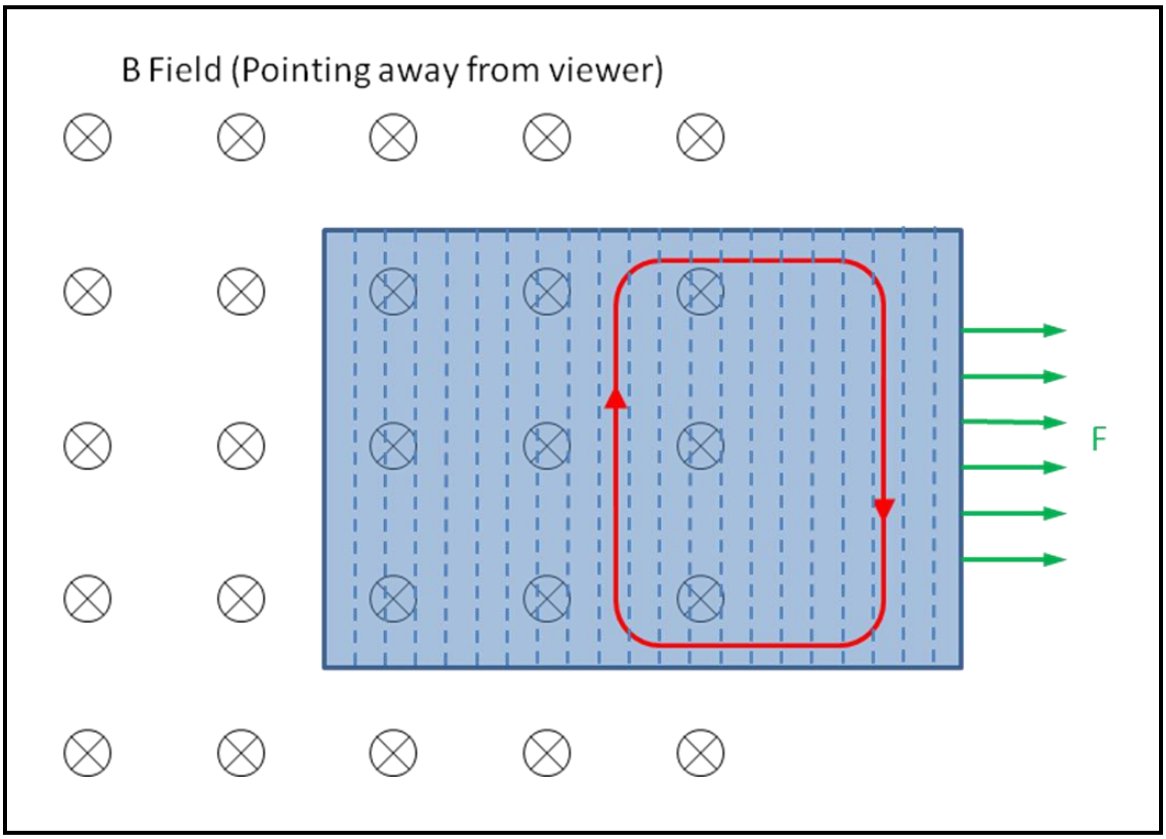

Figure 3. Eddy Currents

A conducting sheet, as shown in Figure 3, can be regarded as a parallel combination of conducting wires.[11] When exposed to a time varying magnetic field, a mechanical motion relative to a stationary magnetic field, or a combination of time varying magnetic fields and

mechanical motion, currents are induced in the conductor and forces act upon the conductor to oppose its motion. For example, a powerful magnet moved across the surface of a conducting sheet of copper will cause the sheet of copper to move in the same direction as the magnet. (A similar effect occurs in all conductors. This effect cannot be seen in ferromagnetic materials as the relative motion is overpowered by the magnetic attraction.) This motion "opposes" the change in the magnetic field. Given a perfect copper sheet with no electrical resistance, no frictional losses, and no thermal losses, the sheet would follow the magnet at the same rate. However, due to losses, the copper sheet will eventually fall away from the magnet.

Using Figure 3 to illustrate, the conducting sheet is moved through a static magnetic field as shown by the solid green arrows pointing to the right from the edge of the conducting sheet. By Lenz's Law, a current is set up in the conducting sheet that creates a force to counteract that movement. The differential wire elements, indicated with light blue dashed vertical lines, that are immersed in the B field, conduct current upwards, as indicated by the circulating red current loop. Using the cross product of the current and the B field, the counteracting force is towards the left of the figure. The horizontal sections of the current create forces upwards and downwards, cancelling each other out. The current path outside the B field has no component of force and thus contributes nothing to the overall counteracting force on the conducting sheet. The net result is that the force due to the eddy current points to the left to oppose the applied force to the right. The same effect occurs if the B field is increased. The conducting sheet tends to get pulled further into the field.

It is important to establish a distinction here in nomenclature. An eddy current is the current established when the magnetic field is changed while the conductor is stationary. When the conductor is moved and the magnetic field is stationary, the current induced in the conductor

is a Foucault current. However, this distinction has no basis in physics as the results are identical. One can simply alter the spatial coordinate system to change one to the other. Furthermore, the term “eddy current” is so much more prevalent in the engineering community that it will be used throughout this thesis regardless of which spatial reference is in motion.

If a constant magnetic field is established in one direction, and a conducting volume is passed perpendicular through the field, the differential wires entering the magnetic field first will have a current induced that will be larger than the differential wires further away from the magnetic field.

Since the resistivity of the conductor is uniform, the induced current will establish an induced voltage on the first differential wire that is larger than the second differential wire. The lower voltage on the second differential wire will allow a return path for current flow from the first differential wire, thus allowing the induced magnetic field that opposes the motion of the conducting volume.

In contrast, the differential wire adjacent to the first differential wire, parallel to the magnetic field (in a conducting volume), will at the same time as the first differential wire, have an identical induced current, a resulting identical voltage, and thus prevent current flow parallel to the magnetic field. Therefore, no forces will act on the conducting volume parallel to the magnetic field.

CHAPTER FOUR: MAGNETIC RESONANCE IMAGING

MRI Coordinate System

The MRI system defines the three mutually orthogonal directions as axial, or up-field and down-field, corresponding to the +z and –z directions, respectively. A human subject is placed in the MRI with the up-field or –z direction at the head and the +z direction towards the feet. The sagittal direction corresponds to the x direction with +x at the subject's left and –x at the subject's right. Finally, the coronal directions are indicated with +y at the front of the body, or upwards, and –y at the back of the body, towards the floor.[12] The isocenter of the magnetic system defines the intersection of the axial, coronal, and sagittal planes.

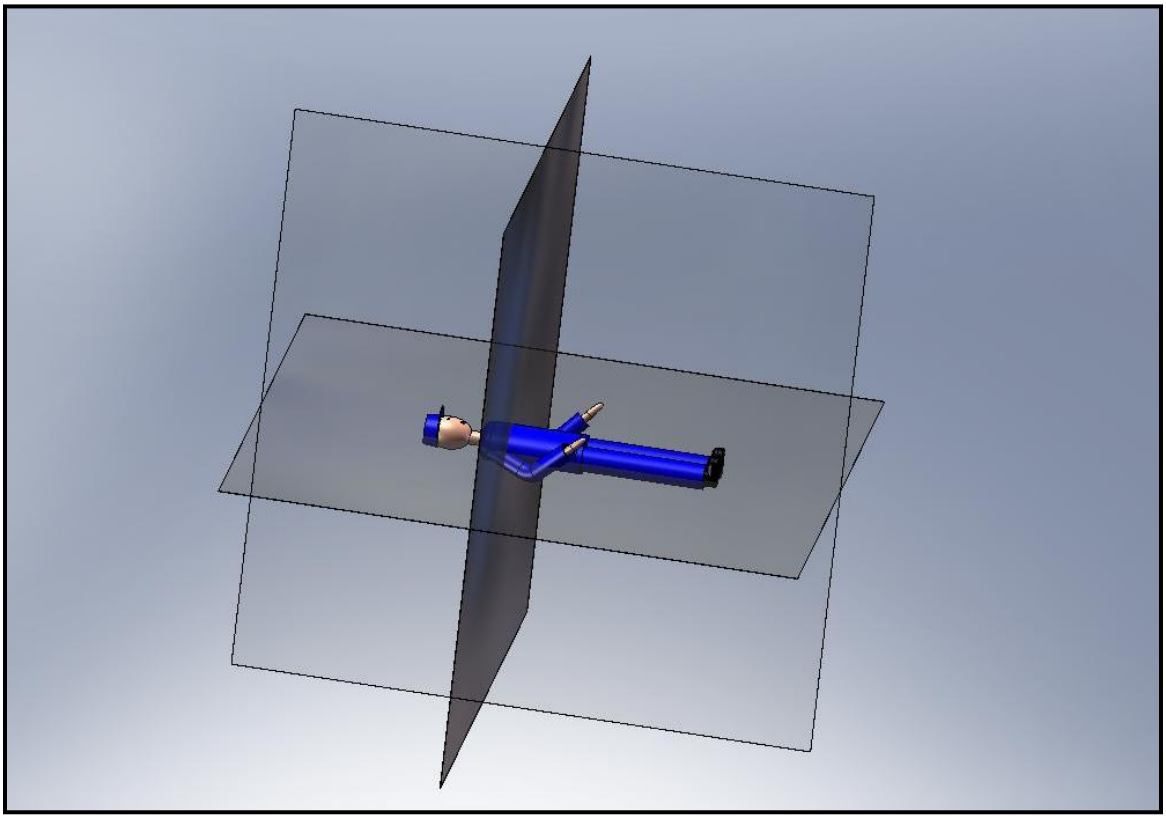

Figure 4. MRI Coordinate System

Figure 4 illustrates the three-dimensional coordinate system employed in MRI systems.

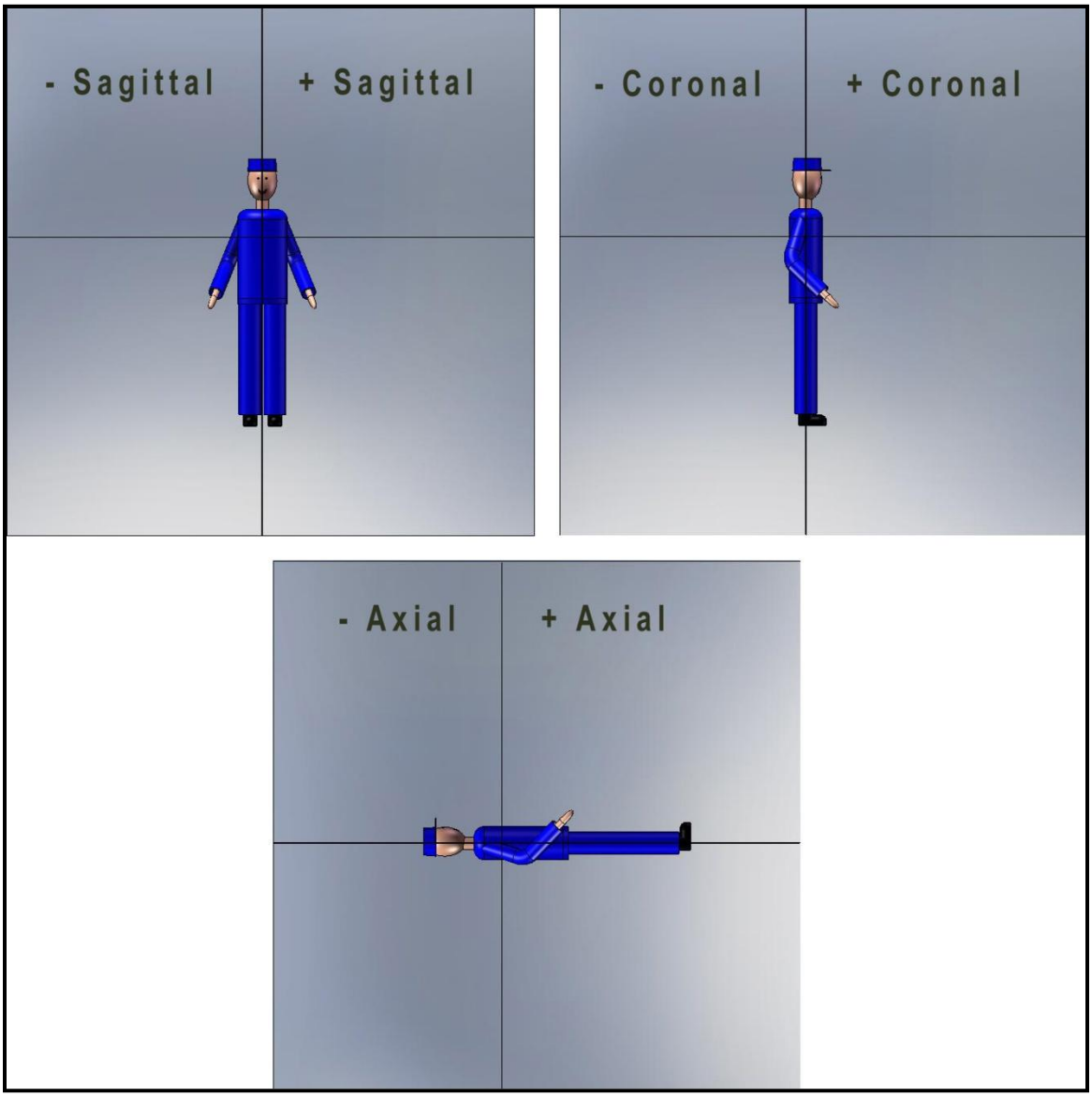

Figure 5. MRI Coordinate Nomenclature

Figure 5 indicates the nomenclature of each of the three mutually orthogonal planes and their directionality.

MRI Basics

The Human Body

Approximately 63% of the human body is composed of hydrogen atoms.[13] For this reason, MRI of the hydrogen atom is of primary interest in medical MRI measurements.

Proton Spin

The hydrogen atom consists of a single proton and single electron. Each of the elementary particles in the hydrogen atom, the proton and electron, has a fundamental property associated with them called spin. (Actual "spin" of the particles has not been directly observed but is used to model the property.) Electron spin, for purposes of this thesis, will be ignored.

The proton also has charge associated with it, and combined with its spin around its axis, produces a current loop, also about the same axis. This current loop produces a net magnetic field and can interact with external magnetic fields. The graphic of Figure 6 shows a single proton spinning around its central axis.

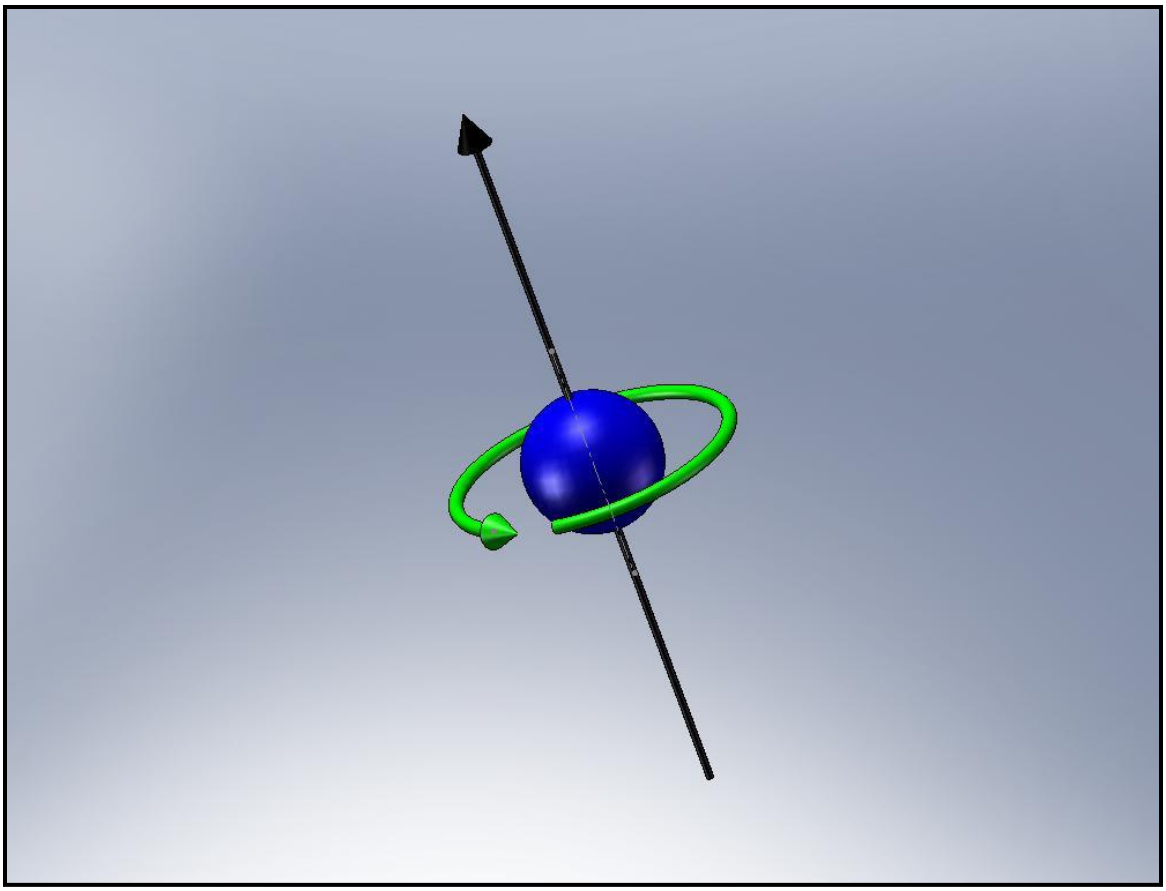

Figure 6. Spinning Proton

Precession

Precession is a description of the circular motion of the rotation axis of a spinning object subjected to an external force, that external force applying torque to axis of the spinning object.[14]

In the case of a spinning toy top, the angular velocity of the particles comprising the rotating wheel (induced by the force of spinning the top) and the angular velocity of the applied torque to the axis of rotation (induced by the earth's gravity acting on the particles in the top's rotating wheel, combine to precess the toy top about a precessional axis. The angular motion of the axis of spin is named precession, and describes a cone centered on the precessional axis.

By eliminating all the friction and thermal loss components of the spinning wheel and eliminating any variations in the external gravitational field, the spinning top would precess about its precessional axis indefinitely. If the external gravitational field is removed, the top would spin around its axis with no precession (the spin axis and precessional axis being coincident). Frictional losses and thermal losses eventually cause the spinning top to stop spinning and fall over.

Similarly, the spinning proton of the hydrogen atom, which has charge, and creates a current loop, precesses about an axis under the influence of an external force, in this case the bore coil's magnetic field. Unlike the precessing toy top, or the gyroscope, the precessing hydrogen nucleus does not fall over or stop spinning. Figure 7 depicts a single proton precessing, the point of the spin axis transcribing a circle about the precessional axis. As shown in Figure 7, the B field points upwards and the precession direction is clockwise viewed from above.

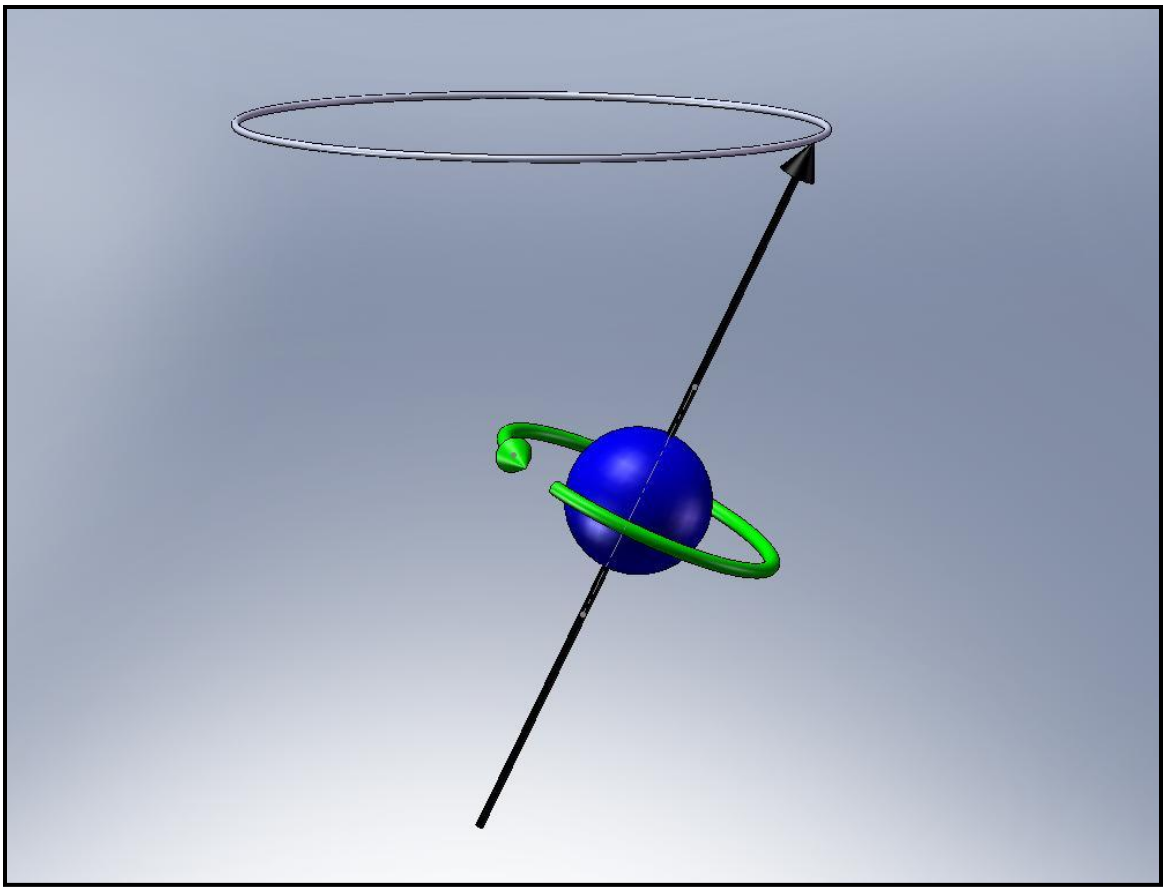

Figure 7. Precessing Proton

Larmour Frequency

The angular frequency of precessional spin of the hydrogen nucleus is a linear function of the gyromagnetic ratio (a physical constant) of the hydrogen nucleus and the magnitude of the externally applied magnetic field. The gyromagnetic ratio of the hydrogen nucleus, γ, and has a value of 2.675×10^8 rad/s/T. Converting to Hertz, the equation becomes $\gamma = 42.574$ MHz/T.[15]

The Larmour equation equates the precessional frequency with the gyromagnetic ratio and the magnitude of the externally applied magnetic field and is:

$$\omega_0 = \gamma B_0 \qquad (7)$$

For an external magnetic field B_0 of 1.5 T, the precessional frequency ω_0 is 63.861 MHz.

Equilibrium Spin States

According to quantum mechanical principles, only two discrete spin states are available for the hydrogen nucleus. The energy levels associated with these two quantum states are $+½\hbar\omega_0$ and $-½\hbar\omega_0$, where the Dirac constant $\hbar \equiv h/2\pi$ and h is Planck's constant (6.626176×10^{-34} kg m^2/s).[16] The spin quanta numbers, -½ and +½ are associated with spins parallel to the external magnetic field and anti-parallel to the external magnetic field, respectively. The spin quanta number parallel to the external magnetic field is the lower of the two energy levels. Subtracting the two, it is noted that the quantum energy difference is exactly $\hbar\omega_0$.

Additional energy sources for hydrogen nuclei include the average thermal energy of the surroundings indicated by kT, where k is Boltzmann's constant (1.380650×10^{-23} kg m^2/s^2 K)[17], and T is the temperature in degrees Kelvin. It is noted that the thermal energy of the system is much greater, millions of times larger, than the quantum energy differences between the two spin states.

If the two energy values of the spinning hydrogen nuclei are compared, that is quantum energy and thermal energy, in the form of a fraction, the "spin excess" is obtained as follows:

$$\text{spin excess} \cong N\,\hbar\omega_0/2kT \quad [18] \qquad (8)$$

where N is the total number of spins present in a sample (N = 2 for hydrogen). Combining the equations, the spin excess is:

spin excess $\cong N \hbar \gamma B_0/2kT$ [19] (9)

With an external magnetic field of 1.5 T the spin excess becomes:

spin excess $\cong [2 \cdot (6.626068 \times 10^{-34} \text{ kg} \cdot \text{m}^2 \cdot \text{s}^{-1}) \cdot (2.675 \times 10^8 \text{ rad} \cdot \text{Tesla} \cdot \text{s}^{-1}) \cdot 1.5 \text{ Tesla}] / [2 \cdot (1.380650 \times 10^{-23} \text{ kg} \cdot \text{m}^2 \cdot \text{s}^{-2} \cdot \text{K}) \cdot 300 \text{ }^{o}\text{K}]$ (10)

spin excess $\cong 10.2 \times 10^{-6}$ (11)

This fraction indicates that there are approximately 10 extra hydrogen nuclei spinning parallel to the external magnetic field for every million hydrogen nuclei. This exceedingly small fraction is multiplied by the fact that there are Avogadro numbers of hydrogen atoms in the volume being scanned.

The molecular mass of hydrogen is 1.00794 grams/mole and the molecular mass of oxygen is 15.9949 grams/mole, making the mass of water approximately 18.01 grams/mole.[20] The mass of water is also approximately 0.9982 grams/cm^3 at 20 ºC. Therefore the number of molecules of water in a cubic centimeter is approximately 0.055 moles/cm^3. Assuming that the MRI can detect volumes as little as one-eighth of a cubic millimeter, and there are 8000 "voxels" in a cubic centimeter, then there are 6.928×10^{-6} moles of water molecules in a single voxel. To determine the number of hydrogen nuclei in the voxel, the number of moles of water are multiplied by Avogadro's number and again multiplied by two (there are two hydrogen atoms in each molecule of water). The result is approximately 8.34×10^{18} hydrogen nuclei in a voxel.

Further multiplication of the hydrogen spin excess by the number of nuclei results in approximately 8.52×10^{13} hydrogen nuclei that can be measured.

System Magnetization

The average proton magnetic dipole moment M_0 is defined as:

$$M_0 = \rho_0 \gamma_0 \hbar^2 B_0 / 4 k T \quad (12)$$

where ρ_0 is defined as the proton unit density or "spin density." The magnetic field produced by the excess spin magnetic dipole moment M_0 is detected by applying a RF pulse tuned to the Larmour frequency. The resonance of this RF pulse with the precessing proton ensures that the precessing proton is "pushed" over in a continuous and synchronized fashion. Figure 8 depicts a proton precessing at the Larmour frequency along a flat circular trajectory.

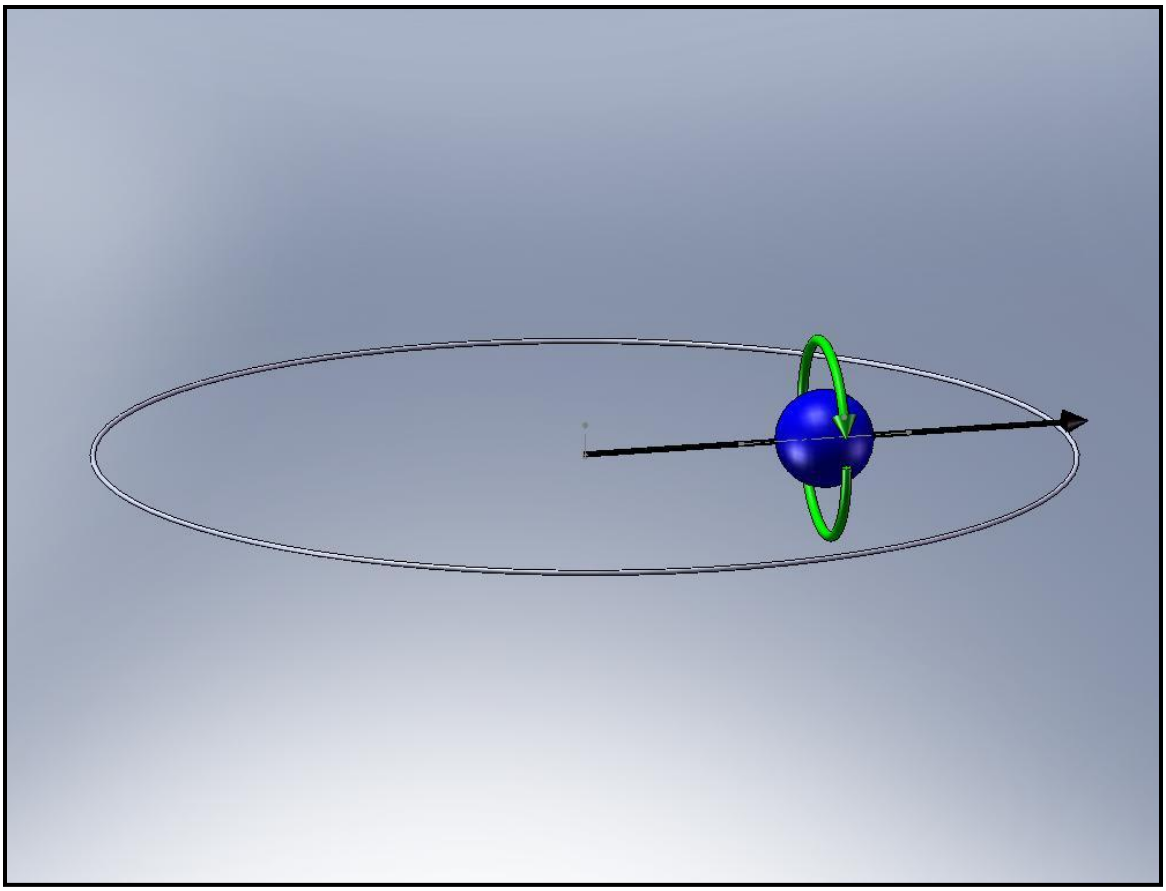

Figure 8. Flat Precession Proton

This is important to consider when the gradient coil fields are superimposed to localize the resonance. An RF pulse that is capable of pushing the precessing proton all the way over by 90 degrees (from the z plane into the x-y plane) is called a $\pi/2$-pulse. This hydrogen nucleus, now spinning in the x-y plane at the Larmour frequency, produces a time-varying magnetic flux that is coupled to a receiver coil and produces a measurable electromotive force in the receive coil.

Bore Coil Design

Bore Coil Shape

The MRI bore magnet is generally designed in a solenoid shape with varying designs of shim coils to produce the most homogenous magnetic field possible, usually to within 1 ppm.

Magnetic Field Intensity

The magnetic field intensity is primarily based on the magnetic properties of the atoms of interest and a trade-off between various physical properties of the magnet itself, such a size, weight, power, cooling, cost, etc. However, a significant consideration for designing the bore magnet is the increase in signal-to-noise (SNR) ratio as the field strength increases.

Gradient Coil Design

Gradient Coil Shape

The MRI gradient coils come in two varieties. The axial gradient coil, which varies the magnetic field along the z-axis (head to foot), consists of an arrangement of Helmholz coils placed on either end of the bore field.[21]

The gradient coils that vary the magnetic field along the sagittal and coronal directions are much more complex. They take the shape of a "saddle" similar to the beam forming coils found on CRT tubes, and are called "Golay coils."[22]

Magnetic Field Intensity

The magnetic field strength of the gradient coils is not as important as the uniformity of the gradient field. The uniformity does not necessarily imply linearity; rather, as long as there are no points within the B field that have the same values, a Fourier transform can be constructed. Knowledge of the Fourier transform and the magnetic field can then be related to position and frequency information to create a faithful image of the subject. However, linearity is a design goal.

CHAPTER FIVE: MRI INDUCED EDDY CURRENTS

The eddy currents produced by an MRI system are far too complex to be completely described within the scope of a single thesis. In fact, the eddy currents produced by the simulation of a single non-optimized MRI gradient coil and a first-order bore coil quickly becomes too complex for a thesis. Therefore, only a few selected geometries and their results will be modeled.

Given a simple experiment using a rare-earth magnet and a thin sheet of copper, and if the magnet is dragged over the copper, the interaction between the magnet and the eddy currents produced in the copper can be easily observed. What is not obvious is the interaction between the eddy current and other magnetic fields. For example, the eddy current produced by the rare-earth magnet reacts with the magnetic field of the earth, but the interaction is too small to observe relative to the much larger interaction between the magnet and the eddy current it produces.

In order to better understand the graphs and graphics presented in this thesis, it is required to establish a coordinate system and an understanding of the directions of rotation, currents, and torques to be described. It is also important to clearly establish the cause and effect relationship between the various inducing forces and induced results. Essentially, it needs to be determined what is creating the phenomena and what is reacting with the phenomena.

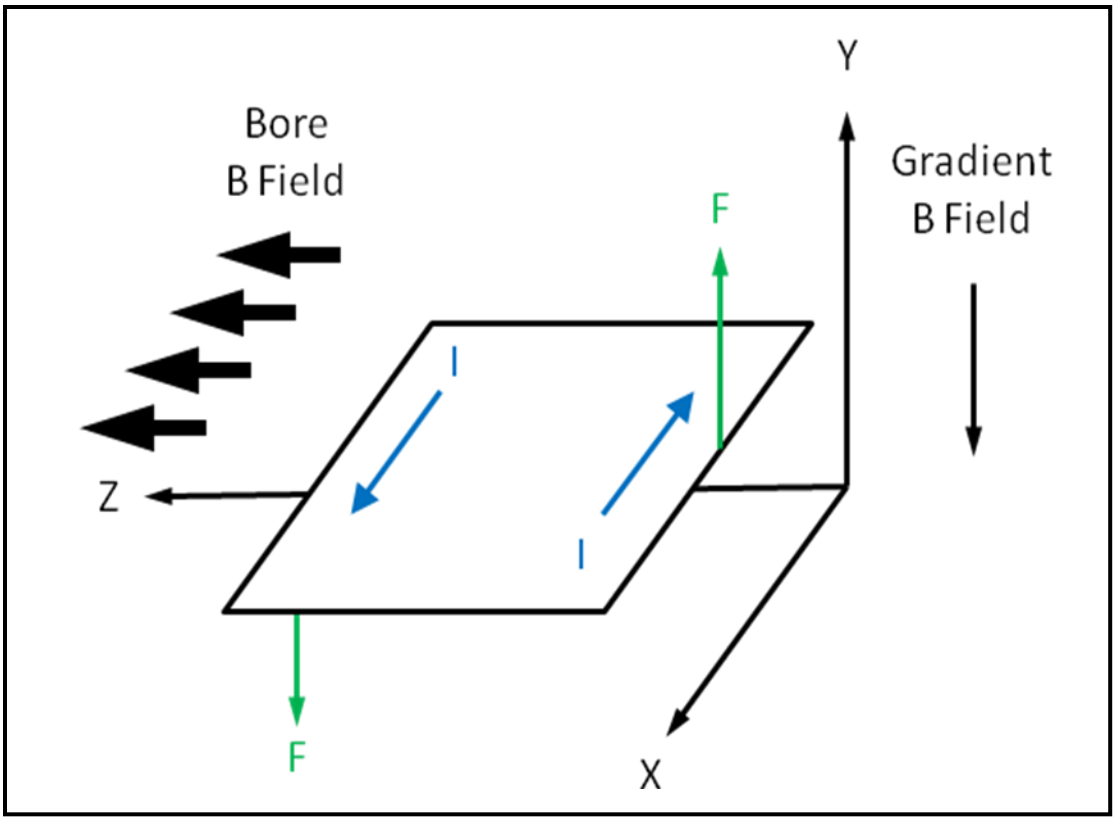

Figure 9. Coordinate Geometry

The coordinate system that is used throughout this thesis, as shown in Figure 9, follows the established coordinate system of a typical MRI system with the x-axis and the sagittal directions being coincident. The y-axis is coincident with the coronal direction, and the z-axis is coincident with the axial direction.

It has already been established that a static magnetic field cannot produce an eddy current if the conductor is stationary. Therefore, since the materials modeled in this thesis are not moving, and the bore field is static, the only item left to produce an eddy current is the gradient coil. Therefore, an established eddy current within the scope of this thesis must be produced by the gradient coil.

The gradient coil is programmed to produce a sinusoidally excited B field that points towards the negative y axis. In conjunction with the static B field produced by the bore coil, the combination of the two fields produces a resultant field by superposition that increases in the positive y direction. This action actually "adds" to the B field of the bore at the positive coronal location in the bore and subtracts from the B field at the negative coronal location in the bore, giving a gradient along the coronal axis. Ignoring for a moment the bore field, it has already been established that a changing magnetic field produces a current that would oppose the field that created it.

Referring to the graphic of Figure 9, the gradient field alone produces a current that circulates ideally along the conducting sheet as shown by the current vectors. Using the right hand rule, and curling the fingers along the path of current, the thumb points upwards; opposite that of the gradient field. If the gradient field were uniform across the conducting surface, only the eddy current would be established and all components of the current, and their associated forces, added together produce no net force on the conducting sheet.

Now, we introduce the bore field, pointing to the left, or towards the positive z-axis. It is this field and the gradient established eddy currents that interact to produce torques on the conducting sheet. Using the right hand rule once again, and pointing the fingers flat in the direction of the current flow, and curling the fingers in the direction of the bore field, the thumb points in the direction of the force applied to the conducting sheet at that point. Using the graphic in Figure 9, the current on the right hand side of the sheet, pointing towards the negative x direction, interacts with the bore field to produce an upwards force (positive y axis) on the sheet. The circulating current on the left hand side of the sheet produces a downward force. The resulting forces on opposite sides of the conducting sheet, also using the right hand rule (for

cross products), indicates that the torque applied in this instance points toward the positive x-axis.

CHAPTER SIX: MRI SIMULATION

Reference Coil Design

Using Ampere's Law to validate the Maxwell software for B field modeling, a solenoid is arbitrarily designed with 100 turns of #18 AWG copper wire, with a diameter or 1.02362 mm, and supplied with 1.0 A of current. Using Ampere's Law for a solenoid:[23]

$$B_0 = \mu_0 n i_0 \quad (13)$$

and replacing $\mu = \mu_0 k$, where k = 1.0000004, we have:

$$B = \mu n i = \mu_0 k n i \quad (14)$$

$$B = [4\pi \times 10^{-7}\ kg \cdot m \cdot A^{-2} \cdot s^{-2}] \cdot [1.0000004] \cdot [100/102.362 \times 10^{-3}\ m] \cdot [1.0\ A] \quad (15)$$

$$B = 1.23 \times 10^{-3}\ kg \cdot A \cdot s^{-2} = 1.23 \times 10^{-3}\ Tesla \quad (16)$$

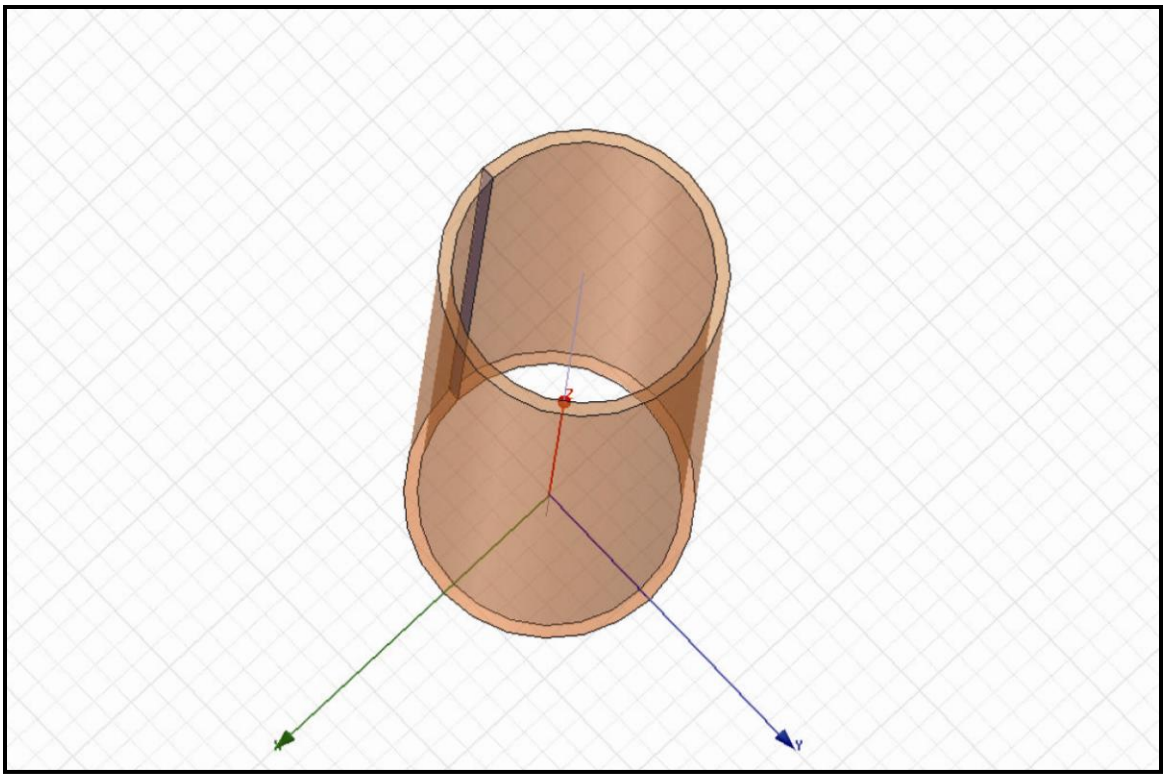

Figure 10. Reference Coil

The reference coil was designed as a solid cylinder with a diameter of 11.02362 mm and a length of 102.362 mm. The coil was created by subtracting another solid cylinder with a diameter of 10.00 mm and a length of 102.362 mm. Copper was assigned as the material and the entire structure enclosed in a space with a minimum of 200% of the dimensions of the solenoid and assigned “air” as the material property.

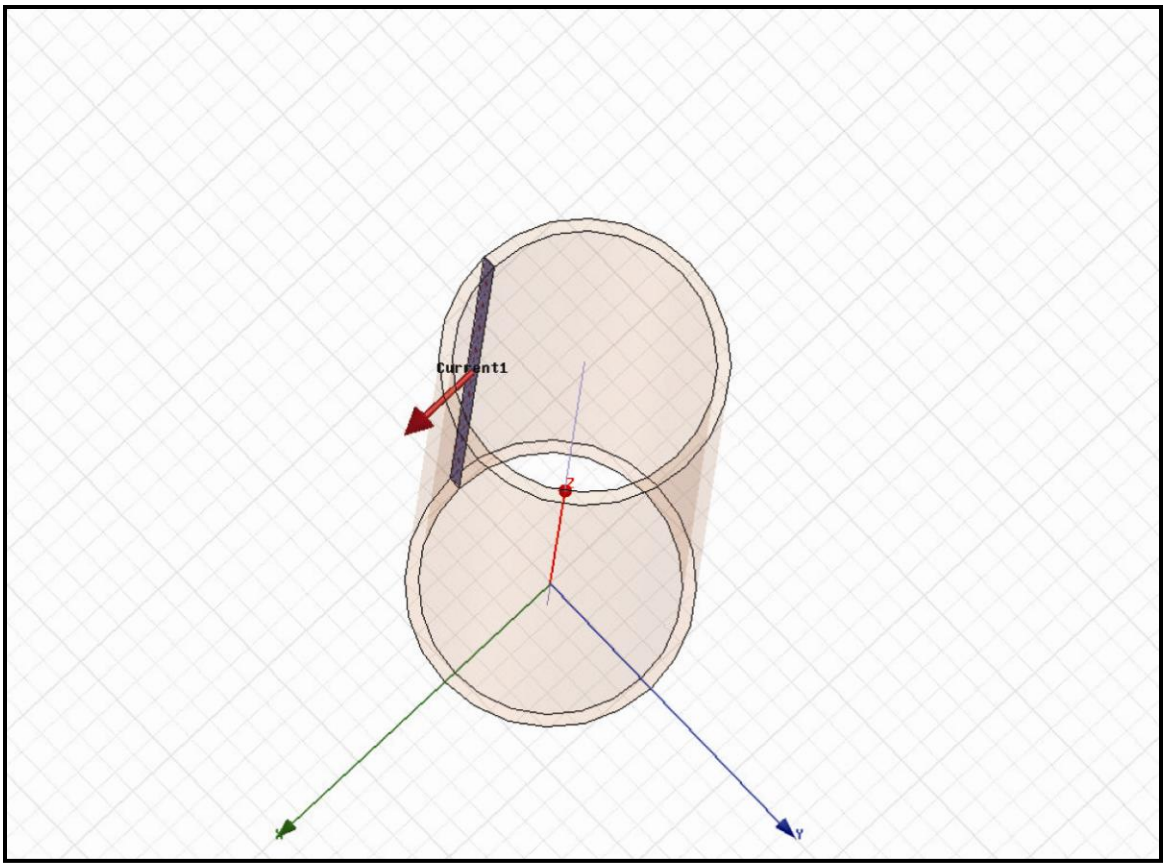

Figure 11. Reference Coil

The cylinder was sectioned and an excitation current of 100.0 Amps applied (Maxwell uses Finite Element Analysis (FEA) and models a solenoid as a solid mass with the currents "stranded" uniformly through the mass. Thus, 1.0 A is modeled for each simulated "strand" or wire with a diameter of 1.02362 mm. The B-Field plot as shown in Figure 12 was obtained.

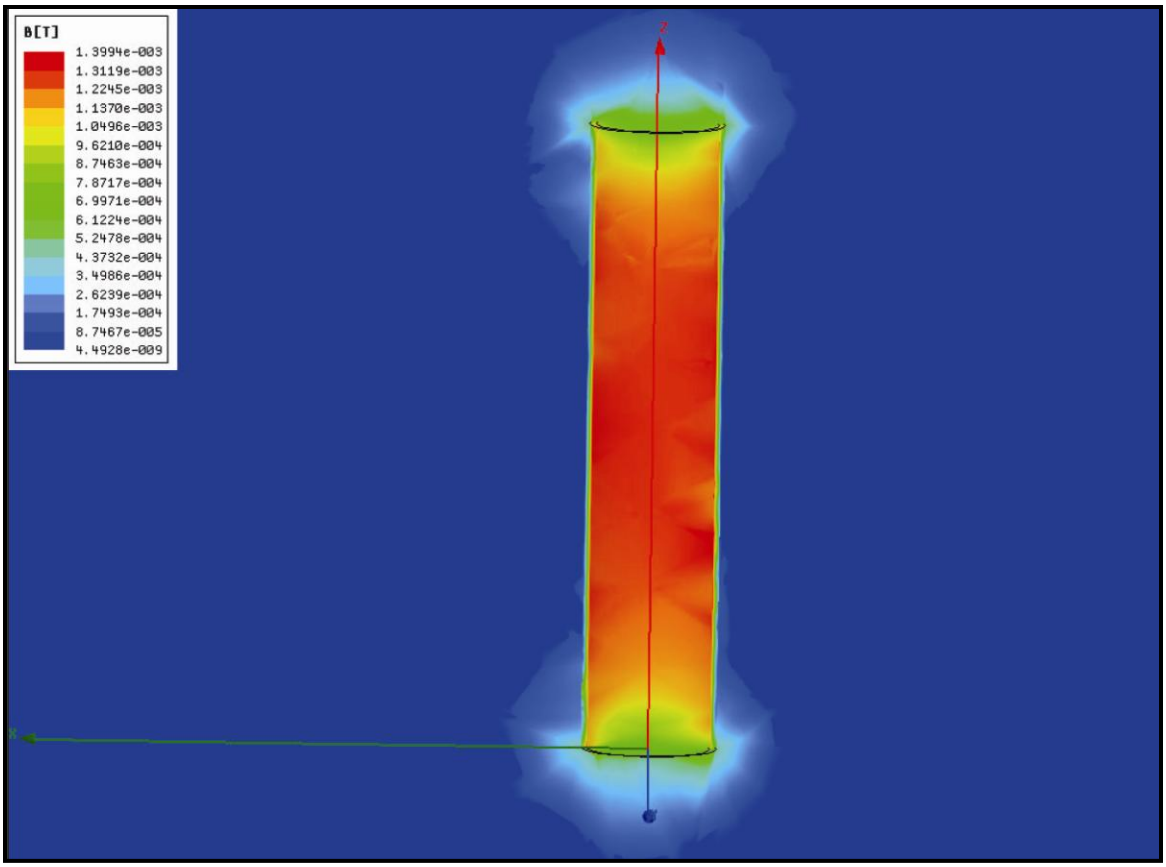

Figure 12. Reference Coil B-Field

As is indicated in Figure 12, the B field is very uniform in the central core. The coil was further enhanced by modeling a polyline through the center, extending 10 mm beyond either end. B field data values were then captured and plotted.

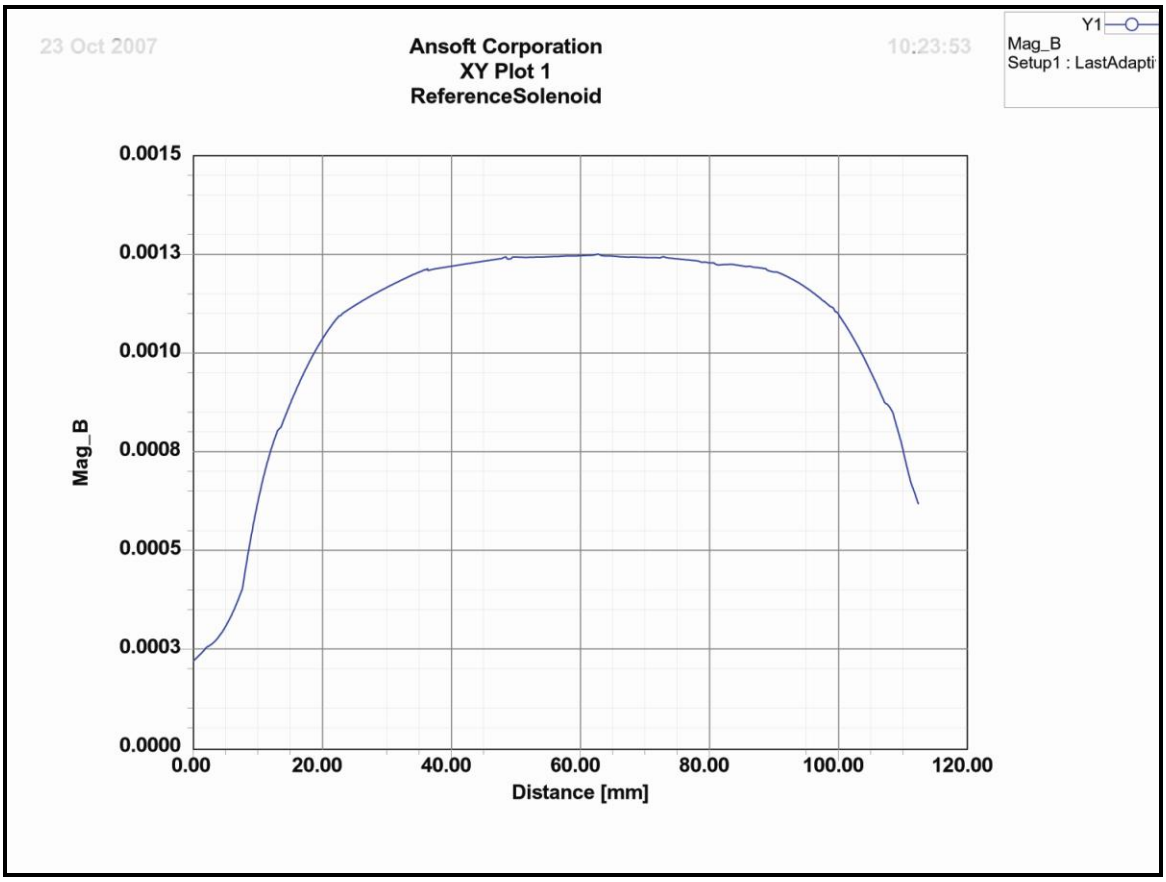

Figure 13. Axial B Field Plot

The horizontal axis of the plot in Figure 13 is the distance in millimeters beginning with the endpoint of the polyline extending through the central axis of the reference coil. The vertical axis of the plot is the magnitude of the B Field in Tesla. At approximately 20 mm (10 mm inside the coil), the B Field magnitude indicated is very close to the 1.23×10^{-3} Tesla calculated previously and remains uniform through the center of the coil. Tabular data collected indicates the maximum value to be 1.247×10^{-3} Tesla, thus substantiating the modeling methods to be adequate for this investigation. Selected tabular data is presented in Table 1.

Table 1 - Reference Solenoid Magnetic Field Strength

Distance	B-Field Magnitude
0.00000	0.000224
10.0002	0.000625
20.0004	0.001037
30.0006	0.001167
40.0008	0.001221
50.0010	0.001244
60.0013	0.001247
70.0015	0.001243
80.0017	0.001230
90.0019	0.001206
100.002	0.001099
110.002	0.000756
112.362	0.000622

Torque Calculations

In addition to the validation of Maxwell's ability to generate B fields, it is also desired to check the validity of the torque calculations. For this check, a well known configuration is used – a square loop. The square loop used in this simulation is a 1 mm square cross section in a 100 mm x 100 mm square loop positioned at the epicenter of the bore field. The square loop is shown in Figure 14.

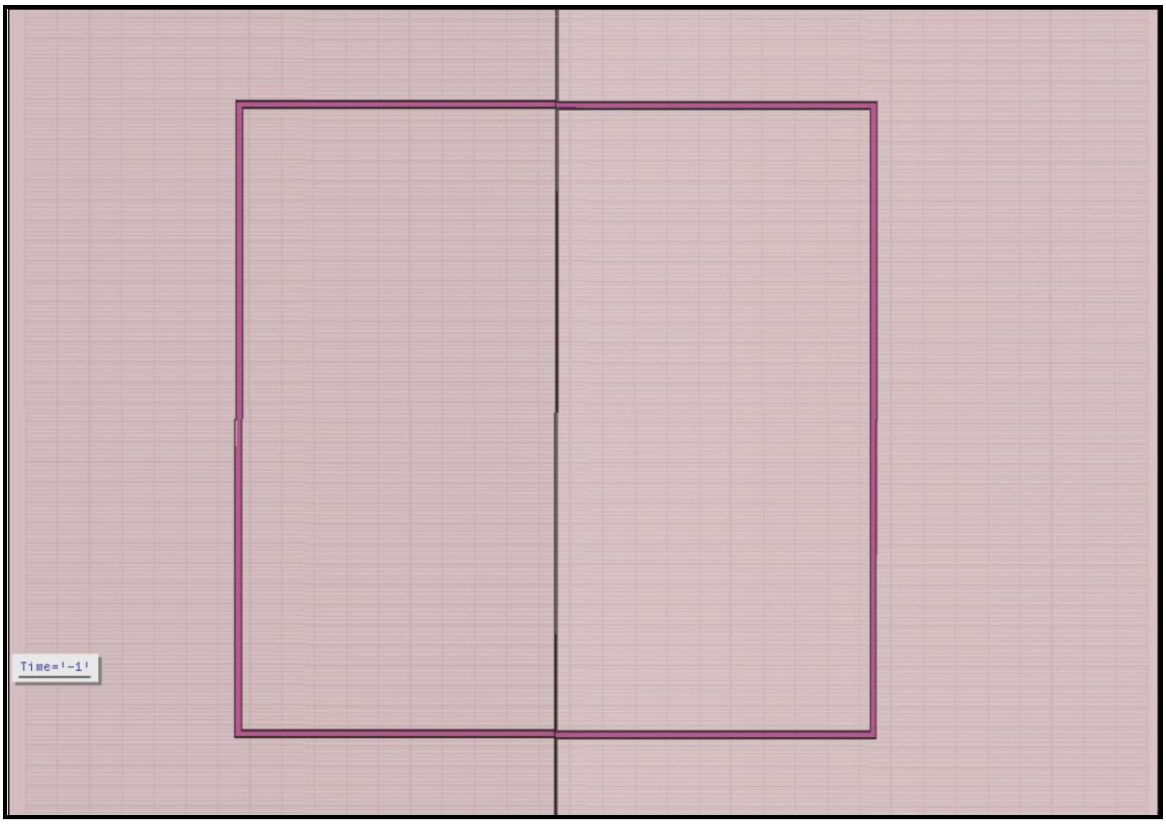

Figure 14. Square Loop

The torque on a current loop is defined by the following equation:[24]

$$\tau = |B||m_t| \sin \theta \quad (17)$$

Where $|B|$ is the magnitude of the B field, $|m_t|$ is the magnitude of the magnetic moment, and θ is the angle between the B field vector and the magnetic moment vector. The magnetic moment of a current loop is simply IA, where I is the current in the loop and A is the area of the loop immersed in the B field. The resulting equation is:

$$\tau = IAB \sin \theta \qquad (18)$$

The next step in the verification process involves calculating the theoretical value of the torque applied to a 100 mm x 100 mm square loop with 1.0 Amp of current, immersed in a uniform B field of 1.564 Tesla. The answer is 0.01564 Nm, or 1.564mNm.

Simulating the 100 mm x 100 mm square loop and establishing a 1.0 amp current as shown in Figure 15, the setup for measuring the torque on the loop is completed.

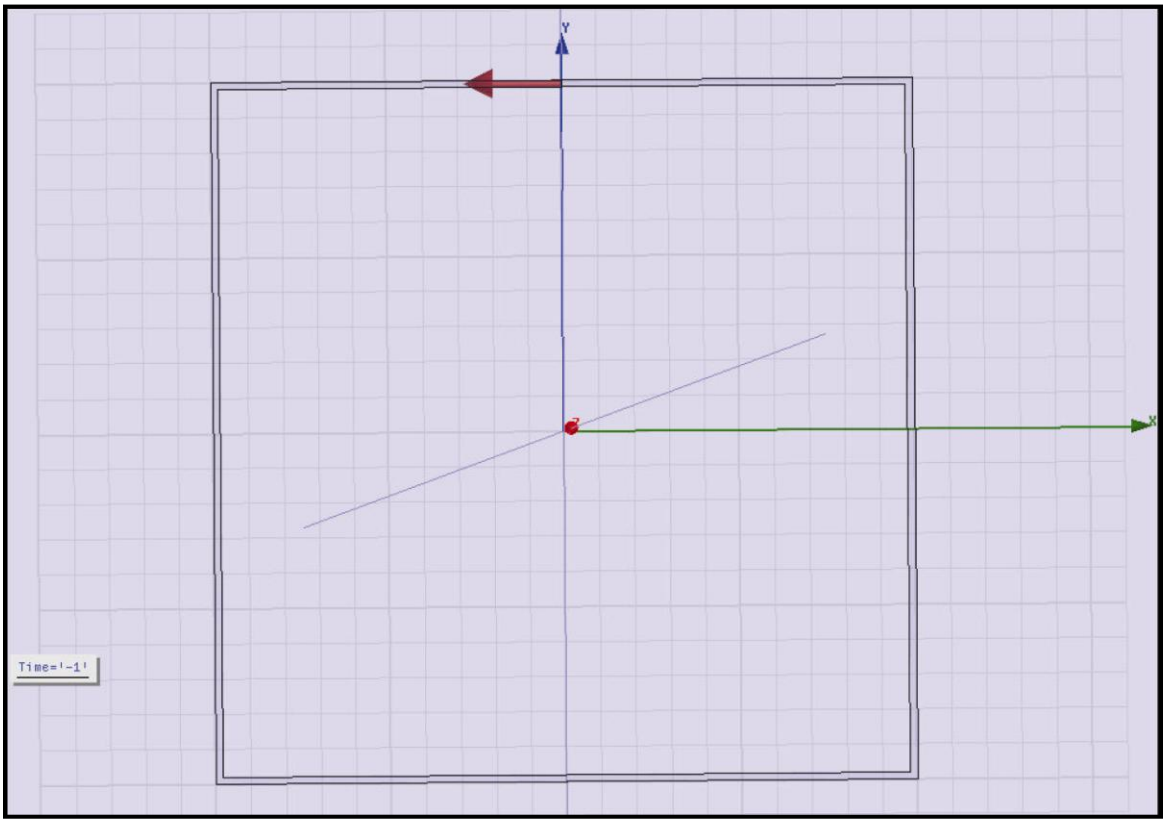

Figure 15. Loop Current

As shown in Figure 15, the current vector in the upper portion of the loop points towards the negative x-axis. The bore field points towards the positive z-axis, pointing directly out of the page as shown in Figure 15. The cross product of the current and the B field will indicate that the force on the upper segment of the loop points toward the positive y-axis. In this orientation there is no net torque. However, if the loop were rotated to lie in the XZ plane, the torque would be maximum and have the value as calculated above. A plot of the torques as a function of the rotation angle of the current loop shown in Figure 16, where zero degrees of rotation indicates the loop lies in the XZ plane is shown in Figure 15. The current loop is sequentially rotated in the x-axis such that at 90 degrees of rotation the loop lies in the XY plane.

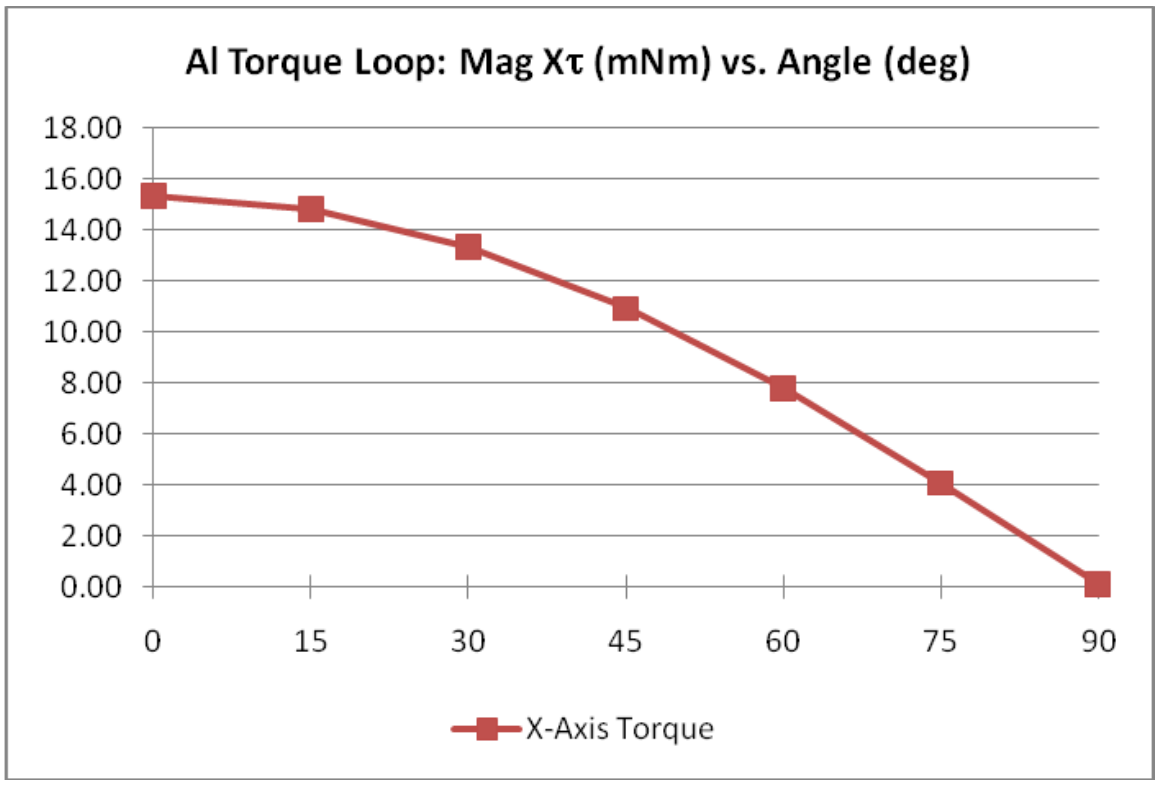

Figure 16. Loop Current

The table below (Table 2) shows a comparison of torque values calculated by Equation (above) and as calculated by Maxwell.

Table 2 - Current Loop Torques

Rotation Angle	Theta	Equation (18)	Maxwell 3D	Difference
		(mNm)	(mNm)	(%)
0	90	15.64	15.3307	2.0
15	75	15.10	14.8192	1.8
30	60	13.54	13.3276	1.6
45	45	11.06	10.9089	1.4
60	30	7.82	7.7653	0.7
75	15	4.05	4.0563	0.1
90	0	0	0.0857	0.0

As can be seen, the values correlate nicely with the theoretical values, thus exhibiting sufficient validation to use Maxwell 3D for torque calculations. For this calculation, the gradient coil current is turned off.

Bore Coil Design

For this simulated MRI bore magnet, the precise dimensions are unimportant as long as the bore magnet forms a relatively long solenoid in order to obtain a uniform magnetic field. Generally the bore dimensions of a typical MRI are approximately 36 inches in diameter and also approximately 36 to 72 inches in length. This design uses a more convenient measurement of 100 cm in diameter and 200 cm in length. To give the bore magnet solenoid sufficient mass for stranded currents, the outer radius of the bore magnet is set at 200 cm.

Figure 17 shows the Maxwell 3D model of the simulated bore magnet with the sectional plane into which Maxell 3D inserts current.

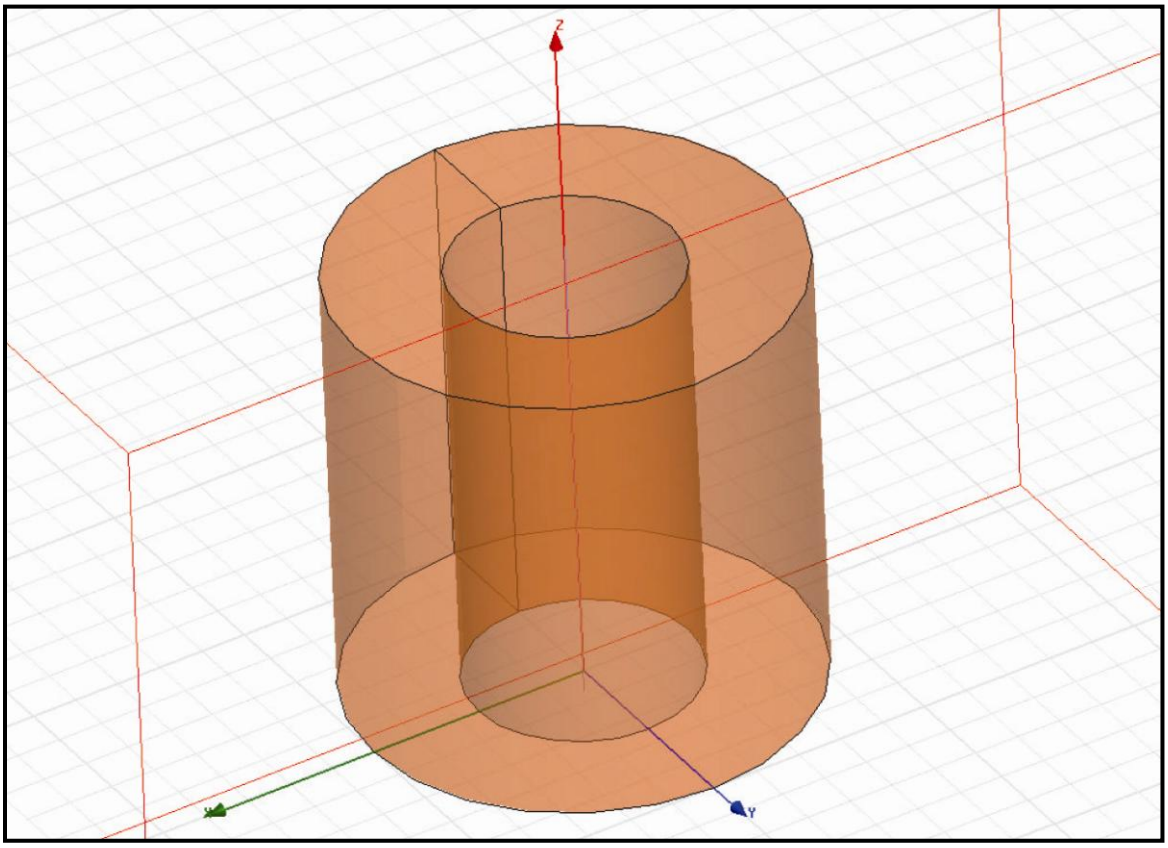

Figure 17. Bore Coil

Figure 18 shows the current and the graphic representation of stranding, the mathematical equivalent to current flowing through multiple turns of wire found in a physical solenoid and in an MRI bore magnet.

Using the right hand rule, and curling the fingers around the central axis of the bore, the z-axis, the thumb points in the direction of positive magnetic field lines. Coincidentally, the legs of a patient inserted into an MRI point in the positive z-axis.

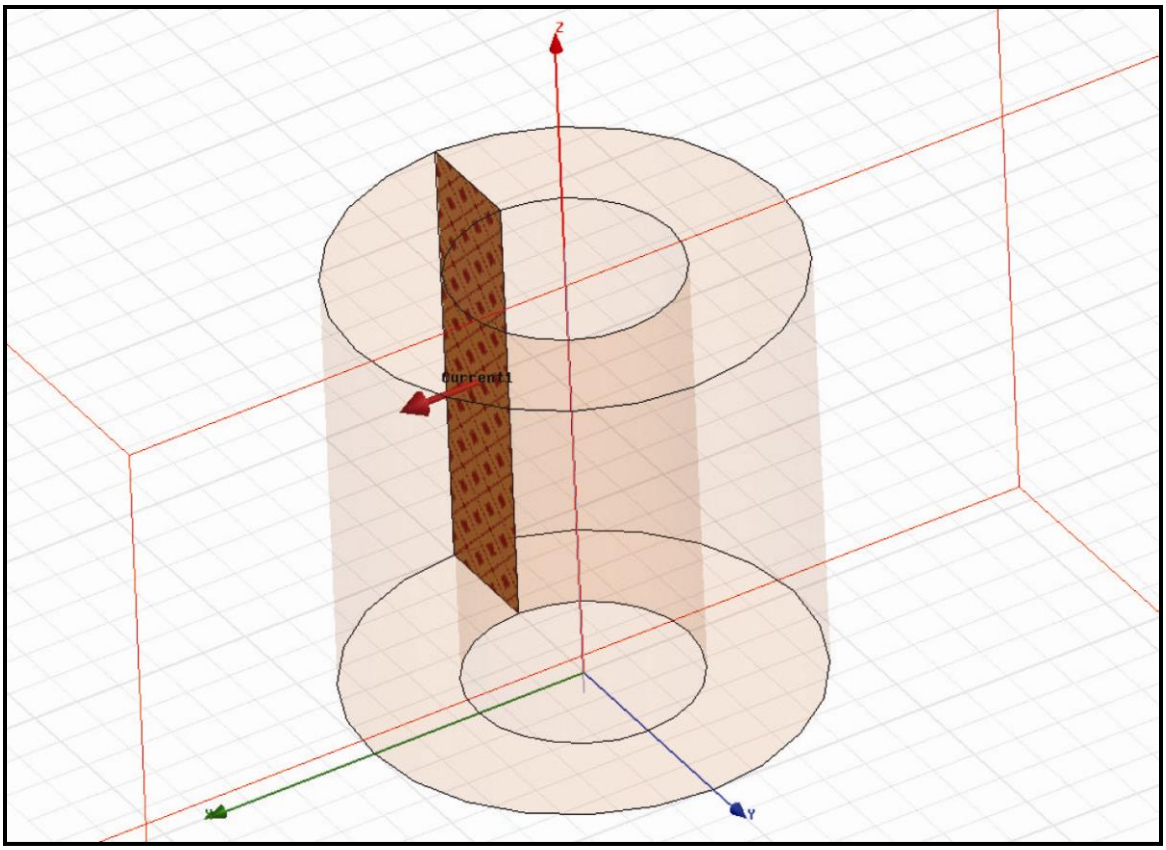

Figure 18. Bore Coil Current

Figure 19 shows a field plot of the magnetic field intensity of the simulated MRI bore magnet. The precise magnitude of the field is not relevant; rather the uniformity in the central region of interest is important, but only for imaging purposes. For purposes of this thesis, precise uniformity of less than 0.5 ppm across the entire region is unnecessary. As shown in the plot, a uniformity of plus or minus 1000 Gauss is well within the area of interest for measuring torques on various materials.

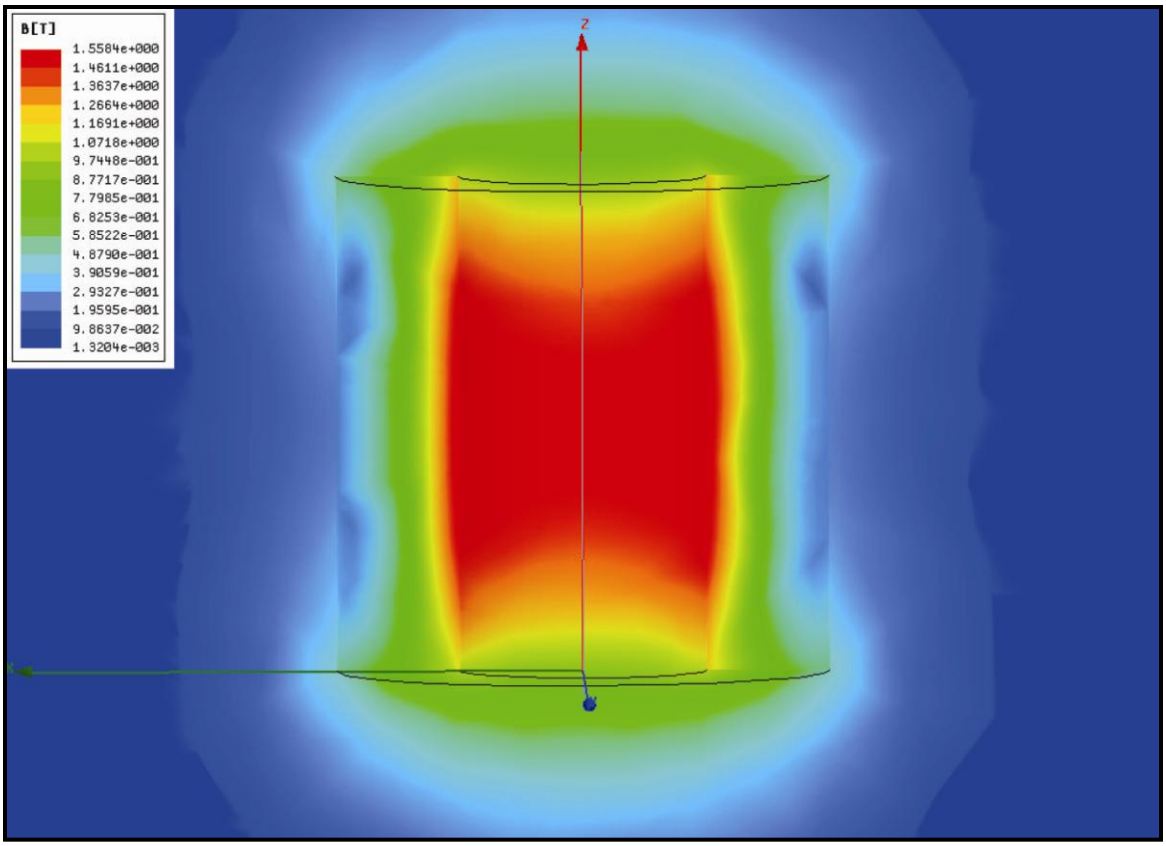

Figure 19. Bore Coil Field Intensity

In order to capture the numerical values of a field, reference geometry is required. In this case a polyline is created along the central axis of the simulated MRI bore magnet and the field intensity calculated along the line. A plot of the field intensity along the line is shown in Figure 20.

The area of interest consists of a small volume of space approximately 100mm on a side located at the isocenter of the simulated MRI bore magnet. The z-dimensions of this volume extend 50mm to each side of the 1-meter vertical axis of the plot.

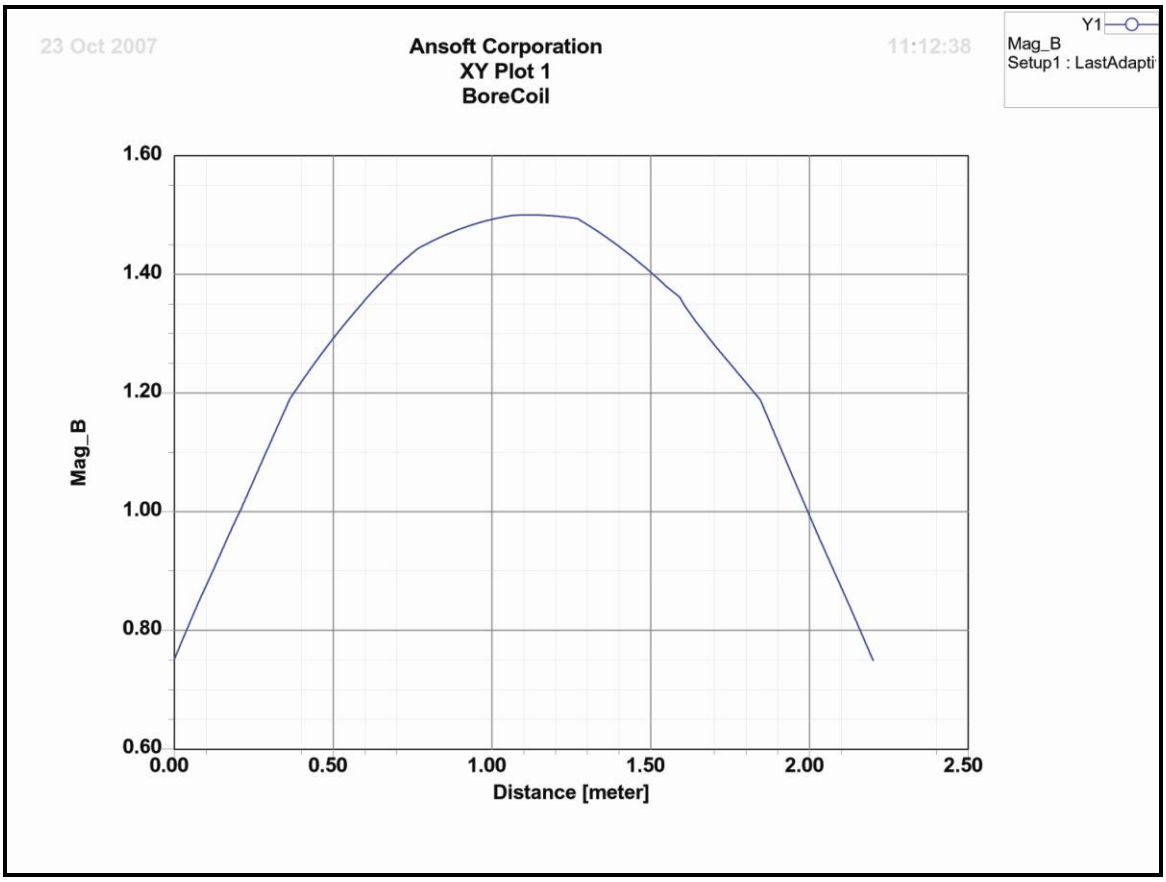

Figure 20. Bore Coil Axis Field Plot

The exact equations used in Maxwell 3D, by Ansoft, Inc., are not published, but the field solution verifies the following two Maxwell's equations:

$$\nabla \times \mathbf{H} = \mathbf{J} \tag{19}$$

$$\nabla \cdot \mathbf{B} = 0 \tag{20}$$

with the following relationship:

$$\mathbf{B} = \mu_0 (\mathbf{H} + \mathbf{M}) \quad (21)$$

where M is the permanent magnetization vector. Since there are no permanent magnets involved in this thesis, and none in the simulations models, the equation reduces to:

$$\mathbf{B} = \mu_0 \mathbf{H} \quad (22)$$

The Maxwell 3D solver considers the magnetic field strength vector, H, at all edges of the mesh such that Ampere's law holds on all contours of all tetrahedral faces. Nodal values for each of the four vertices as well as all six mid-edge nodes are calculated to ensure a good quadratic approximation inside each finite element. This method utilizes fewer computation resources, excellent numerical stability, reducing cancellation errors, and the capability to automatically connect iron regions.[25]

Gradient Coil Design

The design of the gradient coil follows the actual physical configuration of a typical MRI system. There are three sets of gradient coils. The axial gradient coils are simple solenoid or "Helmholtz" coils located at either end of the bore coil and concentric with the bore coil. One of the coils, at the "head" end of the bore coil, is connected such that current flow in that coil matches current flow in the bore coil, thus adding to the magnetic field strength. The other coil, at the "foot" end of the bore coil, is connected such that the current circulates opposite that of the bore coil, thus opposing the magnetic field of the bore. Since the bore field is upwards of 10,000

to 15,000 times stronger than the gradient fields, the gradient fields simply add and subtract, respectively, from the bore field and create an axial gradient that gets smaller as a function of increasing z dimension. Since the configuration of the axial gradient coils is simply "another" solenoid, they were not as interesting as the coronal and sagittal coils.

The coronal and sagittal coils consist each of a set of four "saddle coils" also know as "Golay coils" oriented and connected such that their fields contribute and detract from the bore field along the x and y axes. Using the graphic of Figure 22, and the right hand rule, current flow in the section of the gradient coil near the top of the bore coil, at the "foot" end of the bore coil, pointed towards the negative x-axis, will supplement the field of the bore. In the gradient coil at the bottom of the bore coil, also at the "foot" end of the bore coil, with current connected in such a way that it flows towards the positive x-axis, will detract from the bore field. Using the same analogy with the coils at the "head" end of the bore coil, one can develop an overall supplement to the field at the top of the bore and a detraction at the bottom of the bore for a gradient along the y-axis, greater at the positive y-axis, and linearly decreasing at the negative y-axis extents of the bore. The linear sections of the gradient coils cancel each other out, and the other looped sections are placed sufficiently far from the bore that their fields contribute little to the bore gradient.

Another set of four coils, rotated 90 degrees with respect to the coronal coils, constitute the sagittal coils. For purposes of this thesis, it is not necessary to overly complicate the analysis with the addition of the axial and sagittal coil sets. In fact, the addition of these coil sets will overly complicate the eddy currents and seriously detract from the ability to capture meaningful eddy current data.

The gradient coils used are excited with a 100 Hz sinusoidal current waveform and the data for two cycles of the waveform will be captured.

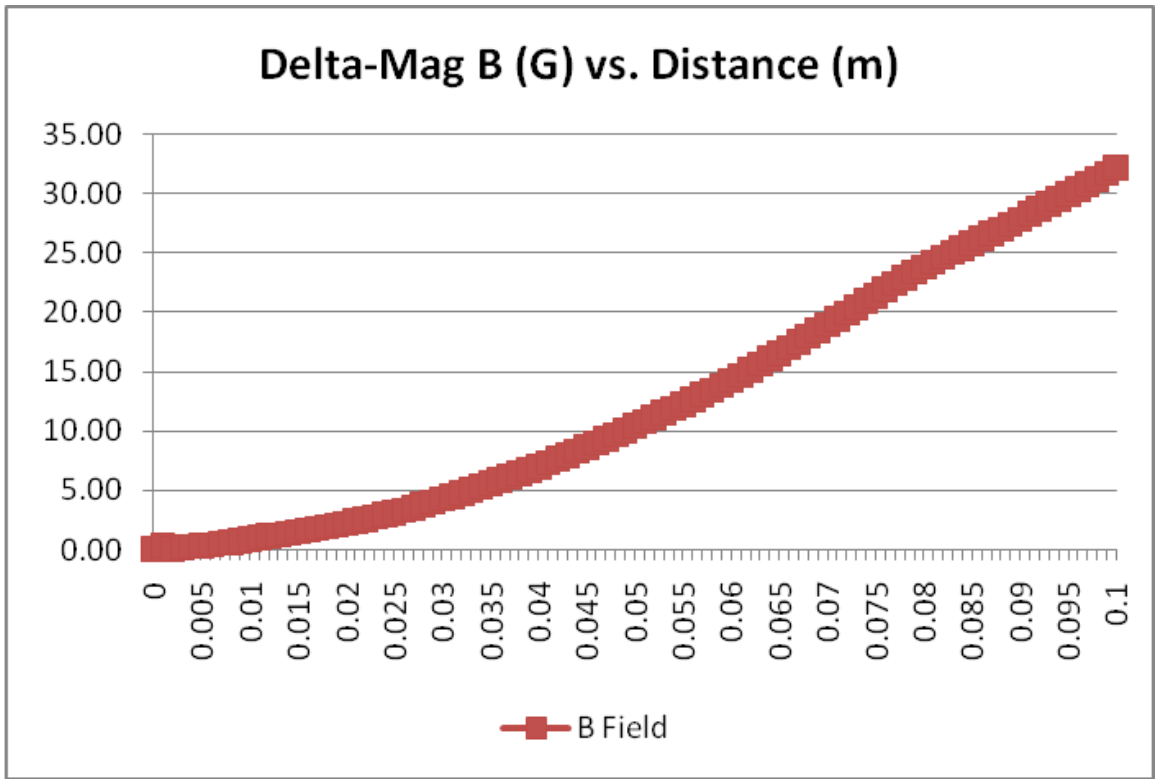

Figure 21. Gradient Field Linearity

The data shown in Figure 21 is a normalized plot of the contribution of the gradient field as a function of distance from the isocenter of the MRI bore. The data indicates that the field is relatively linear with approximately 3.2 Gauss per centimeter gradient at maximum amplitude.

Simulated MRI Design

The simulated MRI is designed using a composite of the simulated bore and the simulated gradient coils. Each gradient coil is separated from the bore by 1 mm and is otherwise concentric with the exact same diameter. The completed simulated MRI is shown in Figure 22.

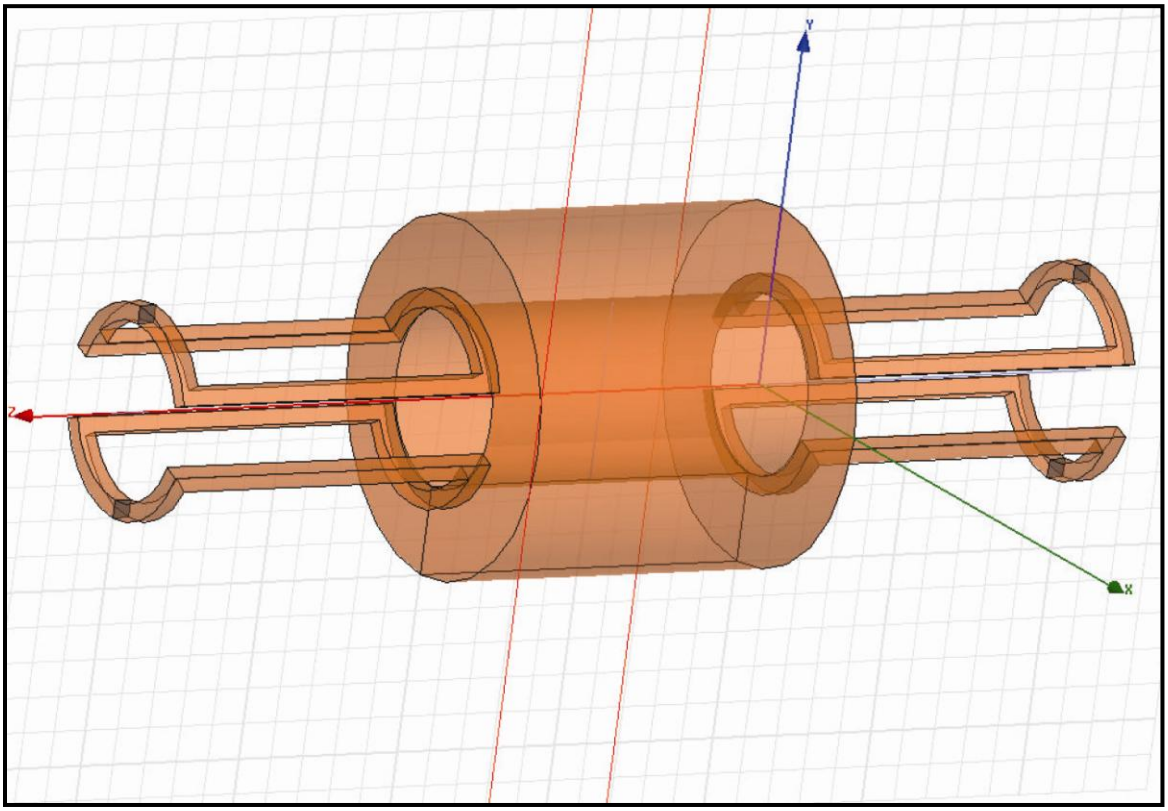

Figure 22. MRI Simulator

Using the exact same current as developed in the bore coil simulation, with the field direction in the positive z-axis, the MRI simulator is established with a static field intensity of approximately 1.5 T field intensity at the isocenter. A graphic indicating the bore coil stranded current flow is shown in Figure 23.

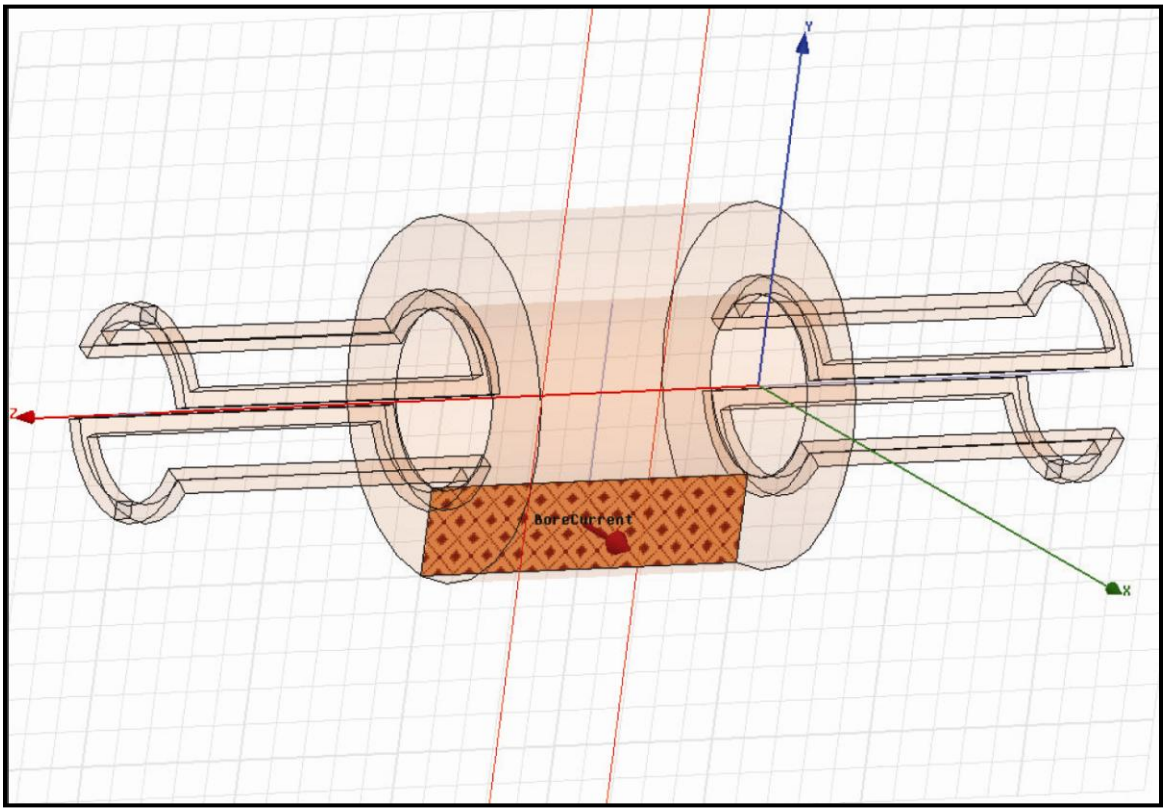

Figure 23. MRI Simulator Bore Current

As described above, the gradient coil at the top of the simulated MRI, at the "foot" end of the bore coil, is excited with a 100 Hz sinusoidally varying stranded current. The graphic of Figure 24 shows the section of the gradient coil where current is inserted and its direction. Following this current through the gradient coil, it can be noted that current flow in the curved section next to the bore coil points in the negative x-axis direction, thus supplementing the bore field at the top of the bore.

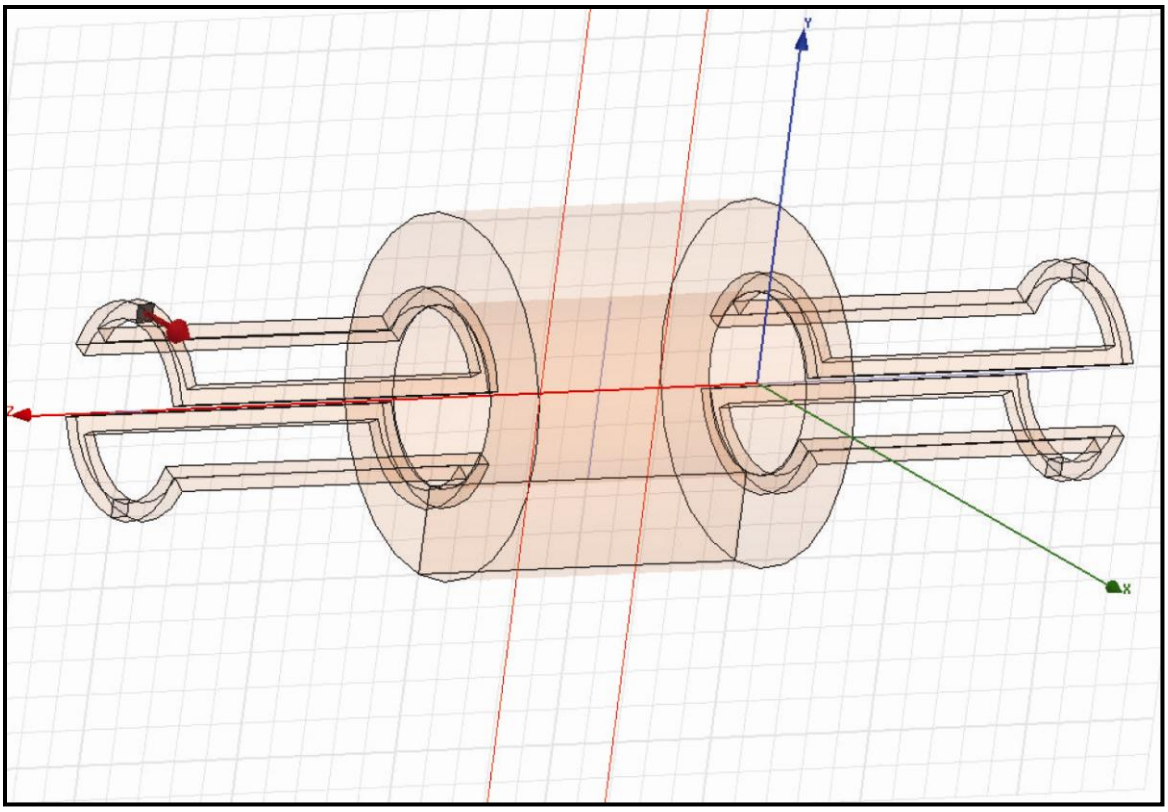

Figure 24. MRI Simulator Gradient Coil #1 Current

A rainbow plot of the field intensity, with the bore field on and the gradient coils excited with a 100 Hz sinusoidally varying current, producing a field gradient of approximately 3.2 Gauss per centimeter at the peak of the current sinusoid, is shown in Figure 25. The field plot is shown for intensity on the YZ plane.

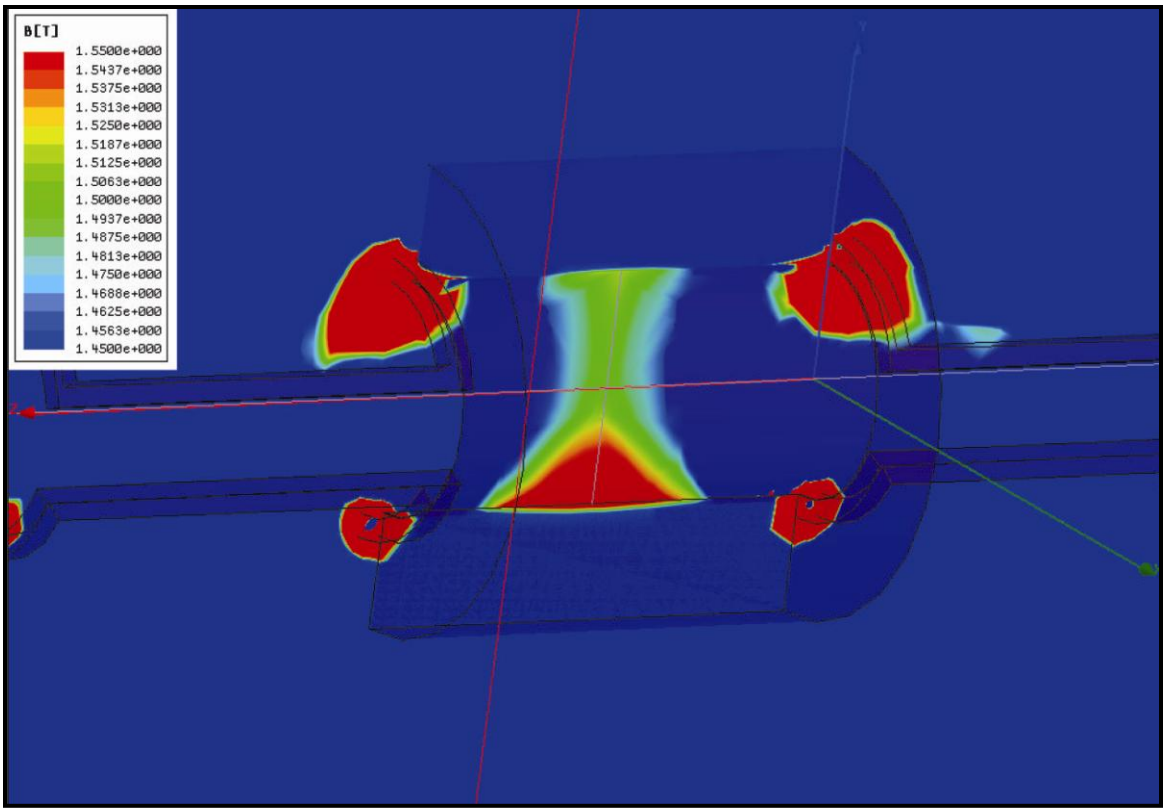

Figure 25. MRI Simulator B Field Intensity

A plot of the field intensity, along the z-axis, is shown in Figure 26. This plot demonstrates that the overall shape of the axial field inside the bore, is unaffected by the addition of the gradient coils (see Figure 26).

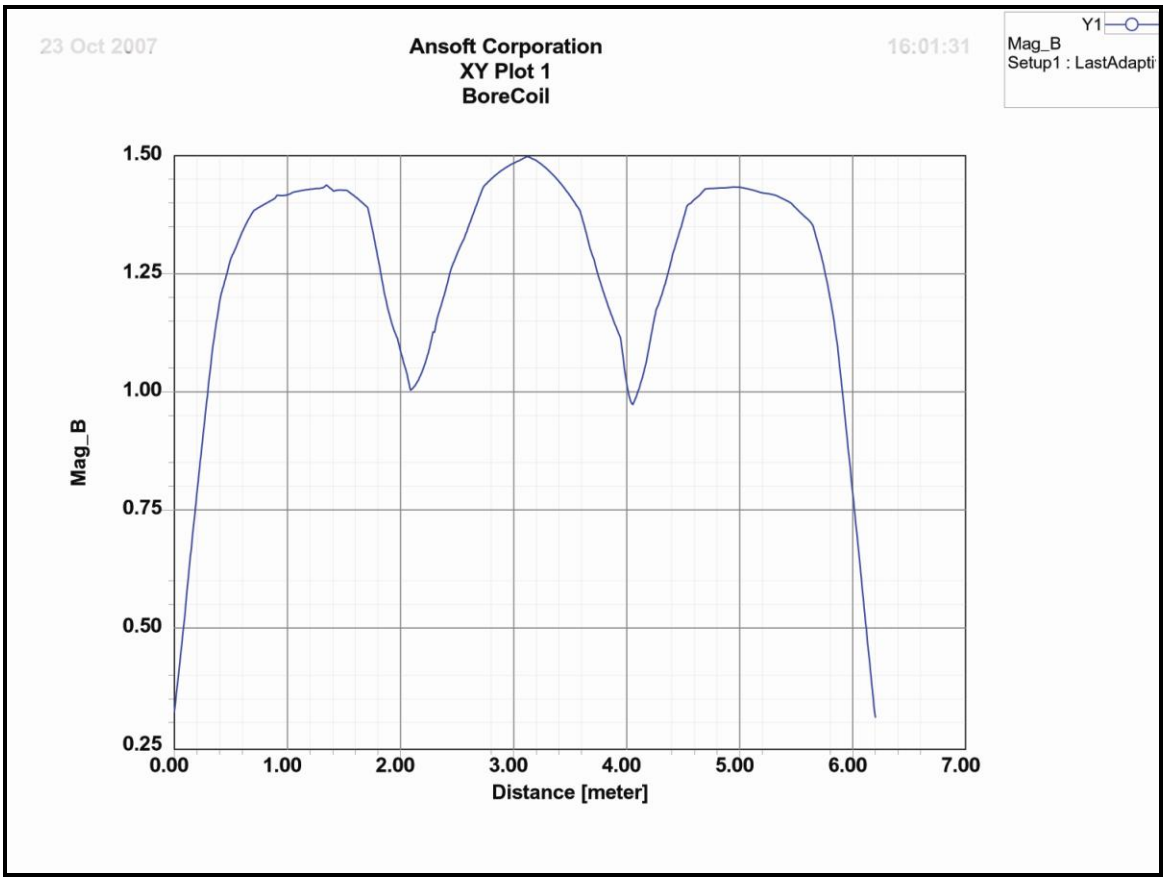

Figure 26. MRI Simulator Axial B Field

Using the bore coil and a single set of gradient coils, a very good approximation of a MRI system is developed, as long as certain limitations are observed. The first limitation is that the simulated MRI in no way is modeled to represent an actual MRI for purposes of field linearity and precision intensity. Nor is it intended to model all possibilities for eddy currents under the influence of the combination of axial, coronal, and sagittal fields with the addition of shim coils and RF coils. Finally, the volume of interest is limited to a section of the simulated MRI bore field that can reasonably used to approximate conditions found in an MRI for the purposes of this

thesis. A colored strip, as shown in Figure 27, indicates the extent of the field that is of interest along the y-axis of the simulated MRI system.

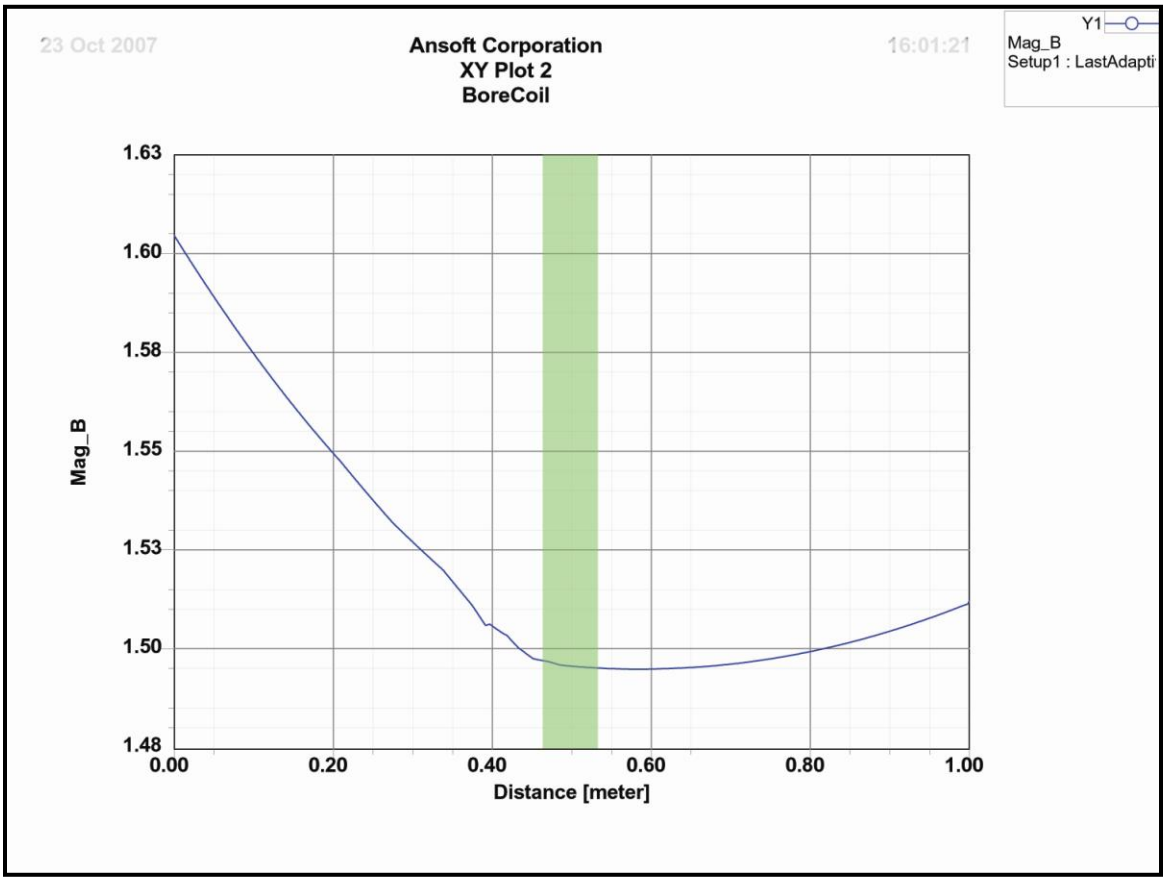

Figure 27. MRI Simulator Coronal B Field

CHAPTER SEVEN: TEST VOLUMES

Now that the MRI simulator is established, a number of test volumes can be inserted and analyzed to form a reference for developing eddy current reduction techniques. An infinite variety of sizes and shapes of test volumes can be developed. It would be impractical to attempt to analyze every possible shape. As is well known in solid modeling CAD programs, and indeed in Maxwell 3D as well, almost every shape can be modeled using only a small subset of geometric shapes, combined in various ways to create more complex shapes. Furthermore, only a small subset of geometric shapes comprises the shapes found in electronic and mechanical devices inserted into MRI fields. For this thesis, a wire, sheet, block, box, sphere, loop, and minor variations will be used. More complex shapes and their effects are left for future work.

Wire Test Volume

The wire modeled for this test volume has dimensions of 100mm x 1mm x 1mm. It is assumed that the torque differences between round wire and square wire for purposes of this thesis are insignificant. The wire is situated with its volumetric center point coincident with the central coordinates of the simulated MRI bore, namely coordinates (0,0,0). The long axis is oriented along the x-axis of the simulated MRI. The graphic in Figure 28 shows the wire in the bore with an orientation of 0 degrees.

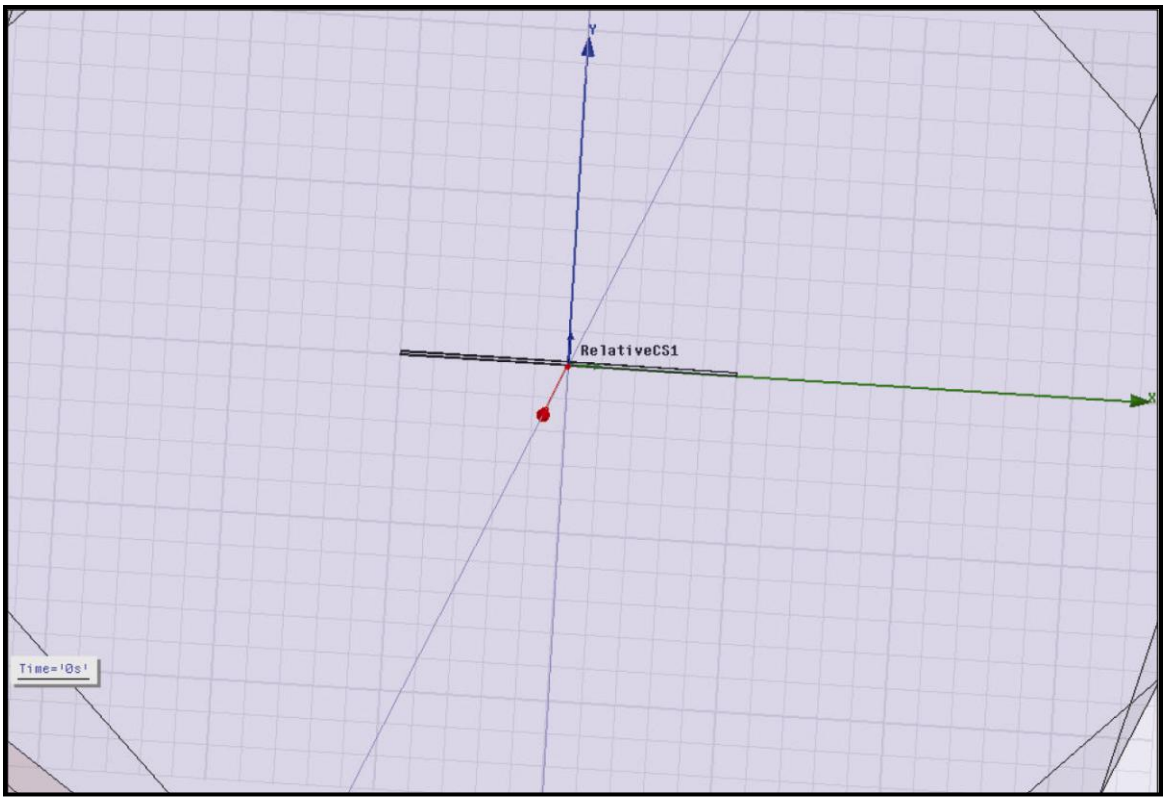

Figure 28. Aluminum Wire

The materials chosen for the wire are Aluminum, Copper, Silver, Stainless Steel, and Iron. Two cycles of 100 Hz AC gradient coil excitation are captured. These materials represent those most commonly found in electronic equipment and mechanical fasteners, as well as a representative material for higher conductivity, silver, and a ferromagnetic material, iron.

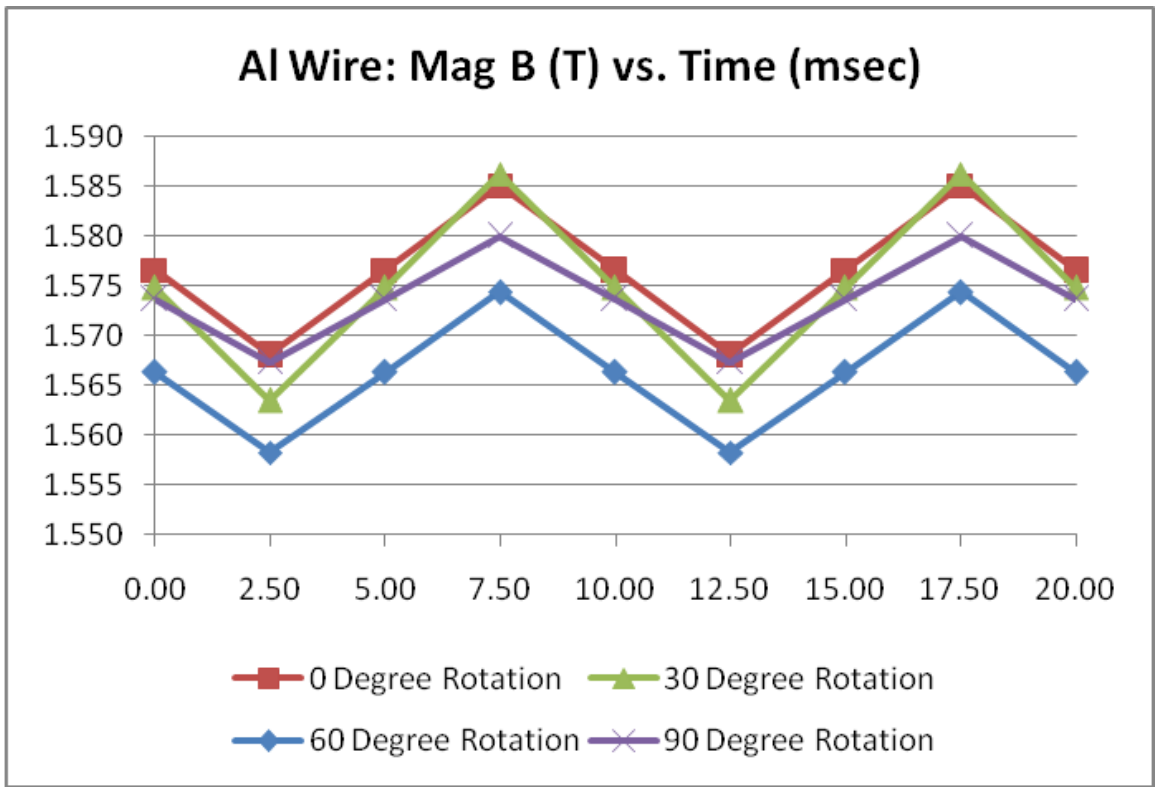

Figure 29. Aluminum Wire – B Field vs. Time

The graph in Figure 29 shows the variation in the magnitude of the magnetic field measured in Tesla at the simulated MRI central volume vs. time in milliseconds for four rotation angles of aluminum wire around the simulated MRI z-axis, with counterclockwise rotation being positive with the z-axis pointing directly at the viewer. As the wire is rotated, variations in the eddy current interactions distort the field, causing the localized field strength to vary. As the wire is rotated, the localized field strength increases until the wire is vertical in the field. The differences in magnetic field intensity, however, contribute little to the overall torques applied to the wires. The primary effect is caused by the gradient coil generated eddy current interacting with the bore static field.

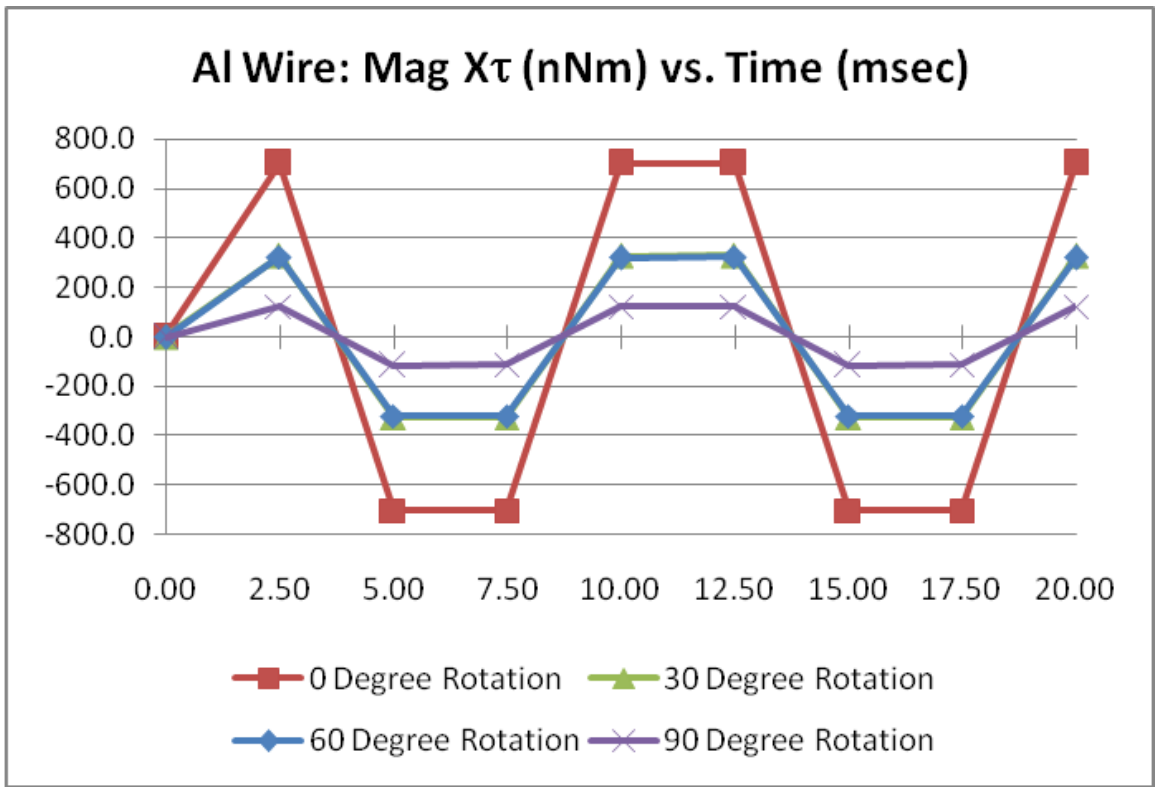

Figure 30. Aluminum Wire – X-Axis Torque vs. Time

The graph in Figure 30 illustrates the variation in torque strength as a function of rotation angle with the vertical axis indicating x-axis torque, in nano-Newton meters vs. time. The important point to note is the fact that the torque in the x-axis is decreasing as the rotation angle increases. Using the cross product of the magnetic field vectors and current vectors, it is clear that the eddy current is circulating around the x-axis in a clockwise fashion as viewed from the positive x-axis.

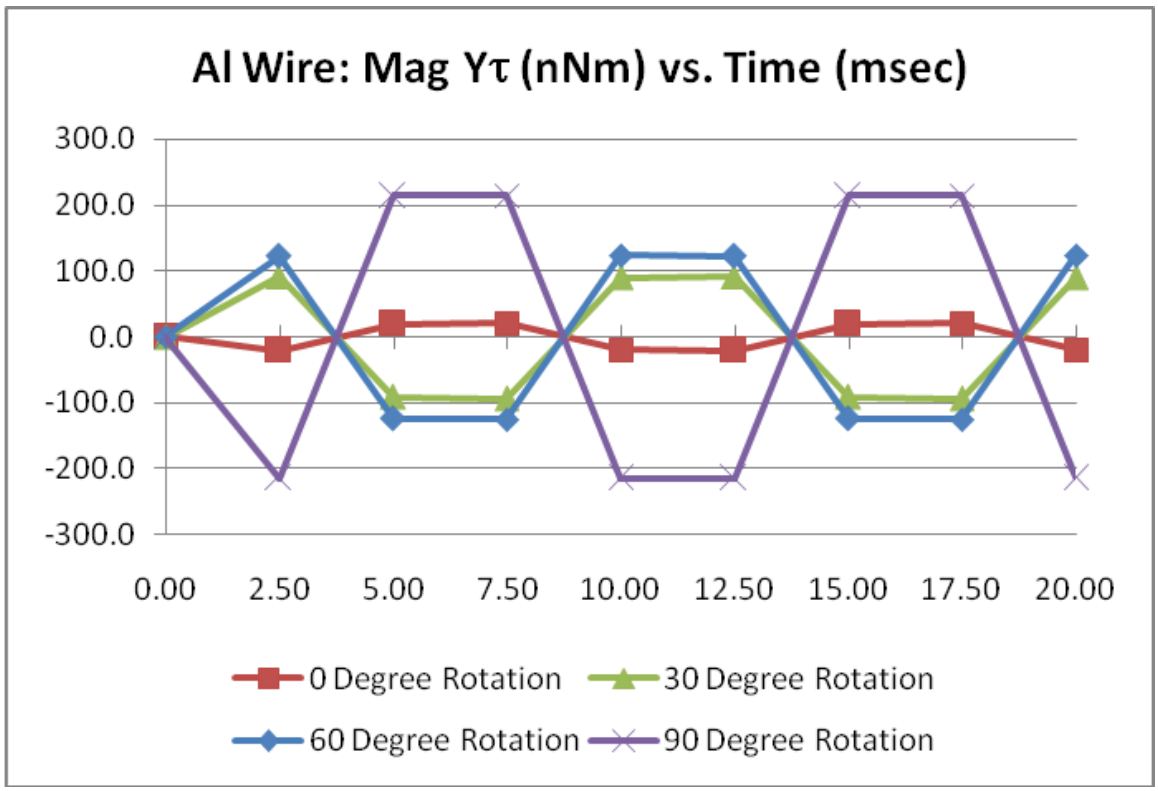

Figure 31. Aluminum Wire – Y-Axis Torque vs. Time

The graph in Figure 31 also shows the magnitude of the torque vs. time, but in this case the torque is around the y-axis and increases as the rotation angle increases. The cross product between the bore field and the eddy current indicates once again that the eddy current circulates clockwise around the y-axis as viewed from the positive y-axis.

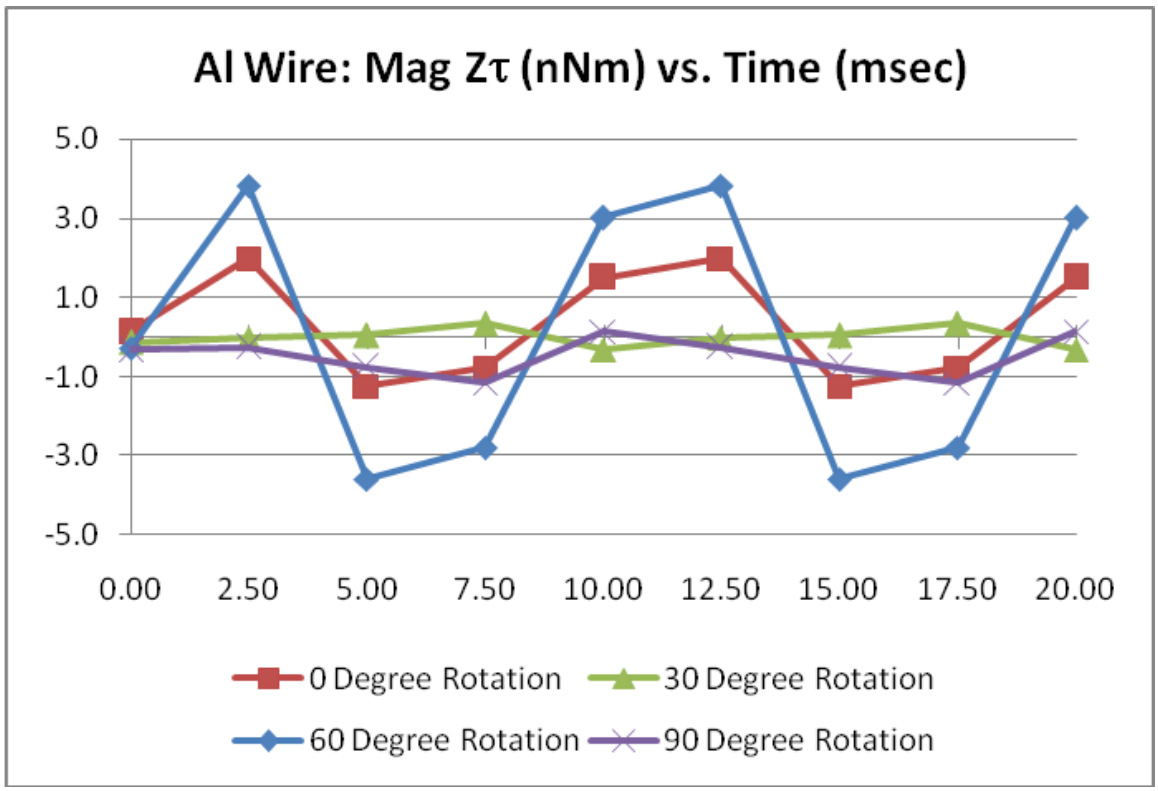

Figure 32. Aluminum Wire – Z-Axis Torque vs. Time

The graph of Figure 32 shows the magnitude of the torque around the z-axis as a function of the rotation angle of the wire, with the magnitude of the torque in nano-Newton meters in the vertical axis and time in the horizontal axis. Note, however, that the scale in the z-axis graph shows torques less than 4nNm in all cases, where the torques in the x and y axes are several hundred times larger.

Based on the magnitudes of the torques, and the relative increases and decreases as a function of rotation angle, it is conclusive that the eddy current acts with the bore field and the gradient field that produced the eddy current has little effect on the torque. It is unlikely that any definitive data can be derived from the z-axis torques due to the tolerances of the Maxell analysis

being of similar magnitude, and the complex interactions between gradient coil induced eddy currents and the much larger bore field.

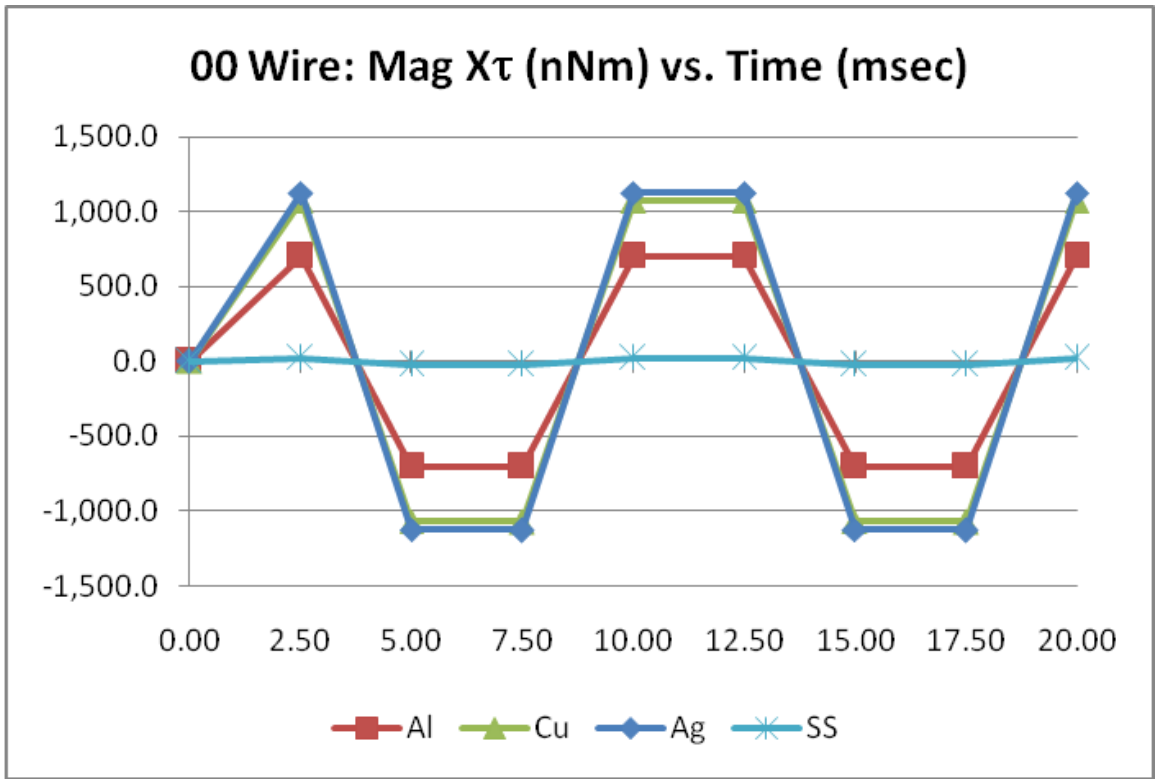

Figure 33. Wire – X-Axis Torque vs. Material

Knowing that the x-axis torque of aluminum wire as a baseline, and establishing that the torque is greatest in the x-axis when the wire is aligned with the x-axis, a comparison of the torque is made for several different materials.

The graph in Figure 33 shows the magnitude of the x-axis torque vs. time as a function of materials. The “00” in the title indicates that the materials are positioned in the 0-degree rotation angle. Copper and Silver have a conductivity slightly less than twice that of aluminum, allowing eddy currents to be established with correspondingly greater magnitude, resulting in an increased

torque. Stainless Steel, however, has a conductivity approximately 40 times smaller than aluminum, and thus cannot carry any eddy current as well as aluminum, copper, and silver. A table of conductivities and the simulation values used by Maxwell 3D is shown in Table 3.

Table 3 - Material Conductivity

Material	Resistivity[26] (micro-ohm-cm)	Conductivity (Siemens/m)	Simulation Value (Siemens/m)
Aluminum	2.6548	37,667,620.	38,000,000
Copper	1.6730	59,772,863.	58,000,000
Silver	1.59	62,893,081.	61,000,000
304	68.97	1,449,905.7	1,100,000
Iron	9.71	10,298,661.	10,300,000

Iron was purposefully left out of the graph of Figure 33. The metals listed in Figure 33 are non-ferrous metals with a magnetic permeability of approximately 1.0. The magnetic relative permeability of a substance is the ratio of the magnetic inductance in the substance to the magnetic field to which it is exposed. The permeability of free space is exactly $4 \cdot \pi \times 10^{-7}$ N A^{-2}. By definition, the relative permeability of free space is unity. This means that the magnetic field is not influenced by these materials much more or less than air or free space influences the field. However, iron has a magnetic permeability of 4000, meaning that iron reacts with the magnetic field intensely compared to aluminum, copper, silver, and stainless steel.

Table 4 - Material Magnetic Permeability[27]

Material	Relative Permeability
Vacuum	1.0
Air	1.0000004
Aluminum	1.000021
Copper	0.999991
Silver	0.99998
304 Stainless	1.0
Iron	4,000

Thus, the eddy current effects in iron (and other magnetic materials) will be insignificant compared to the material itself. Table 4 lists the relative permeabilities of selected materials, as used by Maxwell 3D.

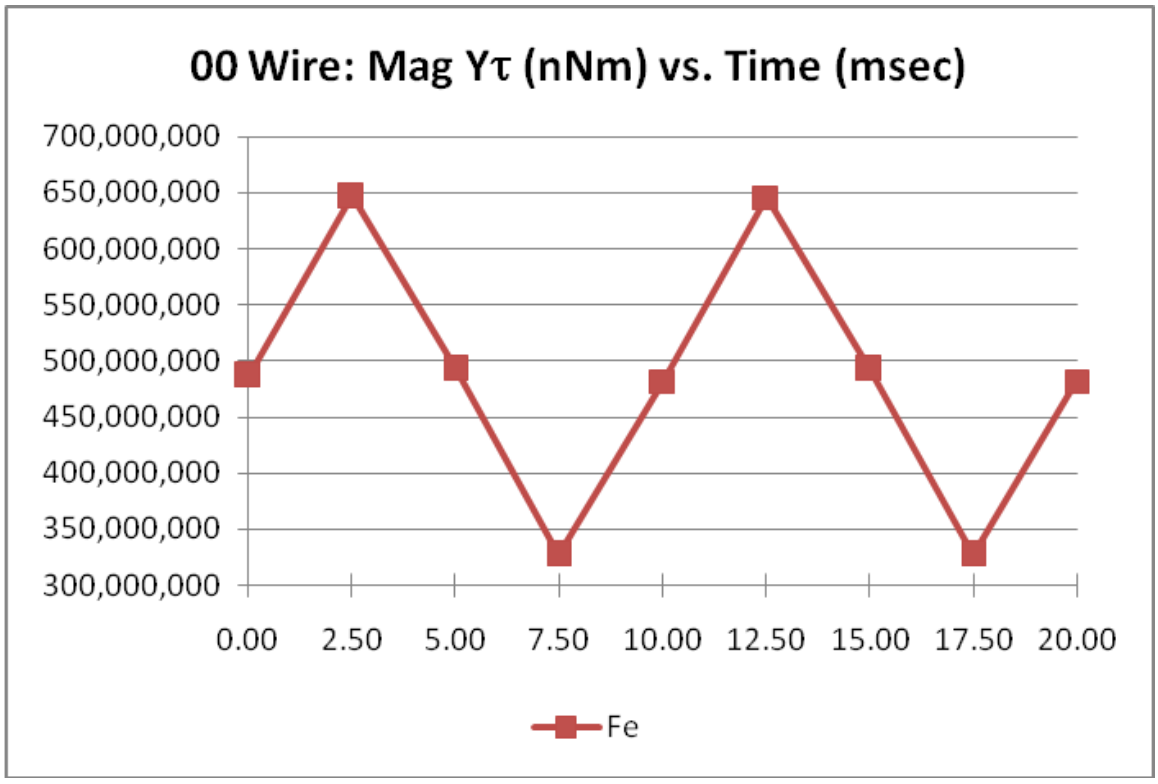

Figure 34. Wire – X-Axis Torque vs. Material

The graph in Figure 34 shows the x-axis torque of the iron wire with the vertical axis showing torque and the horizontal axis showing time. (The “00” in the title indicates that the materials are positioned in the 0-degree rotation angle.) Although iron still reacts sinusoidally with the time-varying gradient coil, this influence is based on the sinusoidal magnetization of the iron and its coincidental attempt to line up with the bore field. The magnitude of the average torque, roughly 0.49 Nm, indicates that approximately 0.1 pounds of force is exerted on the end of the wire, or approximately 1.7 ounces of force.

Sheet Test Volume

The torques experienced on a sheet of conductive material can be thought of as a summation of the torques on individual wire segments comprising a sheet. When immersed in a uniform magnetic field, and acted upon uniformly, the torques experienced by a single differential element of the sheet, a wire, is summed. But, this analogy extends beyond just the simple summation of the torque effects. A sheet of conductive material contains many more conductive paths than a wire, and thus allows eddy currents to be established more efficiently than in a wire. Comparison of the magnitudes of the torques experienced in a wire (nNm) and those in sheets (mNm) indicate many orders of magnitude greater eddy currents in a sheet as opposed to a wire. However, torque components experienced in the wire that is in the plane of the sheet, and those that are rotational, are cancelled. Only the excess and tangential components of torque are experienced.

The sheet modeled for this test volume has dimensions of 100mm x 1mm x 100mm. The sheet is situated with its volumetric center point coincident with the central coordinates of the

simulated MRI bore with its long dimensions in the x and z directions. The graphic in Figure 35 shows the sheet in the bore with an orientation of 0 degrees.

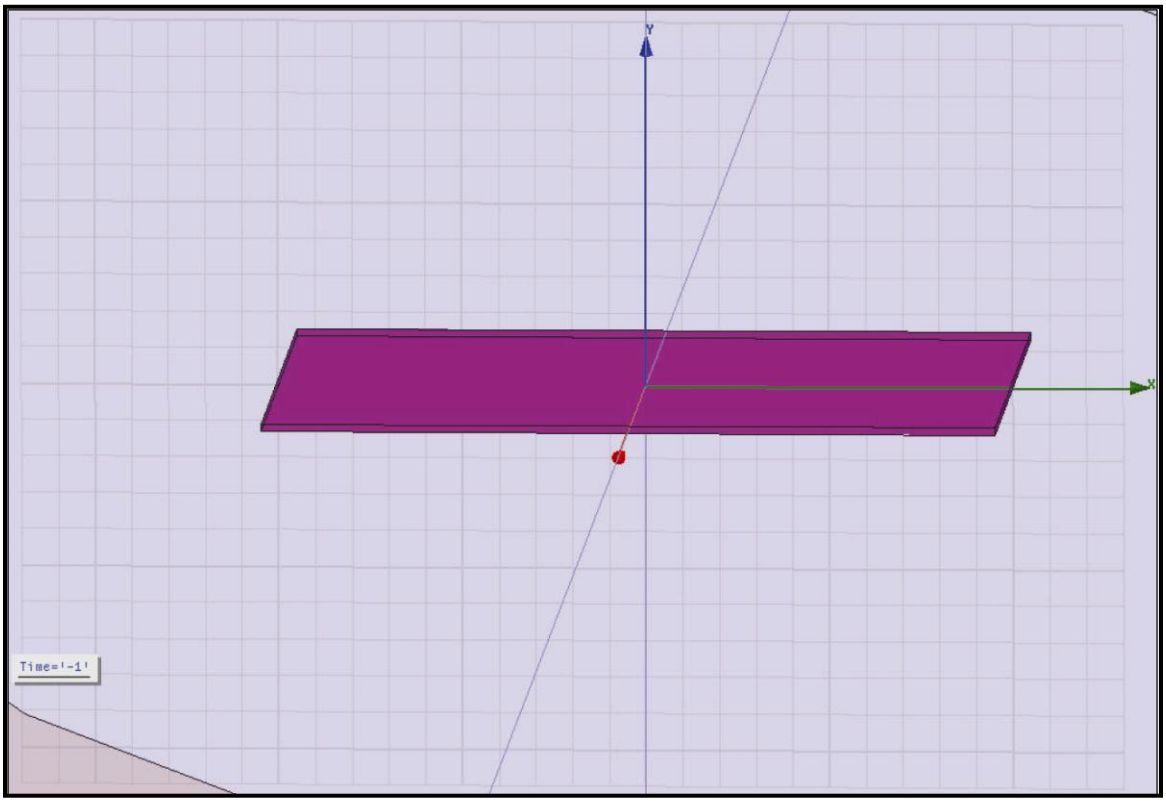

Figure 35. Aluminum Sheet

The materials chosen for the sheets are Aluminum and Copper. Two cycles of 100 Hz AC gradient coil excitation are captured. When capturing data for many of the test volumes, in order to reduce simulation processing, only significant points of interest along the sinusoid are captured. To demonstrate that the data is indeed sinusoidal in nature, a more detailed data capture algorithm was designed and the data captured for the sheet analysis. Subsequent materials and geometries will return to analysis of only certain points along the sinusoidal excitation in the MRI bore.

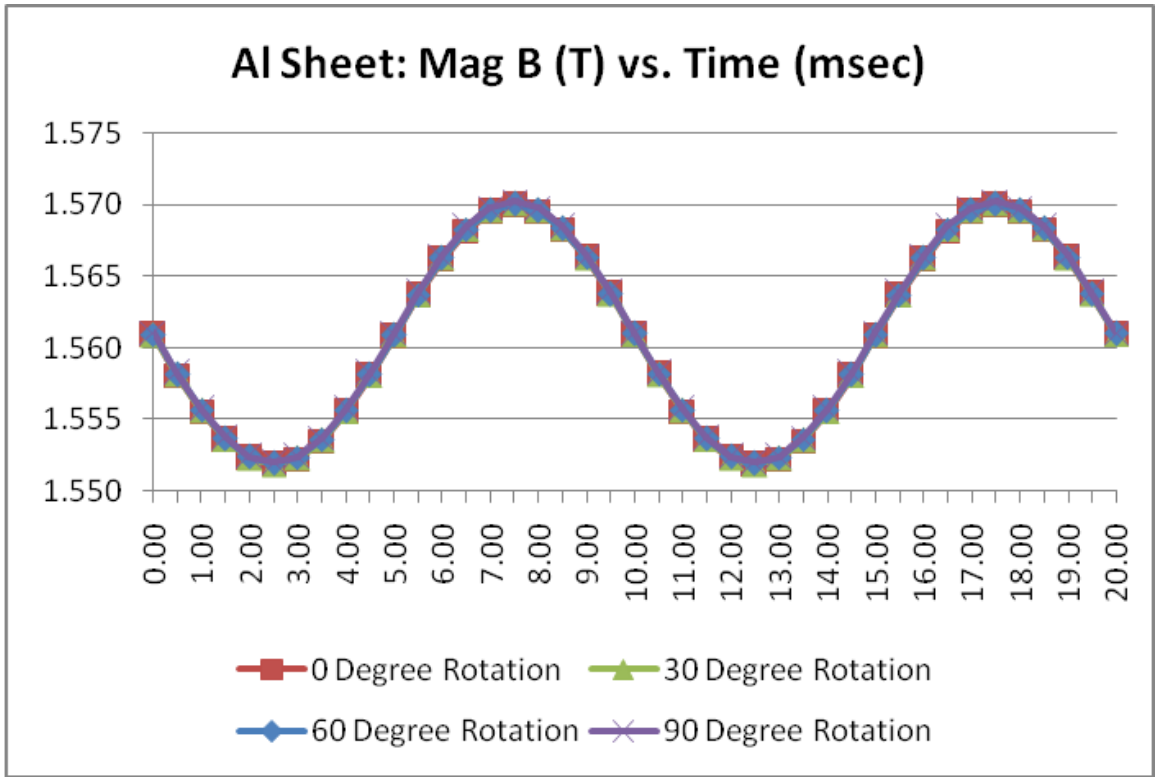

Figure 36. Aluminum Sheet – B Field vs. Time

In the plot of Figure 36, the magnetic field was plotted as a function of the rotation angle of the aluminum sheet. Each plot is coincident (within the tolerance of this simulation), indicating that the non-ferrous material, aluminum, has no significant effect on the magnetic field itself.

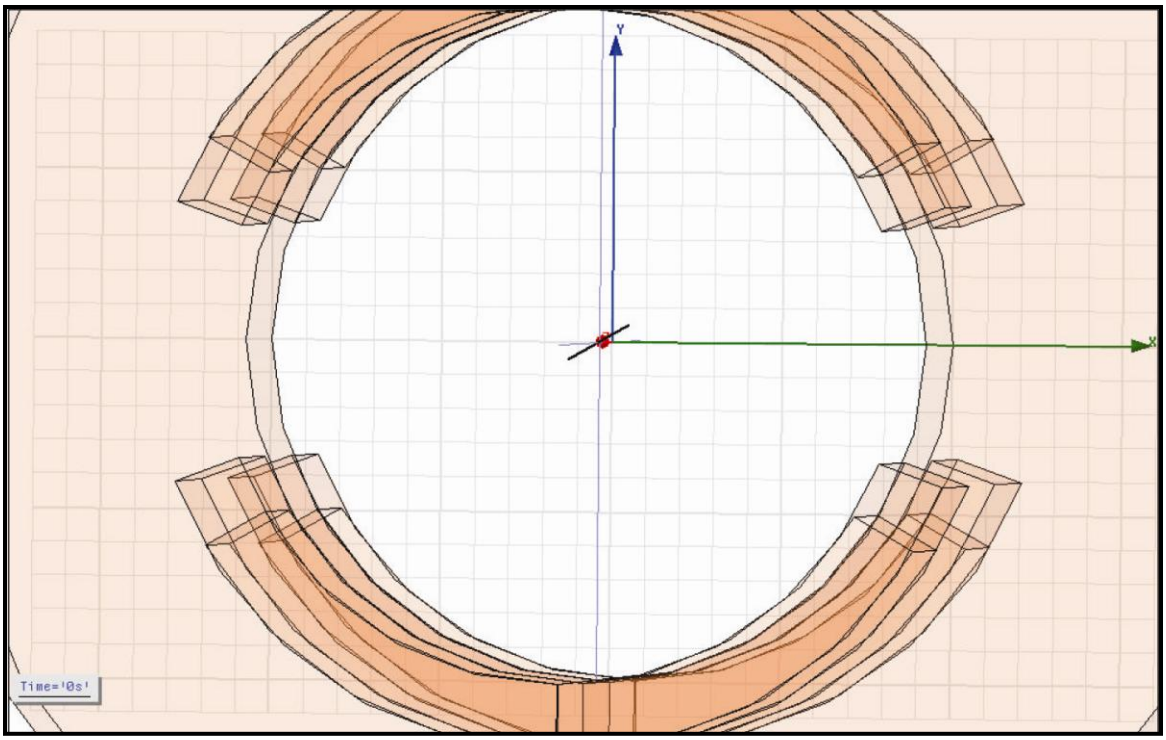

Figure 37. Aluminum Sheet – 30 degree rotation

The graphic of Figure 37 shows the view looking into the positive z-axis (z-axis points out of the page towards the viewer) with the positive x-axis to the right and the positive y-axis pointing upwards. The angle of rotation is zero degrees when the sheet is flat (coincident with the XZ plane). The angle increases in the counter-clockwise direction. The sheet is shown in the 30 degree orientation.

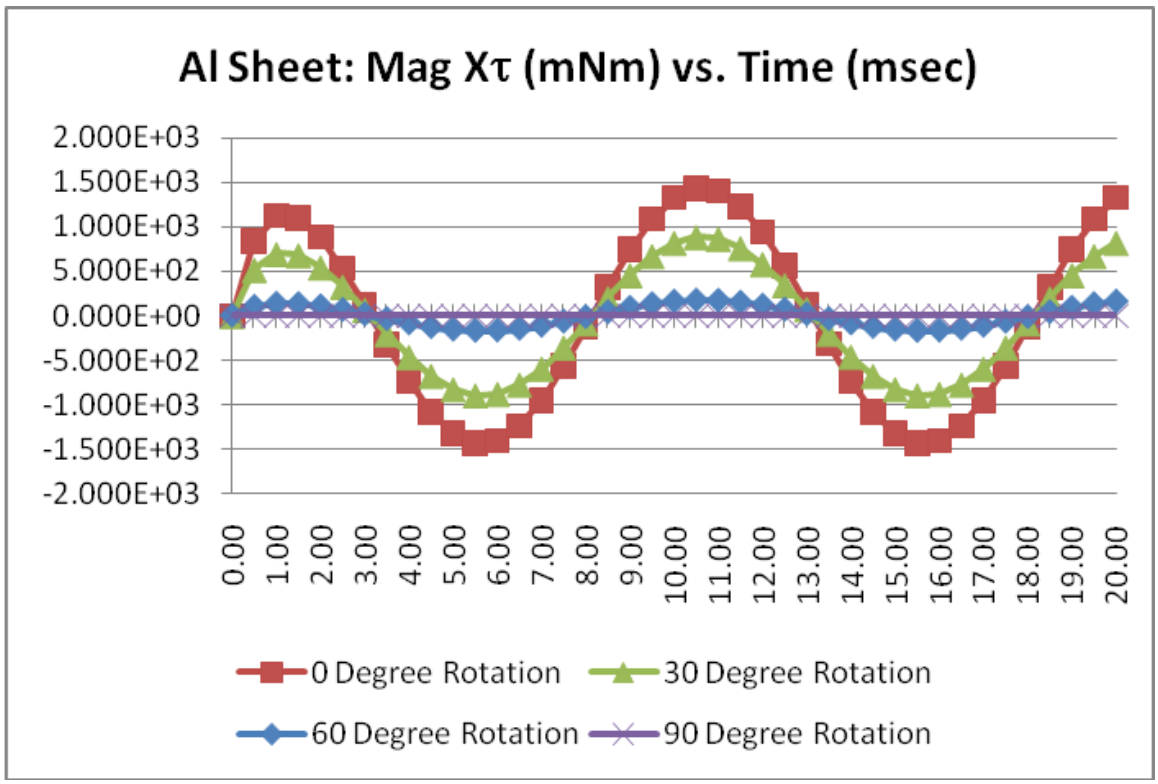

Figure 38. Aluminum Sheet – X-Axis Torque vs. Time

The plot in Figure 38 shows the magnitude of the torque experienced along the x-axis, measured in milli-Newton-meters. The horizontal axis indicates time in milliseconds and the vertical axis indicates torque. The four plots, each indicating a different rotational orientation in the XY plane, demonstrates that the x-axis torque is significant when the sheet is oriented flat (flat relative to a patient lying in the MRI bore), and decreases as the sheet is rotated to a vertical orientation.

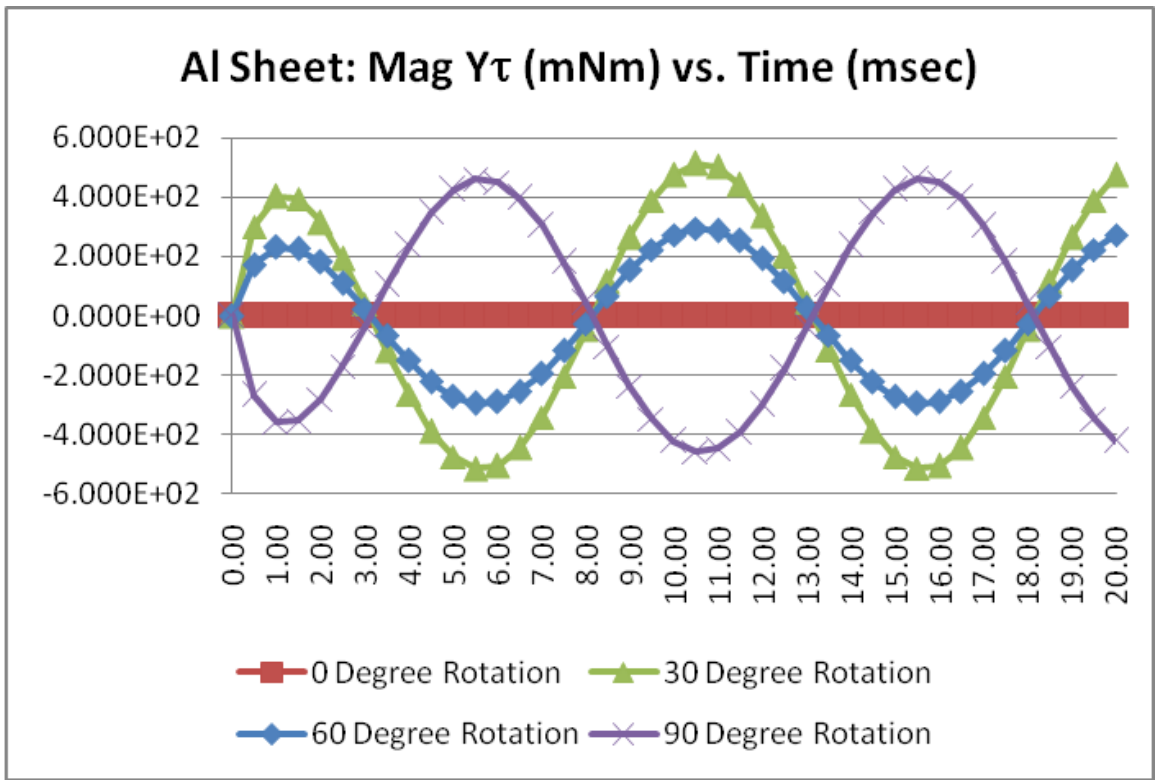

Figure 39. Aluminum Sheet – Y-Axis Torque vs. Time

Figure 39 shows the torque on the aluminum sheet in the y-axis. The horizontal axis of the plot is time in milliseconds and the vertical axis indicates torque, in milli-Newton-meters. In contrast to the torque in the x-axis, the torque experienced by the sheet in the y-axis is minimal at zero degrees rotation and increases as the rotational angle increases. It is interesting to note the phase reversal of the torque at 90 degrees of rotation. This phase reversal would indicate that a sheet that moves between the orientation just less than vertical, say 89 degrees, and an orientation just past the vertical, say 91 degrees, will experience the maximum torque in one direction and then in the other. Thus, the phase reversal supports the contention that vibrations occur in equipment containing metal sheets placed within the MRI bore.

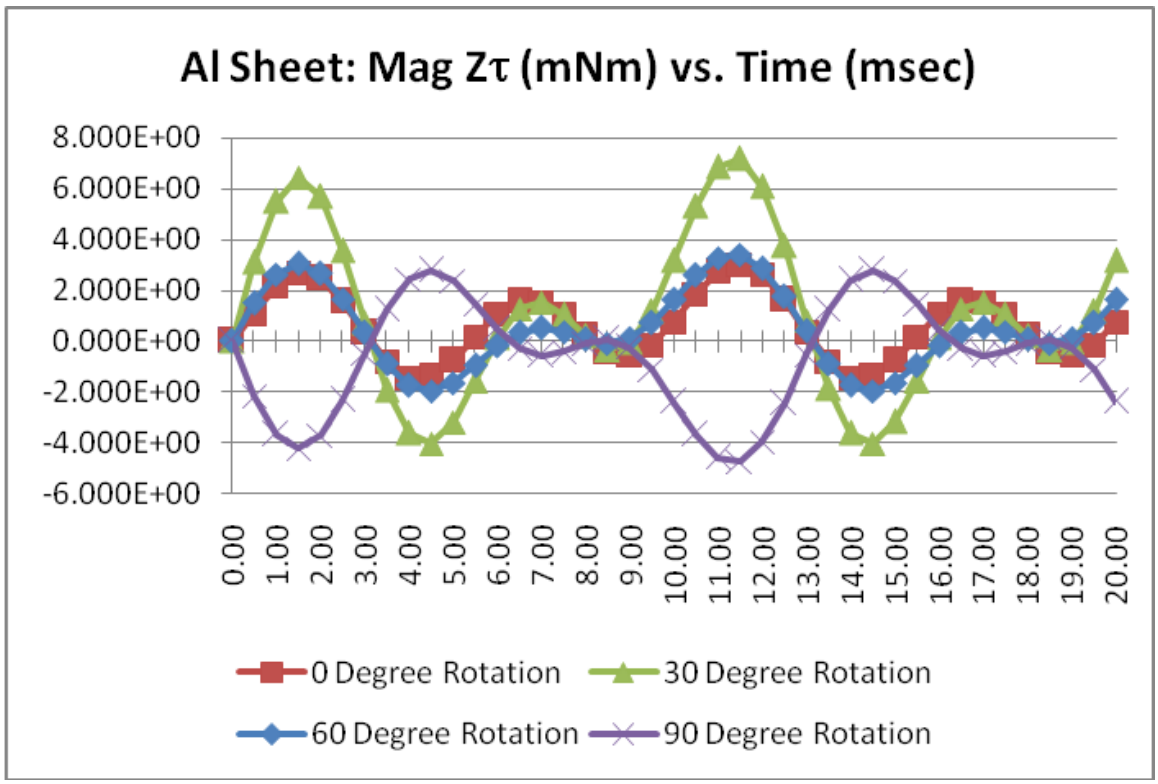

Figure 40. Aluminum Sheet – Z-Axis Torque vs. Time

The plot of Figure 40 shows the z-axis torque of the aluminum sheet as it is rotated in the XY plane. The horizontal axis depicts time in milliseconds and the vertical axis indicates torque in milli-Newton-meters. An examination of the plots, and their various phase shifts, indicate a complex combination of torque components summing and cancelling to produce resultants that are not simple reflections of the excitation fields. Comparing the magnitudes of the forces, it is clear that the x and y torques are two to three orders of magnitude greater than the torque in the z-axis. Thus, the z-axis torque is relatively insignificant.

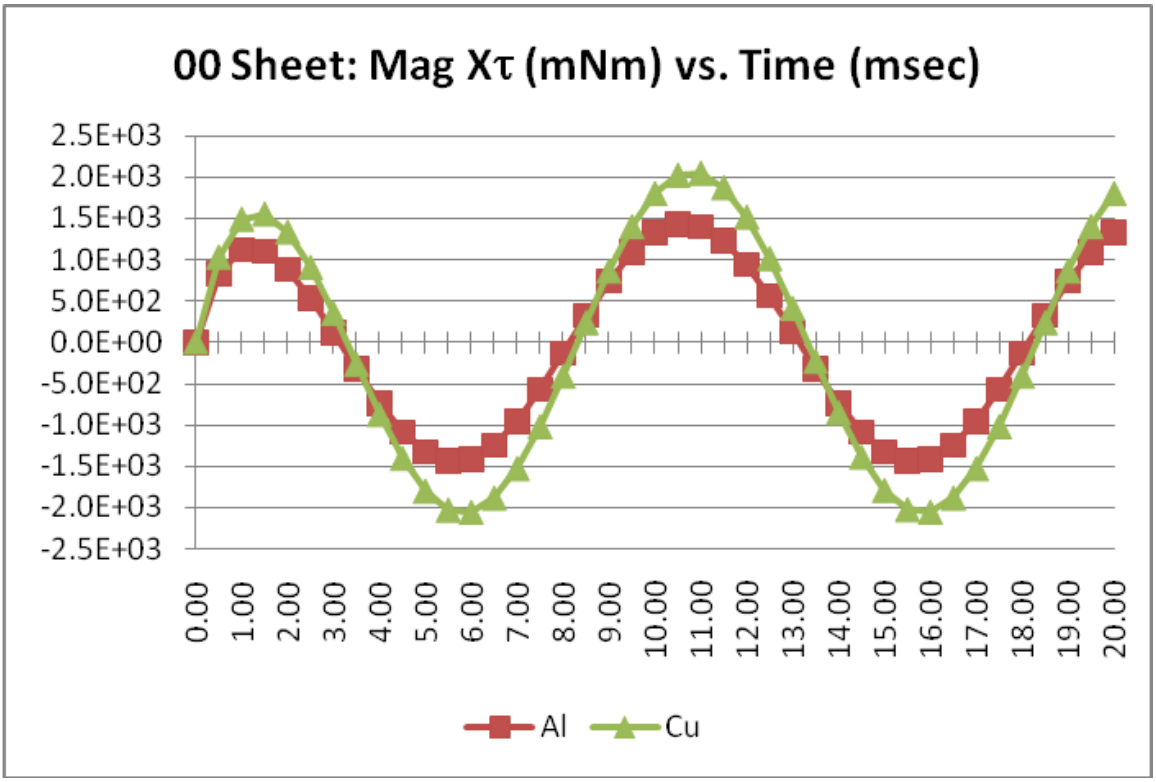

Figure 41. Sheet – X-Axis Torque vs. Material

The plot shown in Figure 41 demonstrates a similar artifact as found in the comparison of materials in the wire test volume – conductivity contributes to the torque. As shown in the plot, copper experiences a slightly greater torque, due to the greater ability to conduct current, and the resulting larger interaction with the static bore field. (The “00” in the title indicates that the materials are positioned in the 0-degree rotation angle.) It is assumed that more conductive materials will exhibit greater interaction, such as silver, and less conductive materials will exhibit less interaction, such as stainless steel.

Block Test Volume

The torques experienced on a block of conductive material can also be extended in a similar fashion as the wire is to the sheet. A block of material is a summation of sheets. Correspondingly, the magnitudes of the torques increase as the conductive volume, and thus the conductive paths, increases.

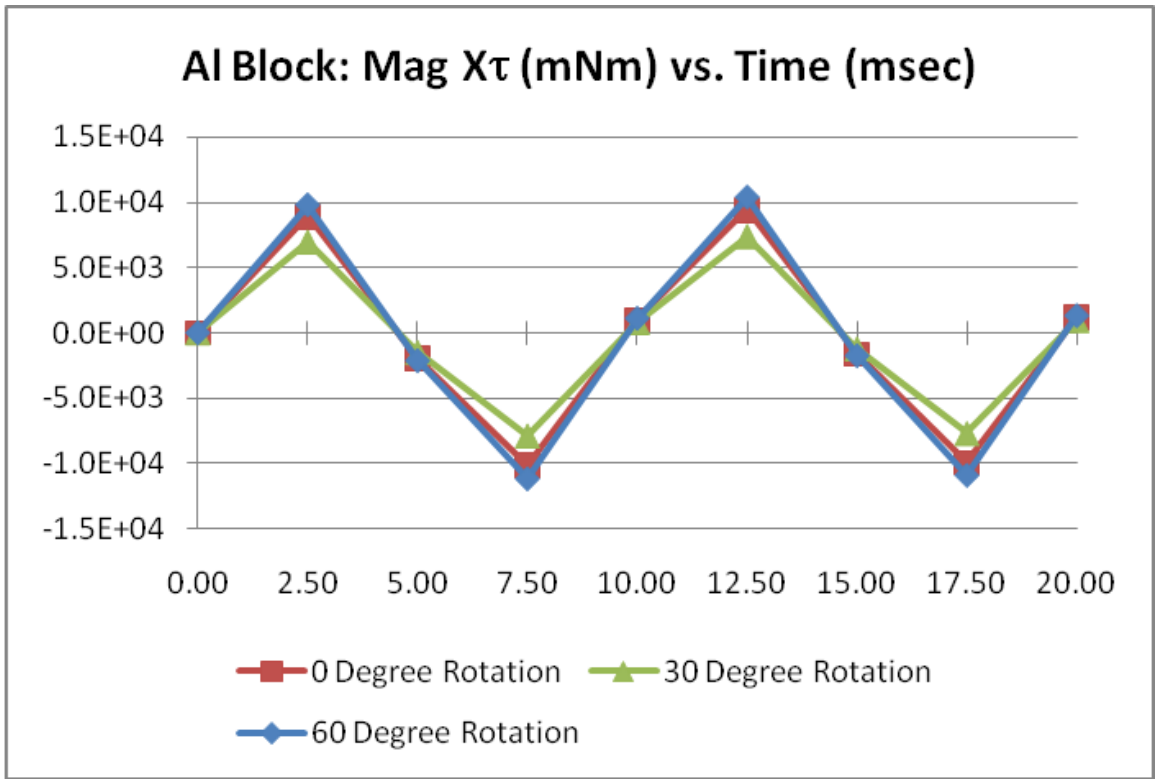

Figure 42. Aluminum Block – X-Axis Torque vs. Time

The plot in Figure 42 shows the torque experienced by a block of aluminum that is 100mm on a side. The magnitude is approximately one order of magnitude greater than a sheet. The horizontal axis of the plot indicates time in milliseconds and the vertical axis indicates torque in milli-Newton-meters. Each of three angles of rotation in the XY plane is shown. Due to

symmetry of the block, the 90 degree rotation angle is identical to the zero degree rotation angle, and therefore, is not indicated. The plot indicates that the x-axis torque, where the conducting volume extends greatly in all three dimensions, is relatively unaffected by orientation. This indicates that there is a preferred current path for eddy currents and the primary contributor is in the x-axis.

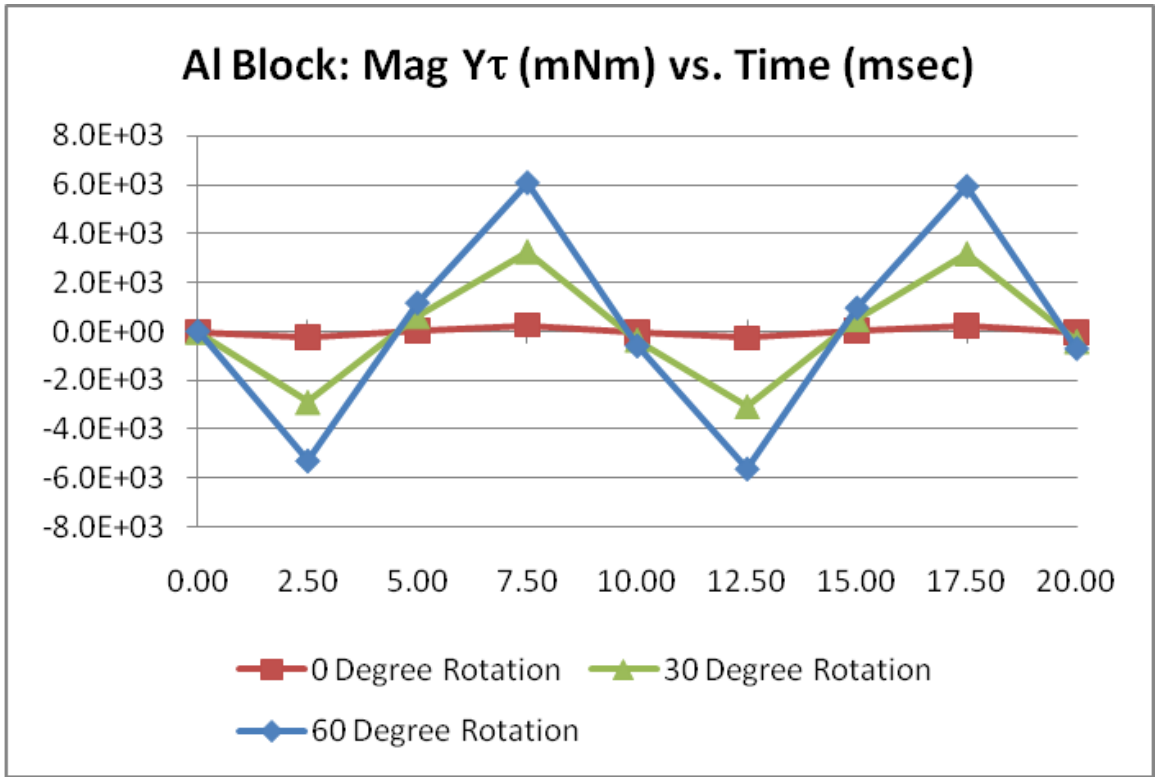

Figure 43. Aluminum Block – Y-Axis Torque vs. Time

The plot shown in Figure 43 shows the torque experienced by the aluminum block in the y-axis. The horizontal axis indicates time in milliseconds and the vertical axis indicates torque in milli-Newton-meters.

This plot indicates that the interaction of the gradient coil induced eddy current and the bore field are more dependent when torque in the y axis is involved. As the block is rotated, the magnitude of the y-axis torque increases. Similarly, the 90-degree rotation angle is identical to the 0-degree rotation angle.

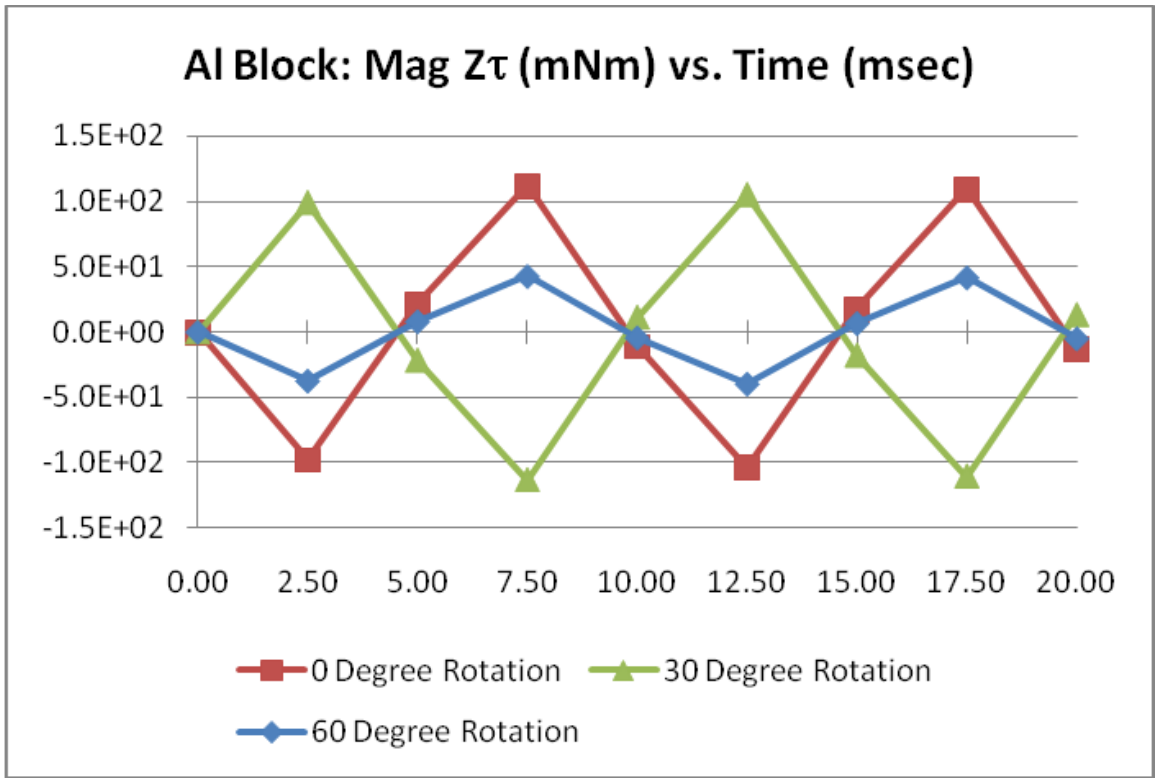

Figure 44. Aluminum Block – Z-Axis Torque vs. Time

In a similar fashion to all previous test volumes, and due to the orientation of the bore field and the selected gradient field, the torque in the z axis remains unimportant. It is interesting to note the phase reversal between 0-degrees and 30-degrees, and yet another one between 30-degrees and 60-degrees. These reversals are indicative of the complex nature of the induced eddy currents due to only one gradient coil. The addition of two more gradient coils as well as various

shim coils and RF coils will quickly create eddy currents much more complex than is the subject of this thesis.

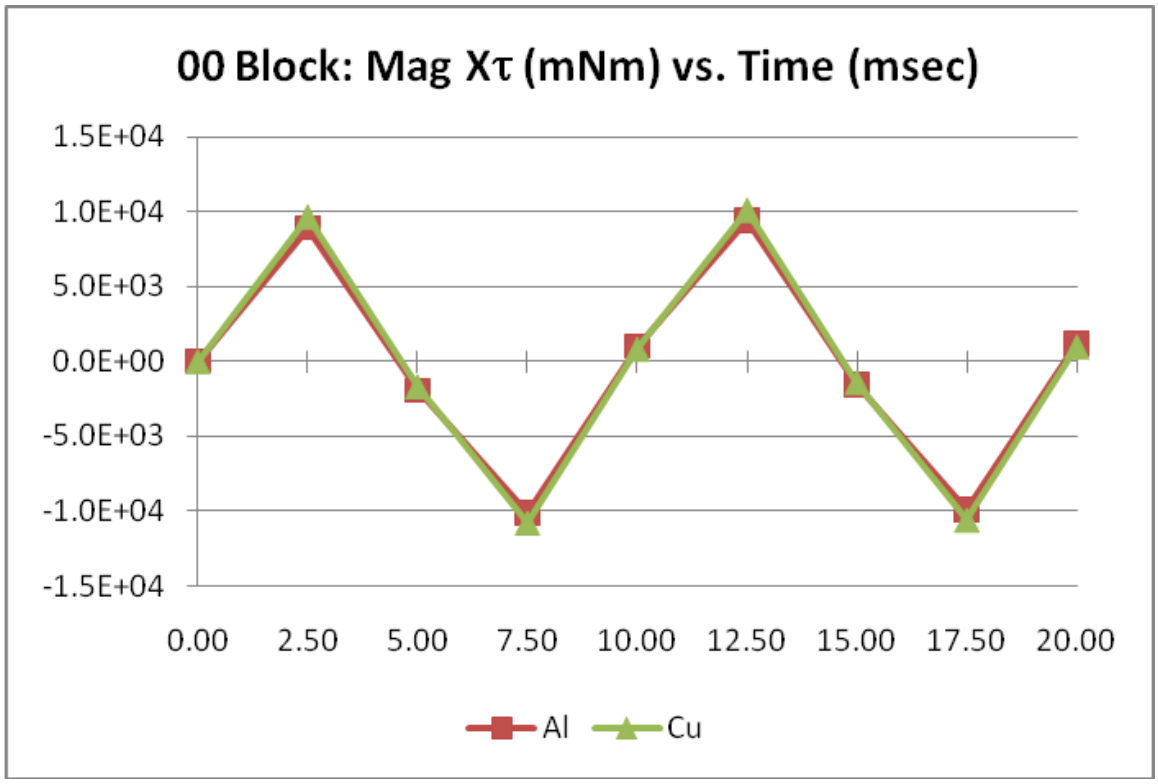

Figure 45. Block – X-Axis Torque vs. Material

The graph in Figure 45 demonstrates that the conductivity of the material still remains of importance, but as the volume of the material increases, the contribution of torque due to additional conductivity decreases as compared to the addition of a multitude of additional conduction paths. (The "00" in the title indicates that the materials are positioned in the 0-degree rotation angle.) In Figure 45, the horizontal axis depicts time measured in milliseconds and torque measured in milli-Newton-meters along the vertical axis. The materials aluminum and copper are compared.

Box Test Volume

The box test volume was modeled in Maxwell 3D as a solid block with a slightly smaller solid block, appropriately positioned, and then subtracted from the larger block. The remaining structure is a box of material with external dimensions of 100 mm on a side and a material thickness of 1mm. The box represents the most prevalent structure found in devices inserted into MRI bores.

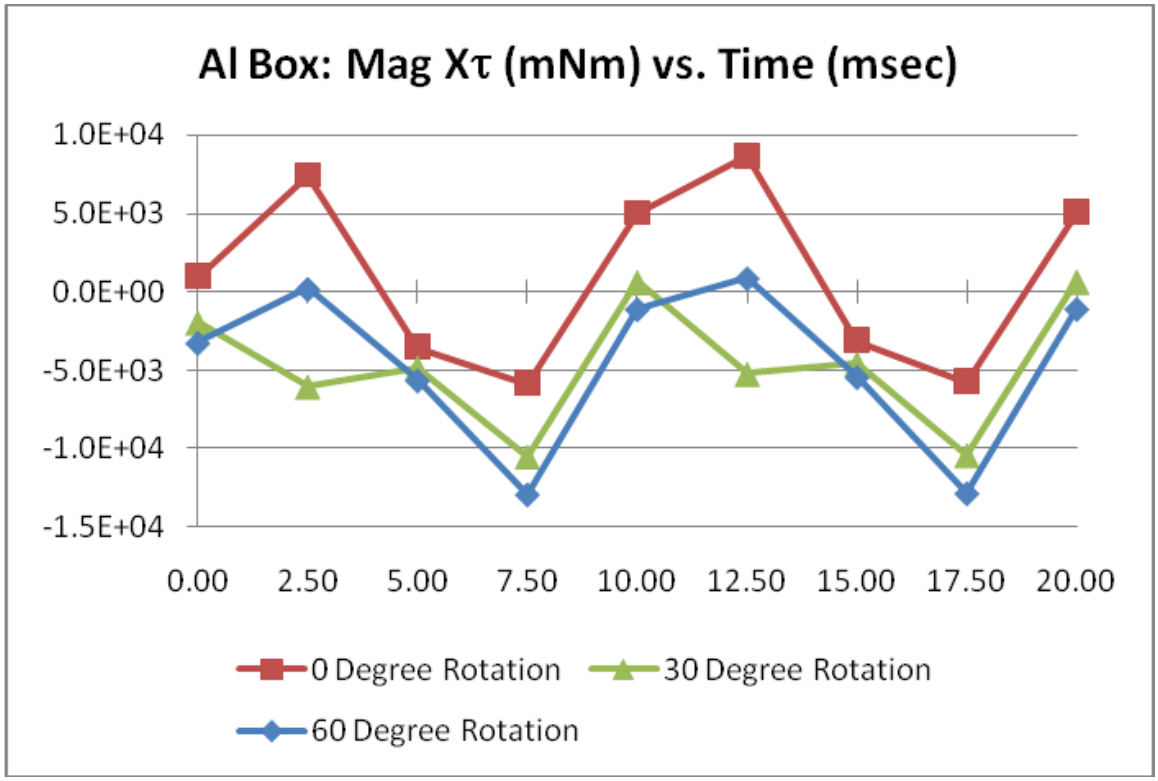

Figure 46. Aluminum Box – X-Axis Torque vs. Time

Based on the graph of Figure 46, it appears that the lack of a central volume disrupts the eddy current paths and is essentially a summation of torques from sheets in orthogonal planes.

This makes the torques on the unit much more complex and variable. At some points the torques are relatively small, at others much larger, contributing to the overall hypothesis that hollow conducting volumes placed in MRI bores experience widely variable vibrations.

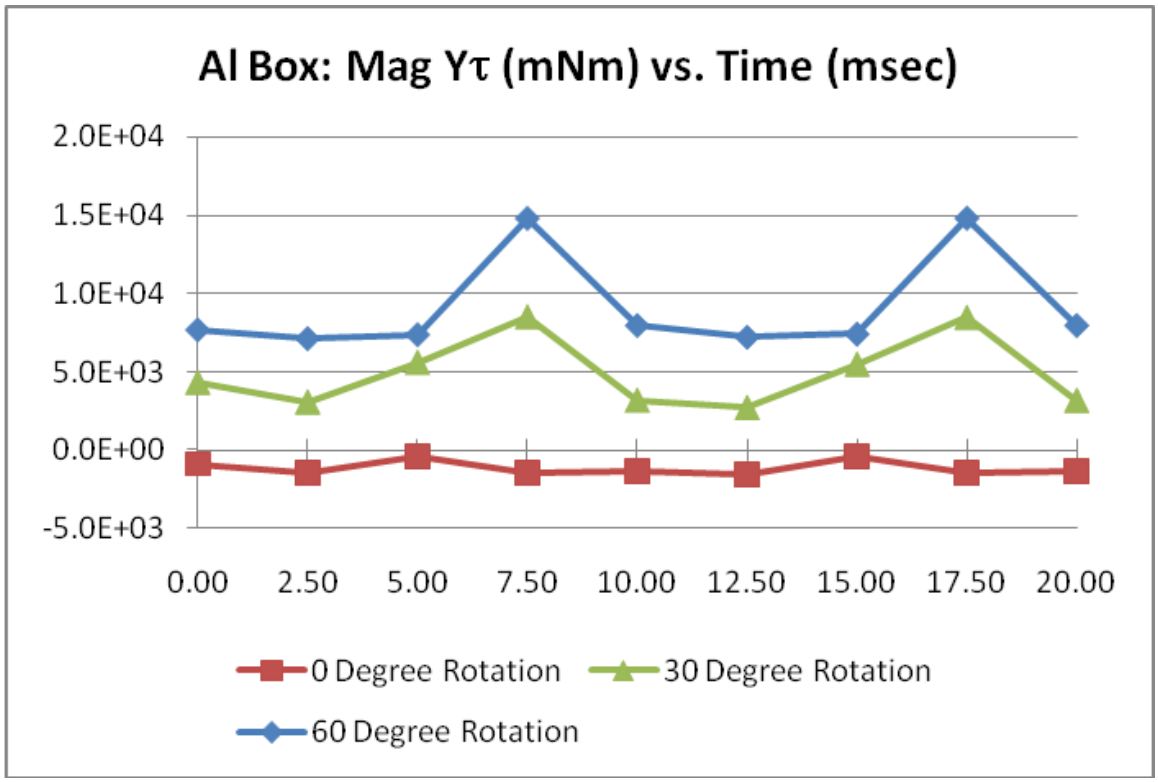

Figure 47. Aluminum Box – Y-Axis Torque vs. Time

Due to the geometry of the bore field and the gradient coil, the y-axis torque is a complex summation of individual torques on sheets in various orientations and has preferred orientation between 30 degrees and 60 degrees to conduct eddy currents that interact with the bore field.

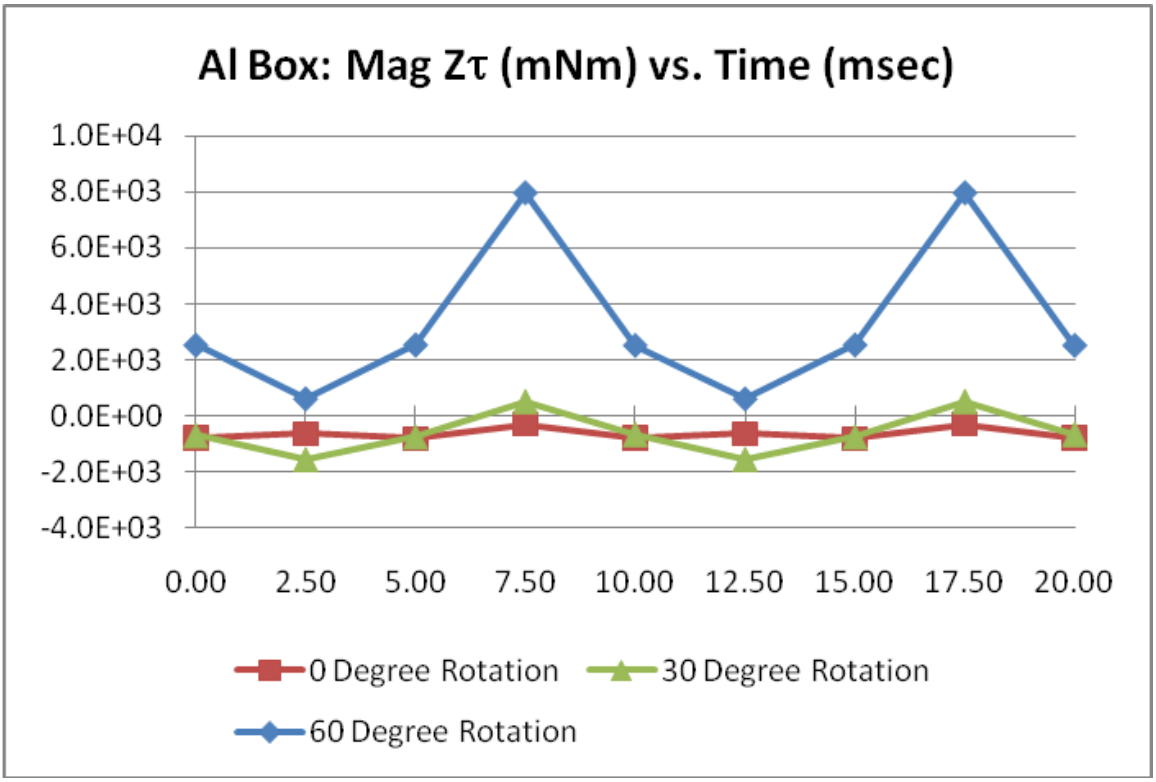

Figure 48. Aluminum Box – Z-Axis Torque vs. Time

Surprisingly, the eddy currents sum in a fashion to create a large z-axis torque as given in Figure 48.

Torus Test Volume

The torus is modeled to determine if any significant eddy current effects can be determined on electrical or mechanical items with circular, torroidal, or cylindrical shapes, such as knobs, indicator bezels, and dials. Hopefully an electronic designer will not be faced with eddy currents established inside a torroidal transformer or coil – it will be shielded or excluded from the equipment placed in the bore.

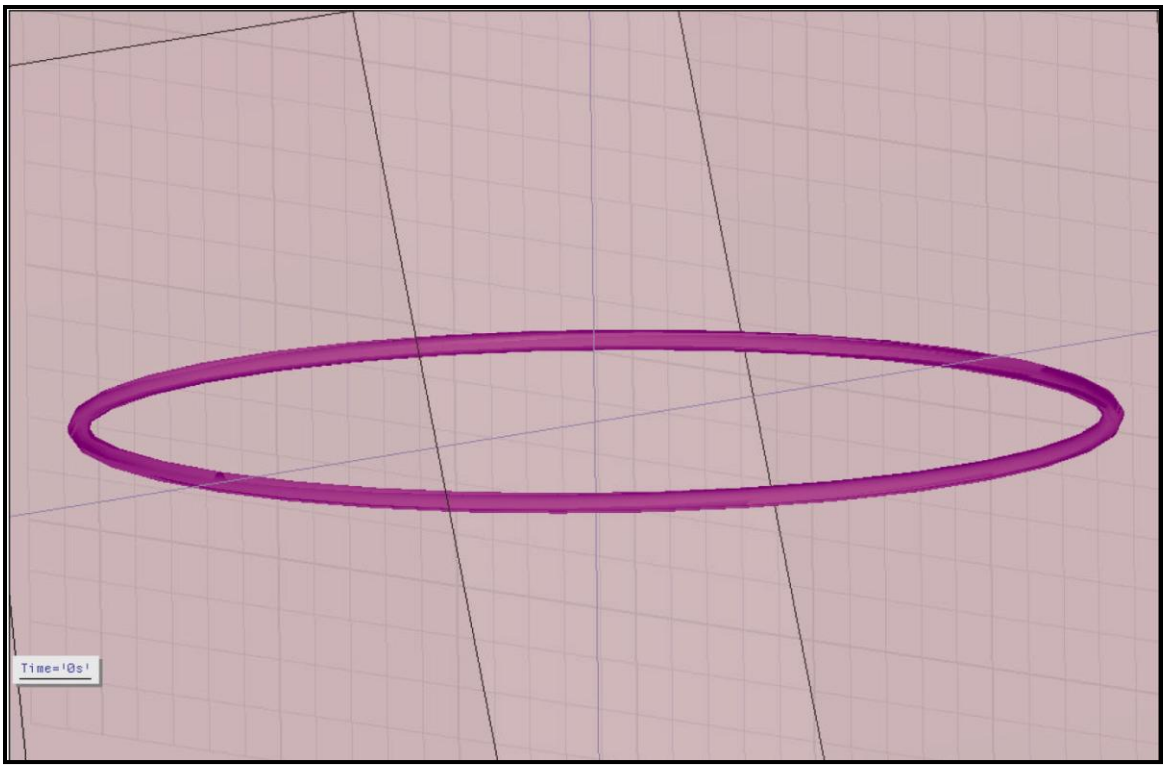

Figure 49. Aluminum Torus

It already has been hypothesized that if eddy currents are reduced, torques will be reduced. It is also surmised that differences in materials produce differences in torque as a function of conductivity, so analysis of the torus is limited to aluminum for material, 100 mm major radius for shape, and the rotational angle about the z-axis. The minor diameter is 1.0 mm.

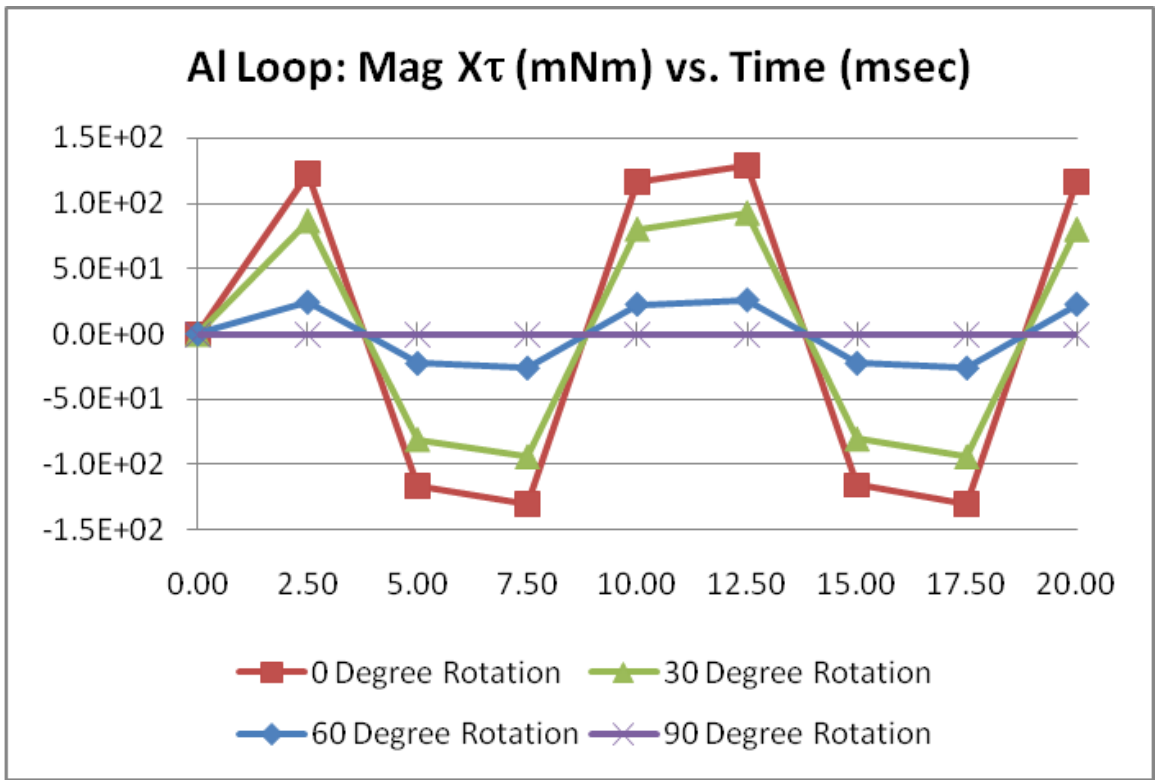

Figure 50. Aluminum Torus – X-Axis Torque vs. Time

Using the right hand rule as established earlier, it is clear that the torus behaves precisely as expected, with a maximum torque when the torus lies completely in the XZ plane and diminishing to zero when the torus is rotated to the YZ plane. In the XZ plane, the torus contains segments that have a maximum cross product between the current and the bore field, producing maximum force on that segment, and thus maximum torque in the x-axis. As the torus is rotated into the YZ plane, the cross products diminish to zero.

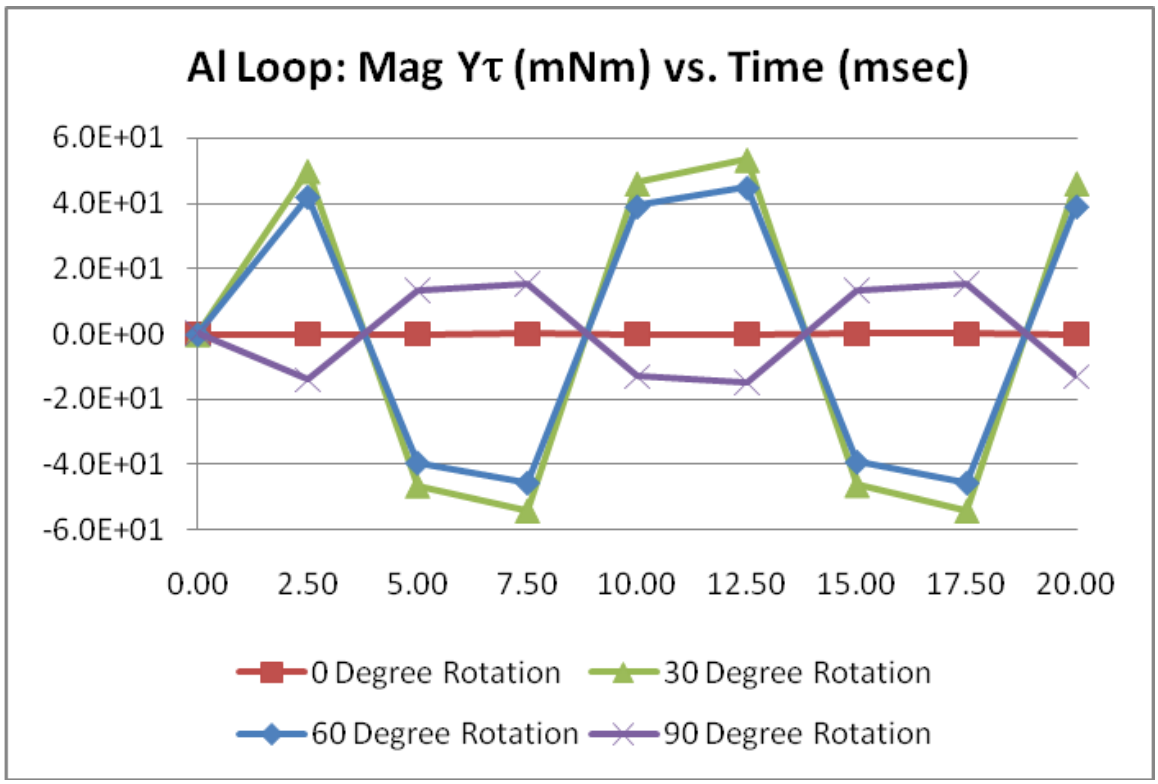

Figure 51. Aluminum Torus – Y-Axis Torque vs. Time

As the torus lies in the XZ plane, the current path is essentially a loop around which eddy currents may flow. All other dimensional characteristics and conductive paths are small in comparison. The graph in Figure 51 demonstrates that no torques in the y-axis exist with any meaning. As the torus is rotated towards the YZ axis, geometries and conduction paths are presented that allow significant cross products producing torque forces in the y-axis. However, as the angle increases to the vertical position, in the YZ plane, the y-axis torques minimize once again. The phase reversal is probably due to the software calculating the torque as 90 degrees belonging to the second quadrant.

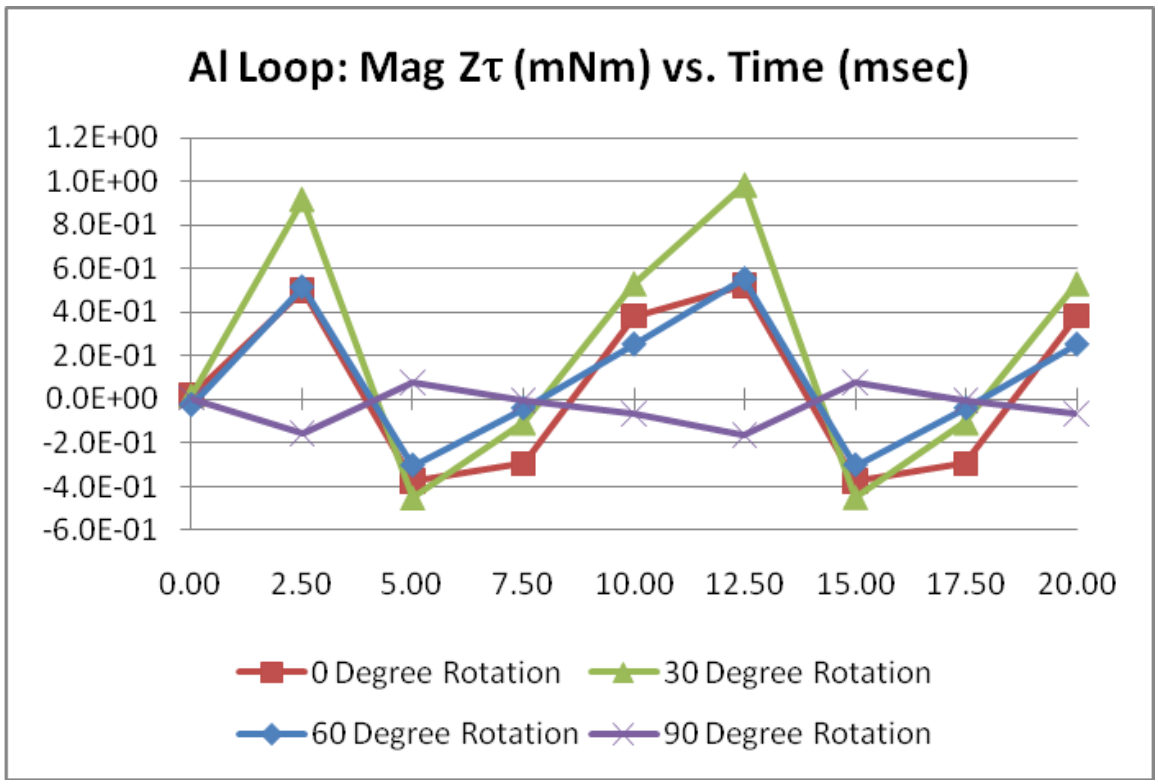

Figure 52. Aluminum Torus – Z-Axis Torque vs. Time

The z-axis torque in Figure 52 is essentially non-existent, with the components shown in the graph of Figure 52 representing imprecision in the calculations of individual tetrahera of the torus mesh.

Sphere Test Volume

A sphere of conducting material is modeled in a similar fashion as the box. A solid sphere of material is modeled and a slightly smaller volume is subtracted. The remaining structure, a conducting spherical shell of material, is then placed in the simulated MRI for analysis.

The sphere is probably the least likely structure to be found in typical equipment placed in MRI bores, but is modeled here as a reference geometry to gain insight into the reaction of this conducting geometry with the magnetic field. Since the symmetry of the sphere precludes differences in rotational orientation, the radius of the sphere is altered to extract any significant data.

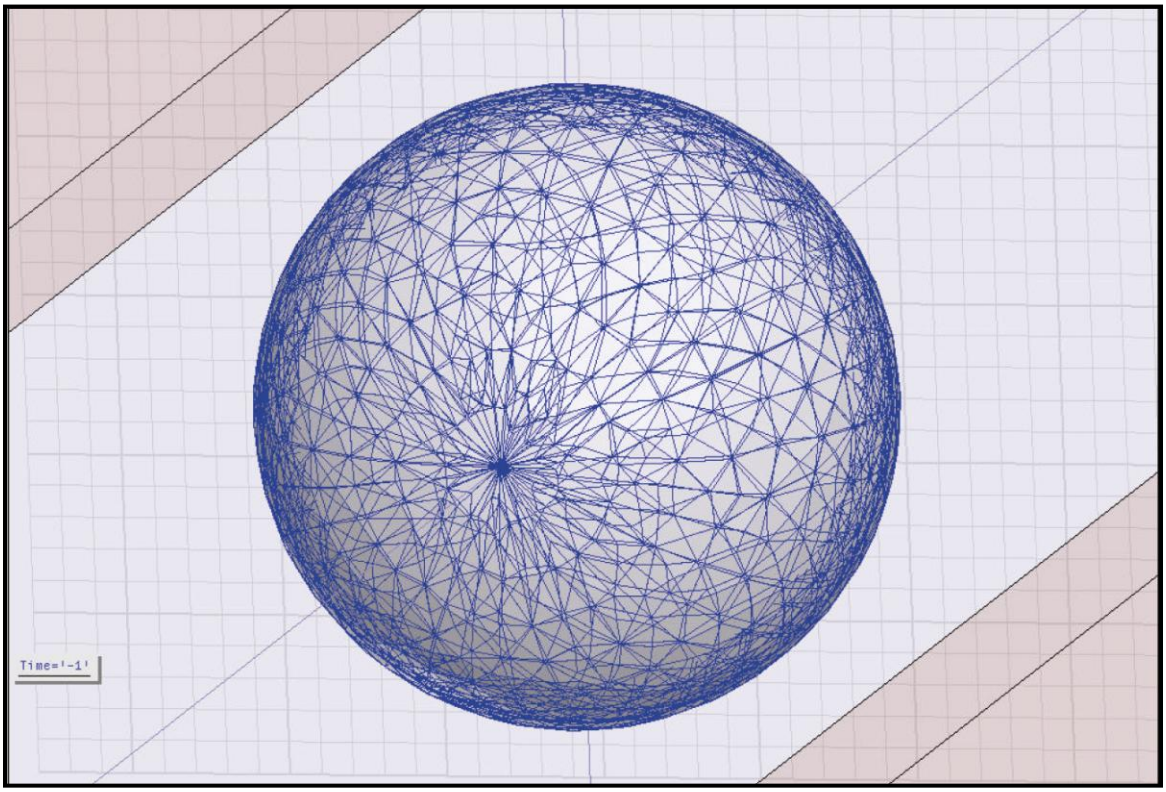

Figure 53. Aluminum Sphere – 50 mm Radius

The sphere shown in Figure 53 depicts the model of the 50 mm radius sphere with the mesh plotted. The internal radius of 49 mm leaves a material thickness of 1 mm and the mesh thus subdivides the material into several thousand tetrahedral elements from which the finite element analysis is performed.

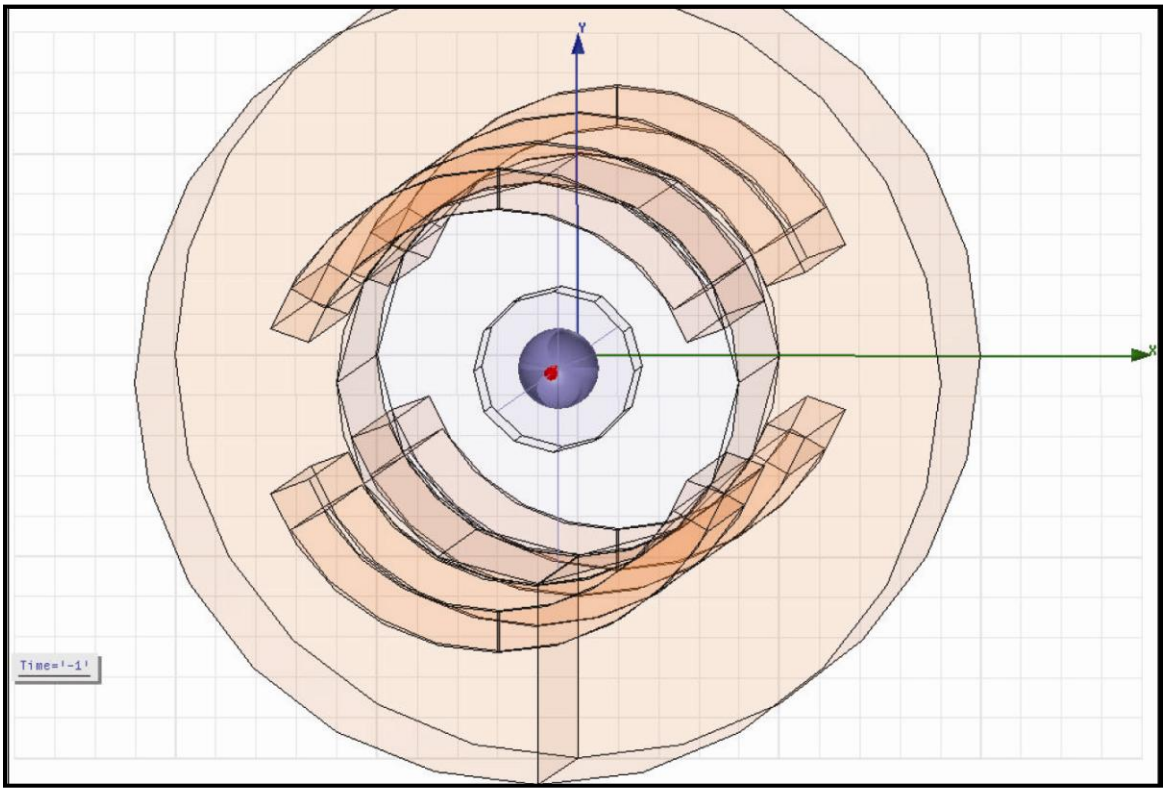

Figure 54. Aluminum Sphere – 200mm Radius

Figure 54 shows the 200 mm sphere at the isocenter of the simulated MRI bore. The 12-sided cylinder of the bore dummy mesh as well as an additional dummy mesh just outside the 200 mm volume of interest, are clearly shown.

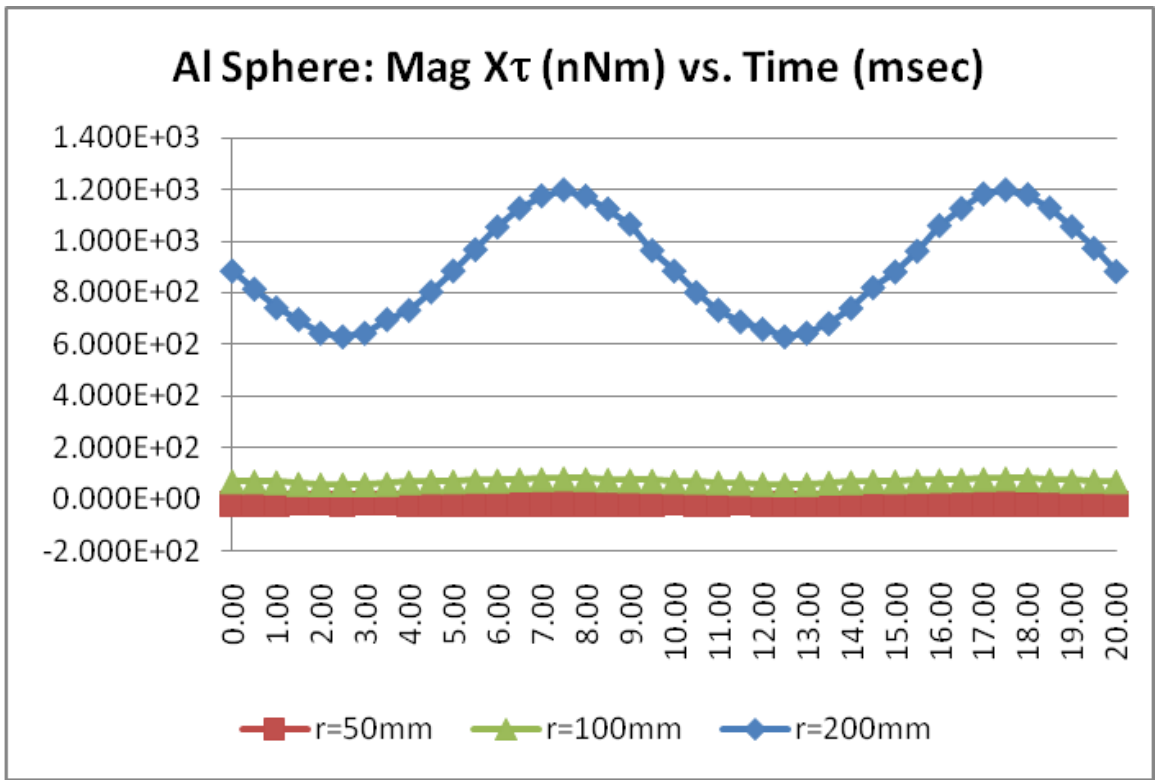

Figure 55. Aluminum Sphere – X-Axis Torque vs. Time

Based on the graph it is probably correct to assume that a sphere must attain a certain minimum size, probably dependent on the magnitude of the field, in order to sustain eddy currents capable of interacting with the bore field. In the graph of Figure 55, the 50 mm and 100 mm spheres show no significant torque while the 200 mm sphere indicates only about 1.2 mNm or torque, significantly less than previous test volumes. Although the sphere has little usefulness as an object within the MRI bore, its configuration contributes the least to torque.

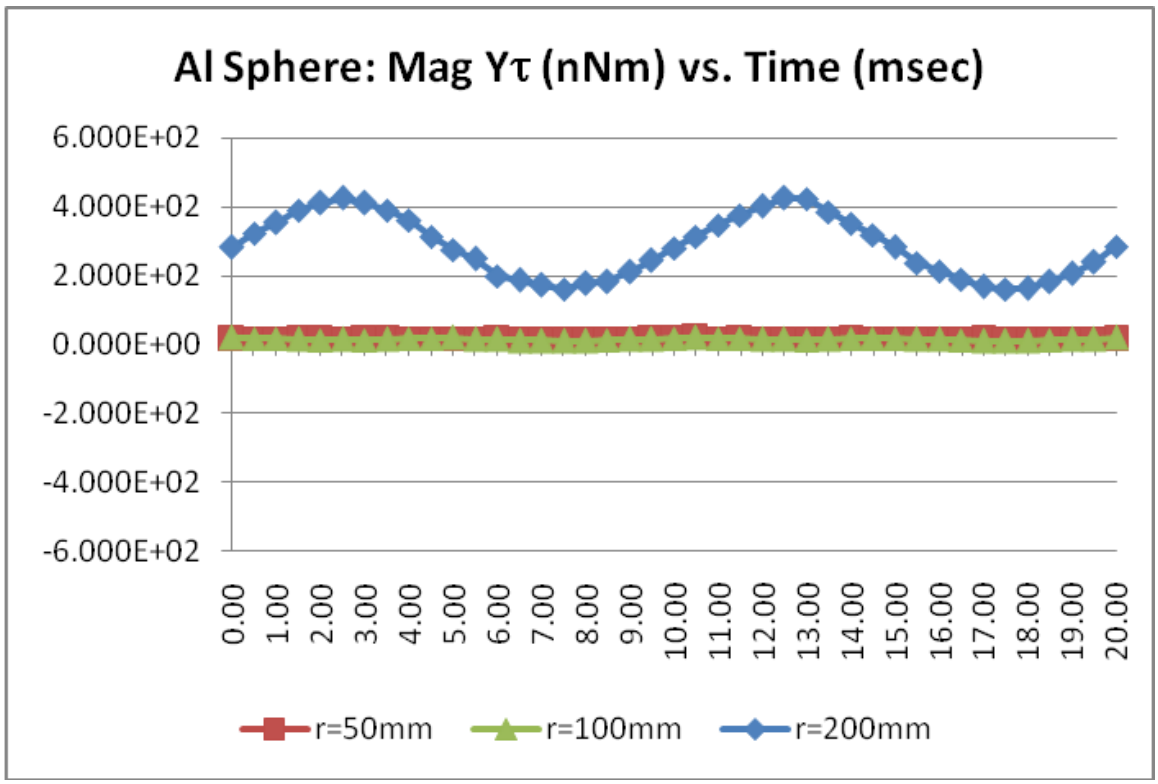

Figure 56. Aluminum Sphere – Y-Axis Torque vs. Time

The y-axis torque shown in Figure 56 for the 200 mm sphere is approximately 3 times smaller than the x-axis torque, indicating that the eddy currents primarily circulate in the XZ planes of the sphere. The eddy currents, however, produce approximately equal torque in the negative z-axis (Figure 57), also supporting the current flow in the XZ plane, and indicating a counter-clockwise rotation as viewed from the positive y-axis (looking along the negative y-axis).

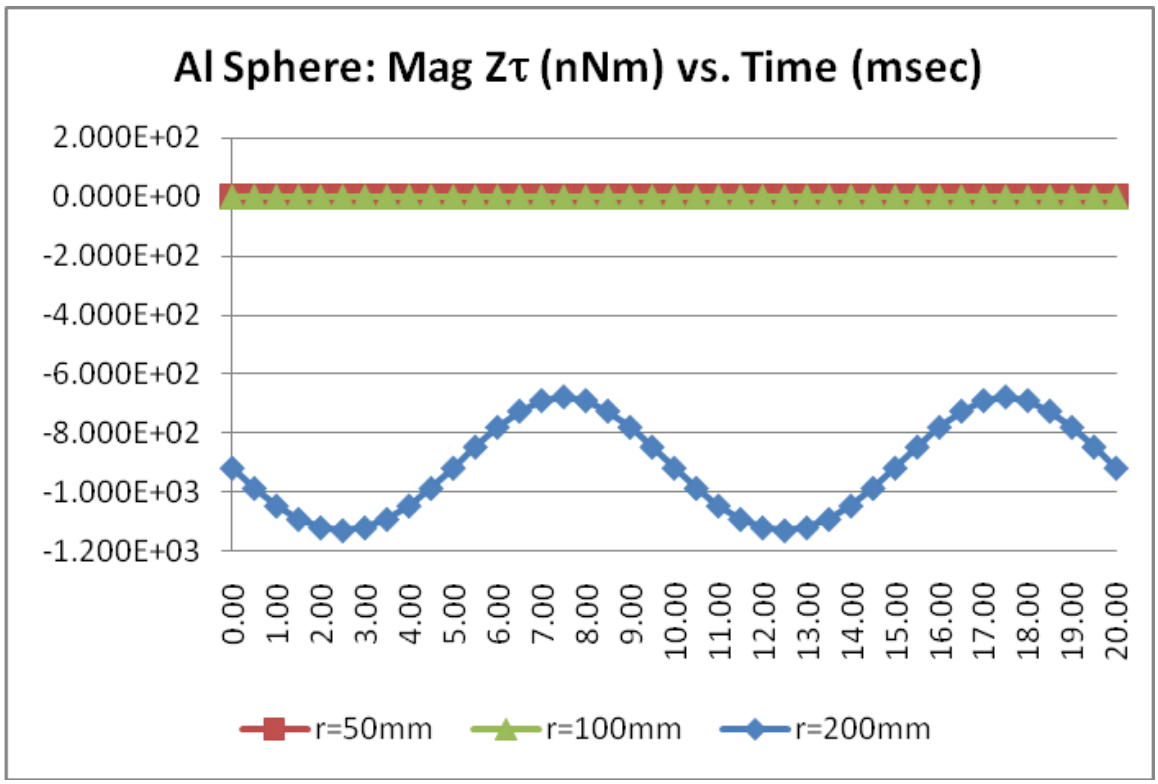

Figure 57. Aluminum Sphere – Z-Axis Torque vs. Time

As a check to verify the torques are produced by the interaction of the gradient coil induced eddy current and the static bore field, and to determine the extent of the contribution of torque from the gradient field itself, the bore field was turned off and the simulation run again. As shown in the graph of Figure 58, the torque on the 200 mm sphere was plotted as a function of time. The x-axis torque is approximately 27 times less than that produced by the interaction of the bore field and the gradient coil induced eddy current. It is interesting to note that the interaction of the sphere and the gradient coil self induced eddy current tend to create a second harmonic, thus validating the slightly distorted graphs of previous test volumes.

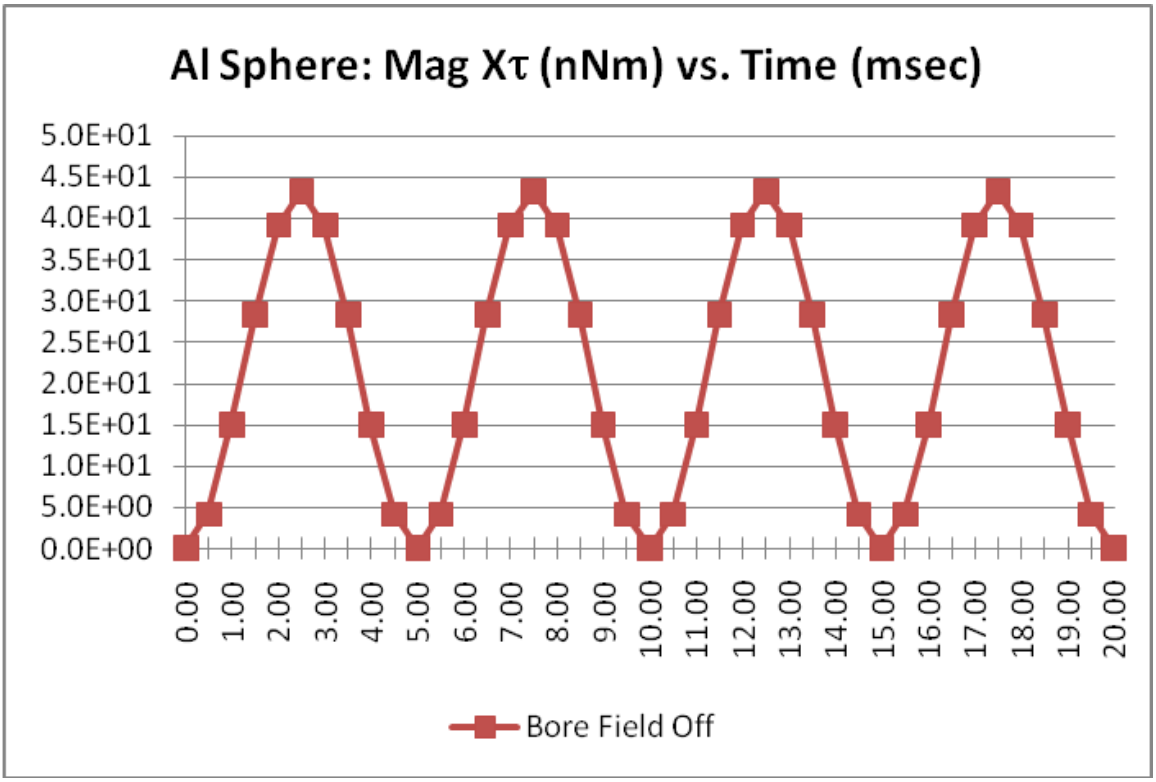

Figure 58. Aluminum Sphere – X-Axis Torque vs. Time

Twin Loop Test Volume

The Twin Loop represents a slightly more complex shape that may be found in electronic or mechanical devices placed in an MRI bore, such as the bobbin of a standard transformer, mounting hardware used to attach larger items (screws used to attach a mechanical fixture), or a mechanical fastener used to hold a patient's sample line or cable.

The Twin Loop in this experiment was devices primarily to determine if it was reasonably possible to determine or predict a specific path for current flow.

As oriented in the XZ plane (zero degrees angular rotation), the Twin Loop presents two major conducting circuits for eddy currents. Using the right hand rule, each of the two loops will conduct current in a counter-clockwise direction as viewed from above (looking in the same

direction as the negative y-axis). This will cause current in the central section of the loop to contain current paths that, if summed together, cancel each other out.

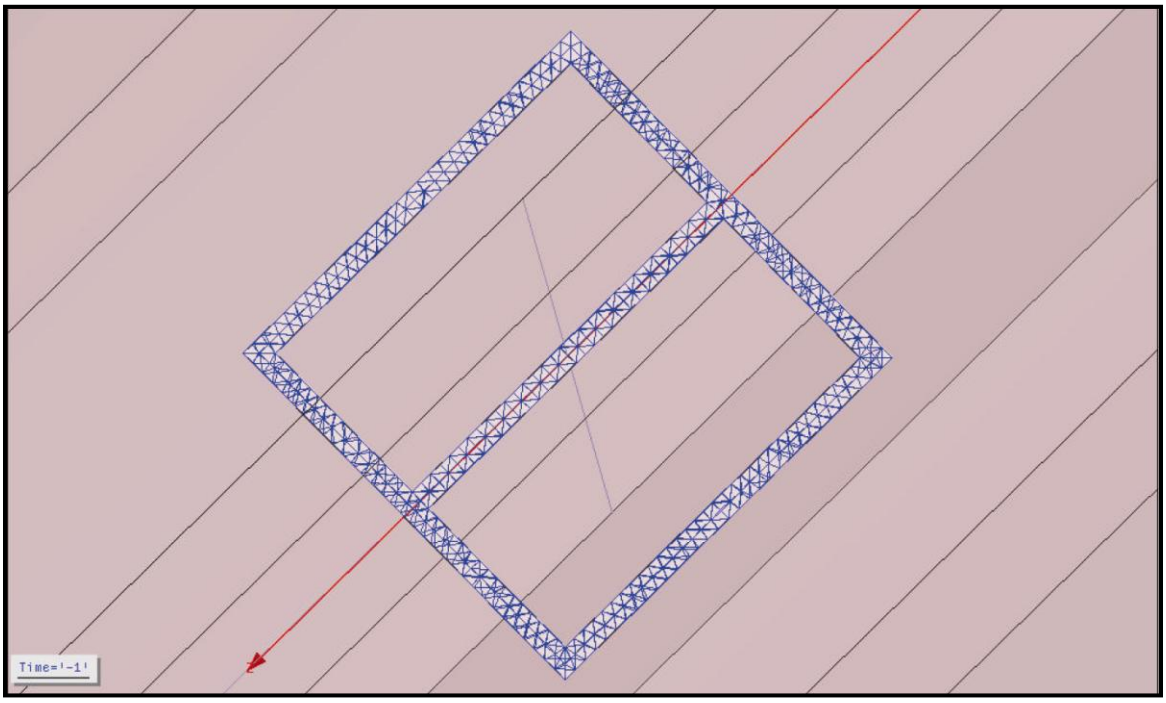

Figure 59. Twin Loop

Figure 59 shows a top view (looking in the direction of the negative y-axis) of the Twin Loop. The arrow running down the center of the central leg of the Twin Loop is the positive z-axis. The element mesh is overlaid on the graphic indicating each of the several thousand tetrahedral comprising the Twin Loop.

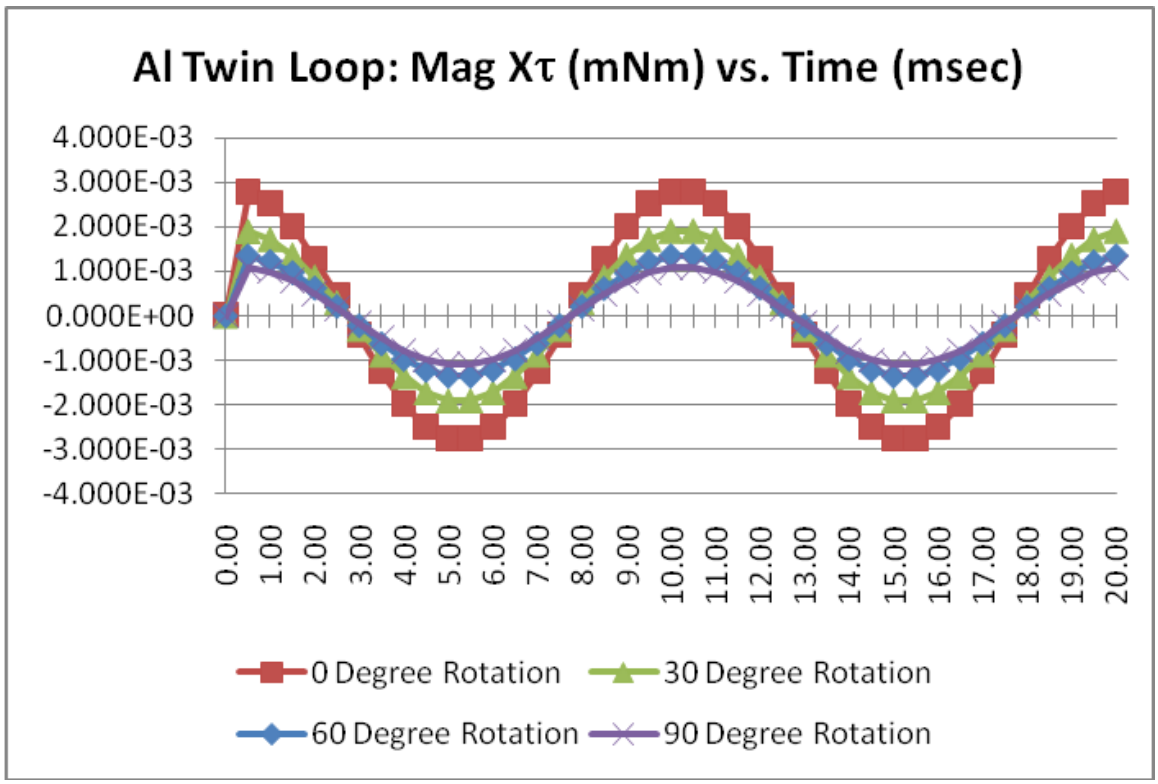

Figure 60. Aluminum Twin Loop – X-Axis Torque vs. Time

The graph of Figure 60 shows the torque on the Twin Loop along the x-axis of the simulated MRI system. The horizontal axis of the graph indicates time in milliseconds and the vertical axis indicates torque in milli-Newton-meters. With the premise that when laid along the XZ plane, the current in the central section of the material will essentially cancel also predicts that the torque also cancels. The graph indicates that this is true. However, as the simulation changes from zero to 1.0 milliseconds, the torque jumps dramatically to a near-maximum value. (The simulation at t = 0 has no previous model upon which to base its calculations, thus jumping from zero to maximum. The difference between 10 milliseconds and 11 milliseconds more accurately reflects the change in eddy current and torque calculations.)

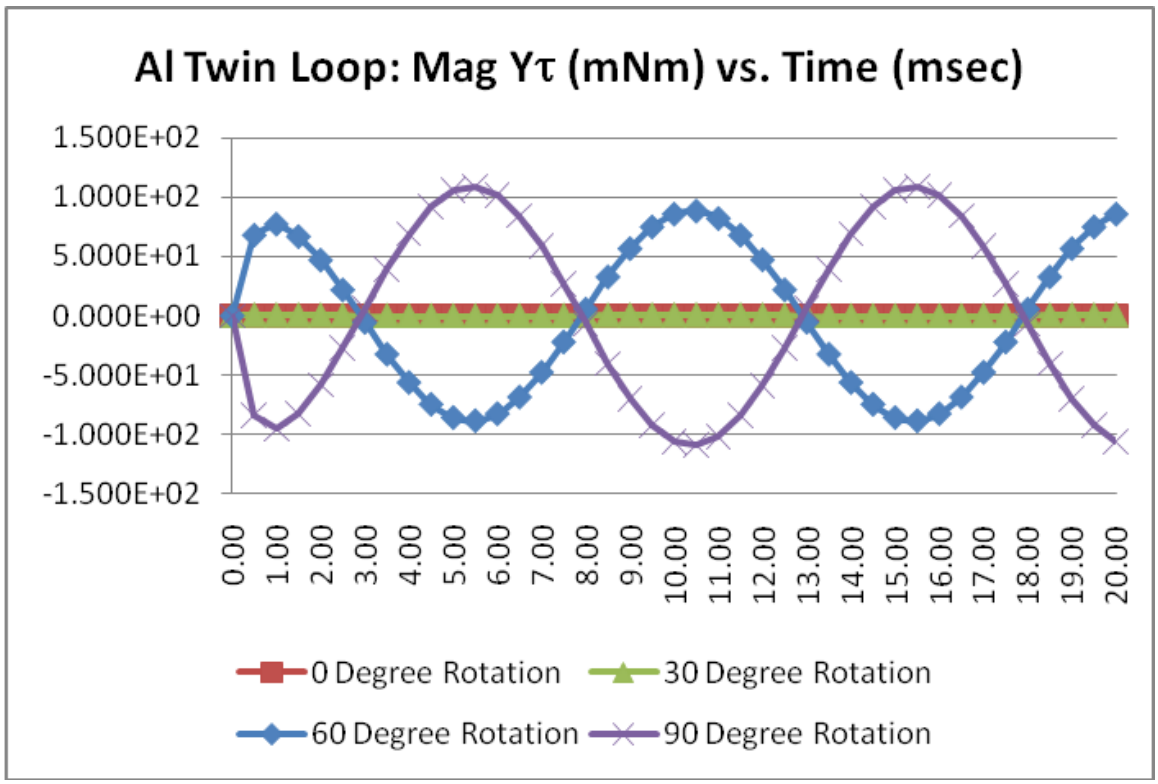

Figure 61. Aluminum Twin Loop – Y-Axis Torque vs. Time

The graph of Figure 61 represents the torque along the y-axis for various rotational angles of the Twin Loop as a function of time. The horizontal axis indicates time in milliseconds and the vertical axis indicates torque in milli-Newton-meters. The torques at zero and 30 degrees of angular rotation show little y-axis torque whereas the 60 and 90 degree rotations show significantly larger torque values.

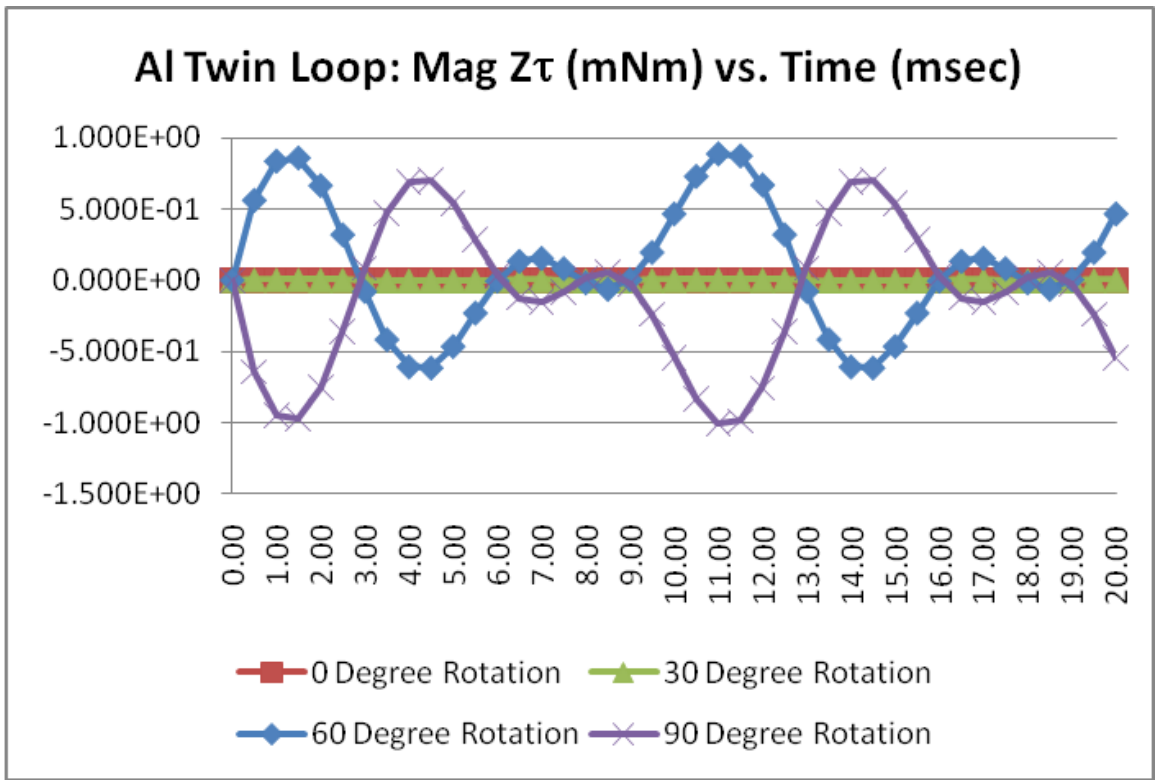

Figure 62. Aluminum Twin Loop – Z-Axis Torque vs. Time

Figure 62 shows a plot of the z-axis torque for various rotational angles of the Twin Loop as a function of time. The horizontal axis indicates time in milliseconds and the vertical axis indicates torque in milli-Newton-meters. The z-axis torque is hundreds to thousands of times smaller than the other two axes, but shows the complex interaction of the eddy currents in the small dimensions of the Twin Loop. This plot shows that many times the eddy current adds, subtracts, and reverses itself within the structure.

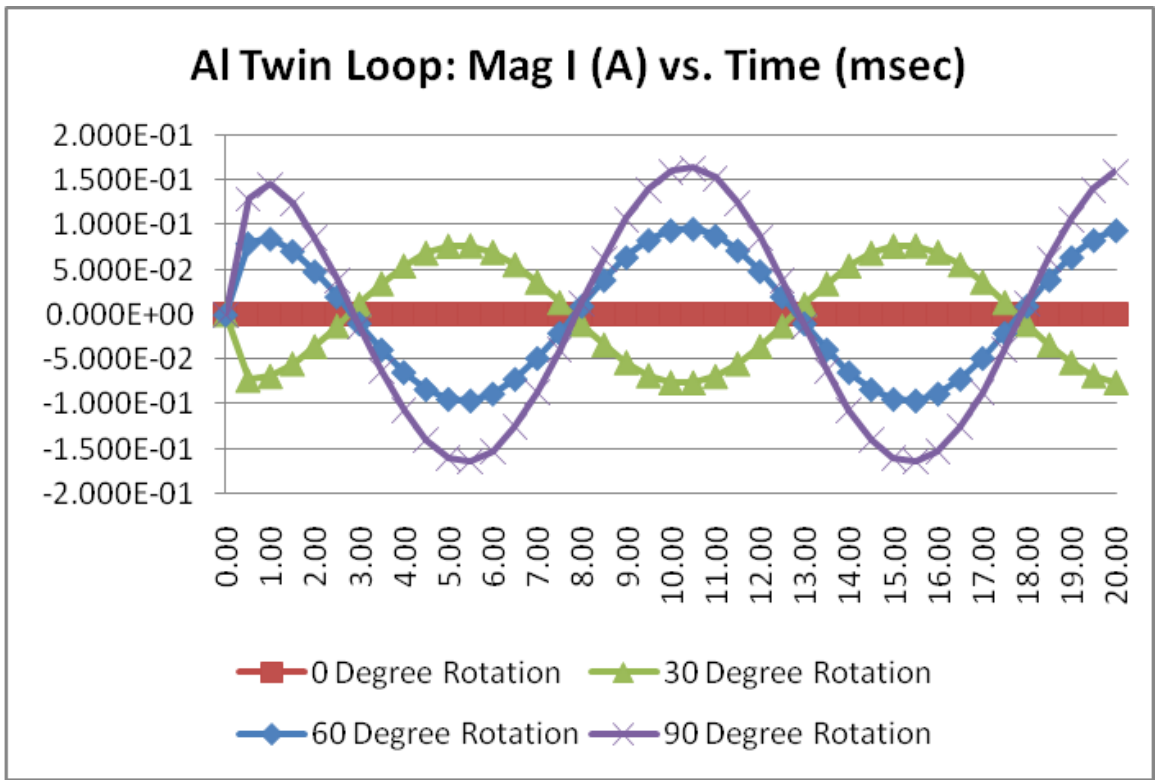

Figure 63. Aluminum Twin Loop – Current vs. Time

A plot of the current as a function of time, for the various angular rotations of the Twin loop is shown in Figure 63. Time is indicated for the horizontal axis in milliseconds and the vertical axis indicates current in amps. Maximum current flow through the central section of the Twin Loop is indicated for the 90 degree rotational orientation with approximately 160 milliamps at peak excitation.

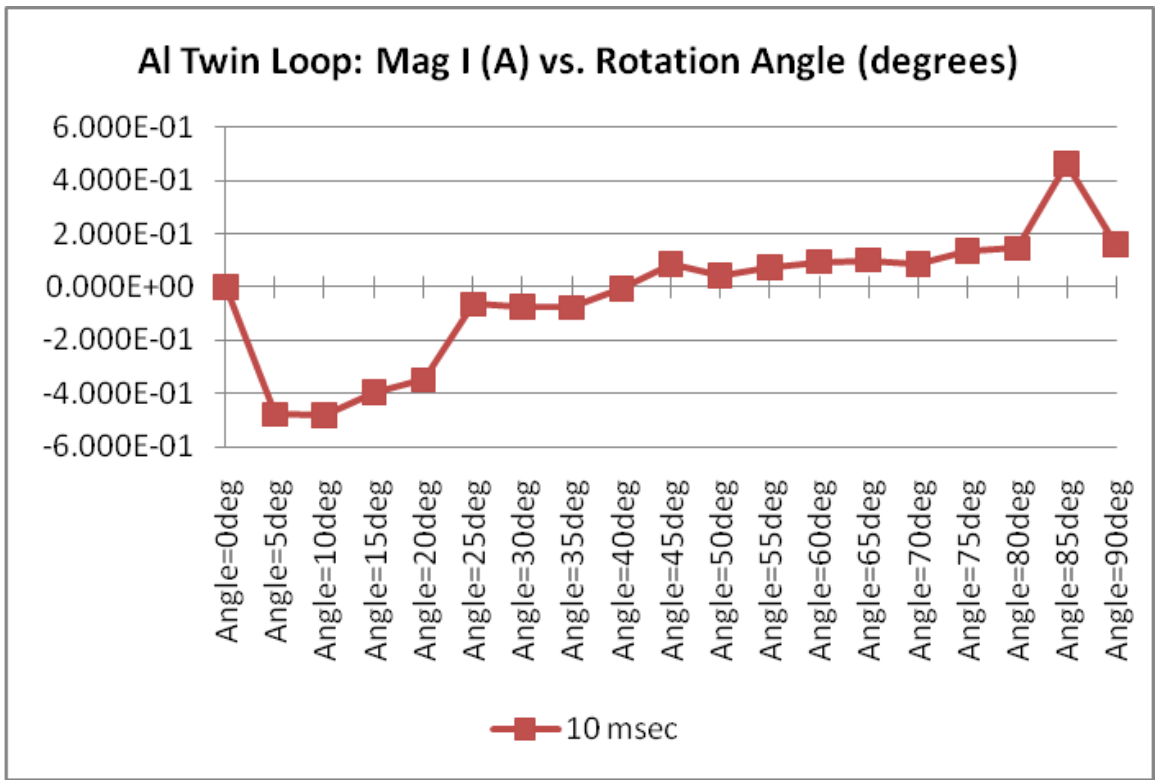

Figure 64. Aluminum Twin Loop – Current vs. Rotation Angle

One goal established prior to simulation was to determine if there was a point at which current flow could be stopped in a conducting path and what the conditions were to prevent this current flow.

In the simulation, a section was created in the exact center of the central leg of the Twin Loop. The section was required in order to establish an element to which an equation could be applied that will calculate the current through that section. The equation is:

$$I = \int_s \mathbf{J} \cdot \mathbf{n}\, ds \qquad (23)$$

This equation is the surface integral (of the section) of the dot product of the current vector through the section and the vector normal to the section. In essence, this equation sums up all the contributing currents through each mathematical element crossing the surface, whether in one direction or the other, which are normal to the section. This equation is created in Maxwell 3D using the field calculator and is described in the addendum.

As shown in the graph of Figure 64, the maximum current is shown as a function of angular rotation and demonstrates that the current flow in the central leg of the Twin Loop stops when the Twin Loop is rotated to approximately 40 degrees. Not surprisingly, eddy currents are highly dependent on physical orientation with relation to the inducing field.

CHAPTER EIGHT: EDDY CURRENT REDUCTION TECHNIQUES

Round Holes Technique

From a manufacturing point of view, a perforated sheet is relatively easy to manufacture. A solid sheet of material is passed through a punch and die set that perforates the sheet, one hole at a time, one row at a time, or several rows at a time, eventually filling the sheet with holes. Thus, the availability of materials with round perforations allows electronic or mechanical devices and other structures to be easily fabricated for use in MRI systems.

The perforated sheet modeled here consists of a 100 mm x 1 mm x 100 mm aluminum sheet with twenty five 5 mm radius holes placed uniformly across the surface. Figure 65 shows a top down view of the aluminum sheet.

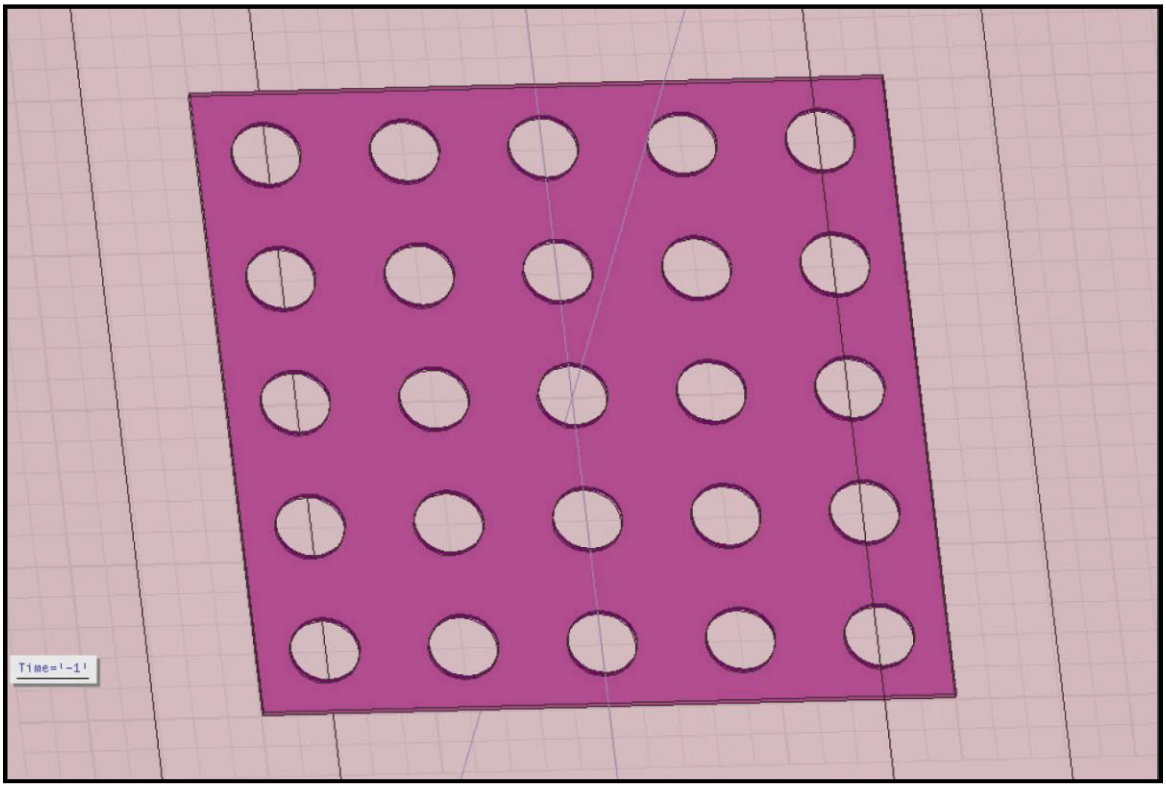

Figure 65. Aluminum Sheet – Round Perforations

The graph of Figure 66 shows the x-axis torque on the sheet as a function of time for various angular rotations about the z-axis. Time is indicated along the horizontal axis in milliseconds and torque in milli-Newton-meters is indicated for the vertical axis.

As with the solid sheet, the magnitudes of the x-axis torques (Figure 66) at 0-degrees of angular rotation are maximum and decrease as the rotation angle increases towards 90 degrees. However, unlike the solid sheet, a preferred orientation appears, in this case at 30 degrees, most likely due to a conduction path that is more efficient in this orientation.

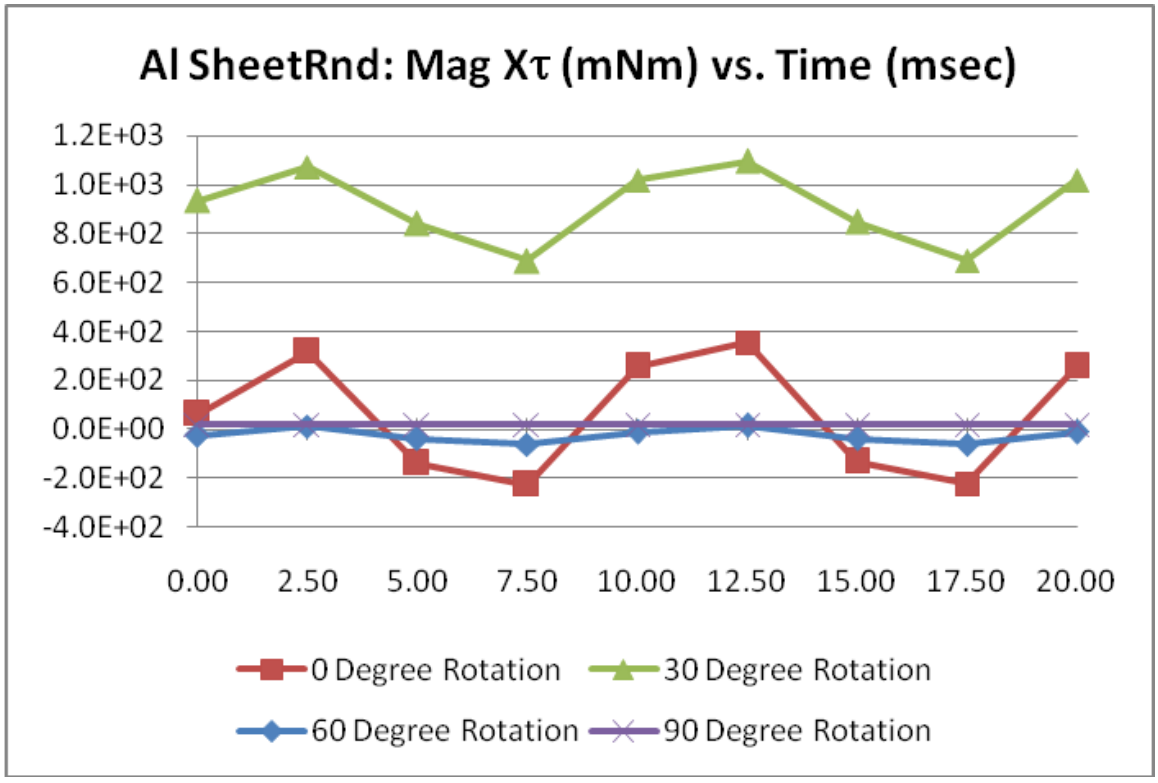

Figure 66. Round Perforated Aluminum Sheet – X-Axis Torque vs. Time

The y-axis torque also shows a preferred orientation, but with opposing direction. In the graph of Figure 67, the horizontal axis indicates time in milliseconds with the vertical axis indicating torque in the y-axis direction in milli-Newton-meters. For the 60 and 90 degree orientation, the y-axis torque is almost non-existent. A positive y-axis torque exists at 0 degree rotation while the 30 degree rotation exhibits maximum torque among these orientations.

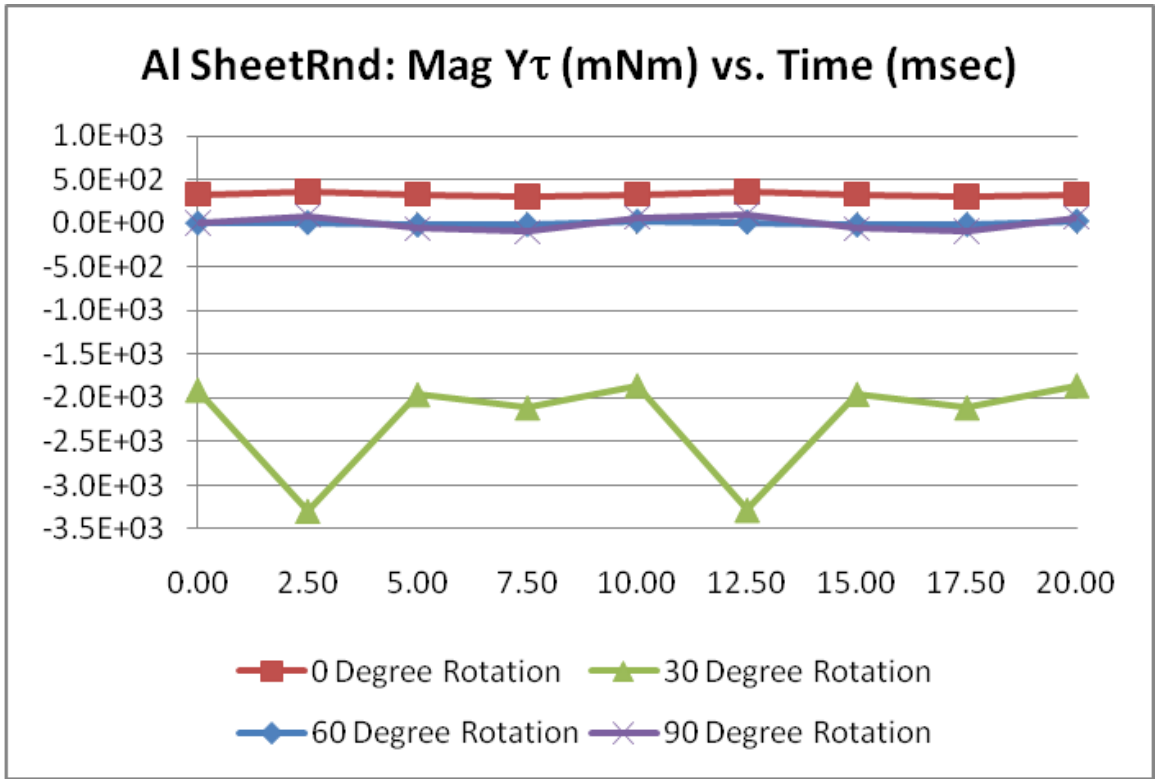

Figure 67. Round Perforated Aluminum Sheet – Y-Axis Torque vs. Time

The z-axis torque also exhibits a preferred orientation, but with much less force, approximately one-tenth that of the y-axis. In this case all but the special 30-degree orinetation exhibits practially no torque. In the plot of Figure 68, the horizontal axis represents time in milliseconds with the z-axis torque in milli-Newton-meters indicated along the vertical axis.

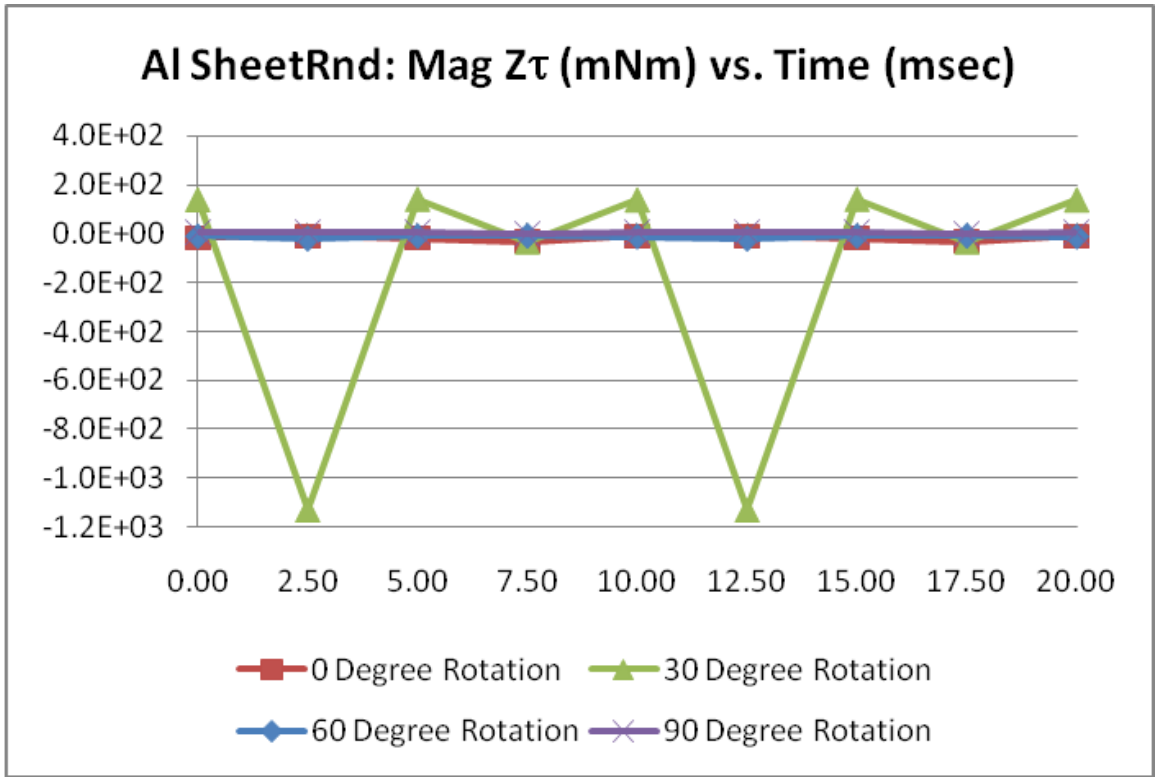

Figure 68. Round Perforated Aluminum Sheet – Z-Axis Torque vs. Time

Square Holes Technique

Square hole perforations are also readily available in prefabricated sheets although the manufacturing process is slightly more troublesome. The punch and dies sets for square holes tend to dull quicker than round holes, especially at the corners, making share hole perforated material slightly more expensive to purchase.

The perforated sheet modeled here consists of a 100 mm x 1 mm x 100 mm aluminum sheet with twenty five 10 mm square holes, placed uniformly across the surface. Figure 69 shows a graphic of the sheet with square holes as seen looking in the same direction as the negative y-axis. In this graphic the positive z-axis is pointing down.

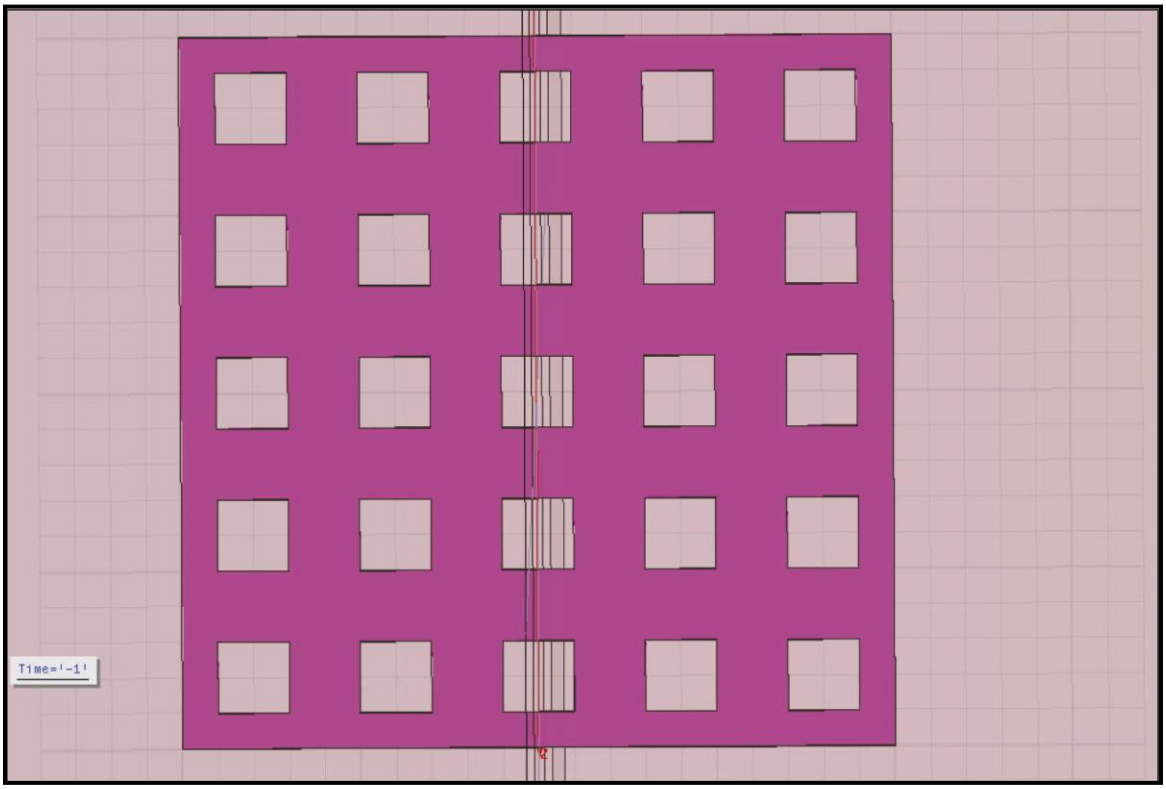

Figure 69. Aluminum Sheet – Square Perforations

In the case of the sheet with square holes, the disruption pattern seems to have a better behavior pattern than the sheet with round holes. It is hypothesized that the square holes disrupt the eddy current flow in such a manner as compared to the sheet with round holes, that a special preferred orientation is not established.

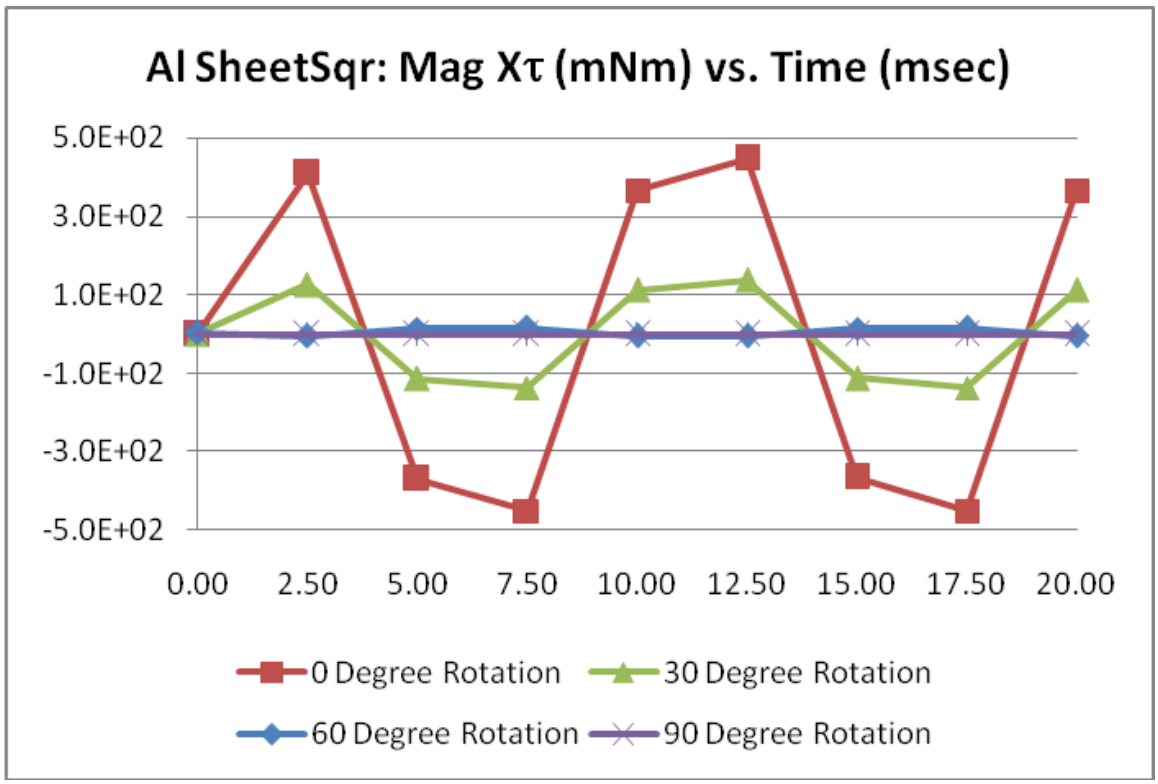

Figure 70. Square Perforated Aluminum Sheet – X-Axis Torque vs. Time

The graph in Figure 70 shows the x-axis torque for each of the four angular orientations of the aluminum sheet with square holes. The horizontal axis indicates time in milliseconds and the vertical axis indicates x-axis torque in milli-Newton-meters. For the zero degree orinetation the x-axis torque is maximum, indicating that the circulating paths around each hole, and perhaps groups of holes, contirbute to the overall torque of the sheet. As the sheet is rotated, however, the circulating paths quickly are distrupted leaving only the small dimensions of the sheet for eddy current circulation.

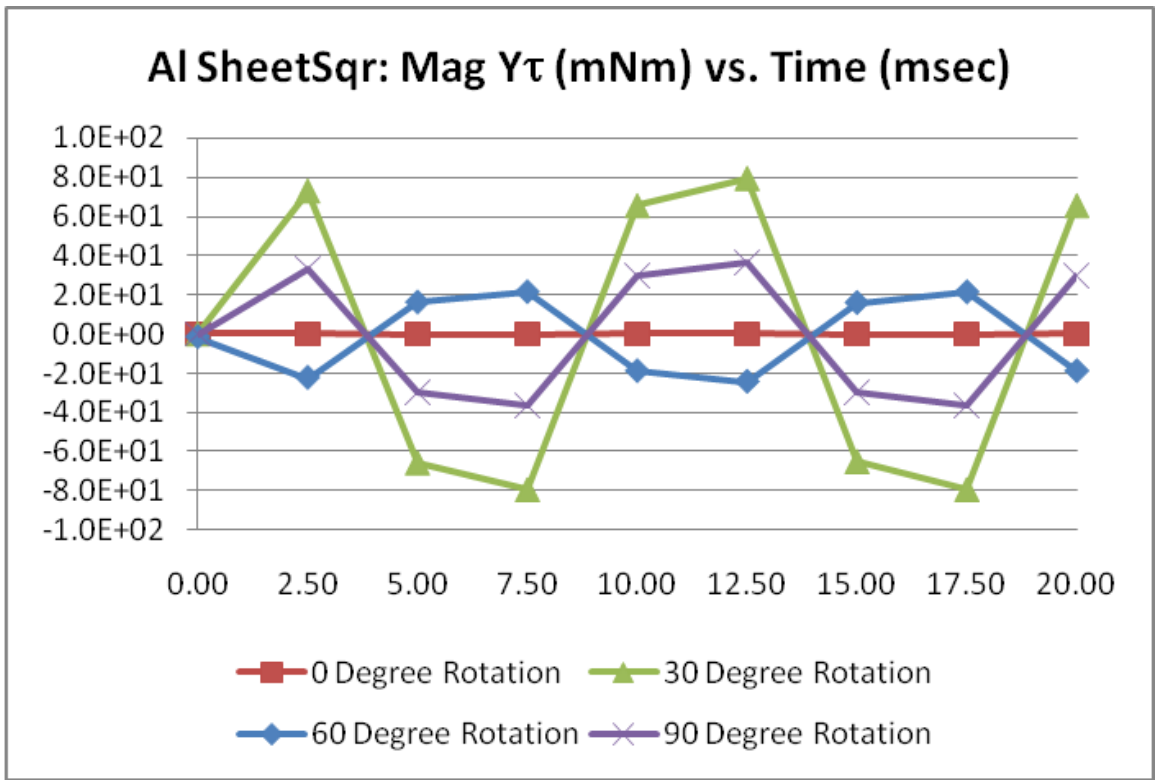

Figure 71. Round Perforated Aluminum Sheet – Y-Axis Torque vs. Time

The y-axis torque exhibits a slightly different pattern as shown in Figure 71. Almost no torque in the positive y-axis is exhibited at zero degrees orientation. As the sheet is rotated the torque peaks and diminishes to a point where eddy currents remain to produce y-axis torque in the 90 degree orientation. Phase shifitng is an artifact of the second quadrant.

The z-axis torque is essentially non-existent, but definitely has a preferred orinetation – zero degrees. The graph of Figure 72 shows the torque in the z-axis. The horizontal axis of the graph indicates time in milliseconds and the vertical axis indicates torque in the positive z-axis in milli-Newton-meters. The overall magnitude is approximately one hundred times smaller than the y-axis and perhaps 50 times smaller than the x-axis.

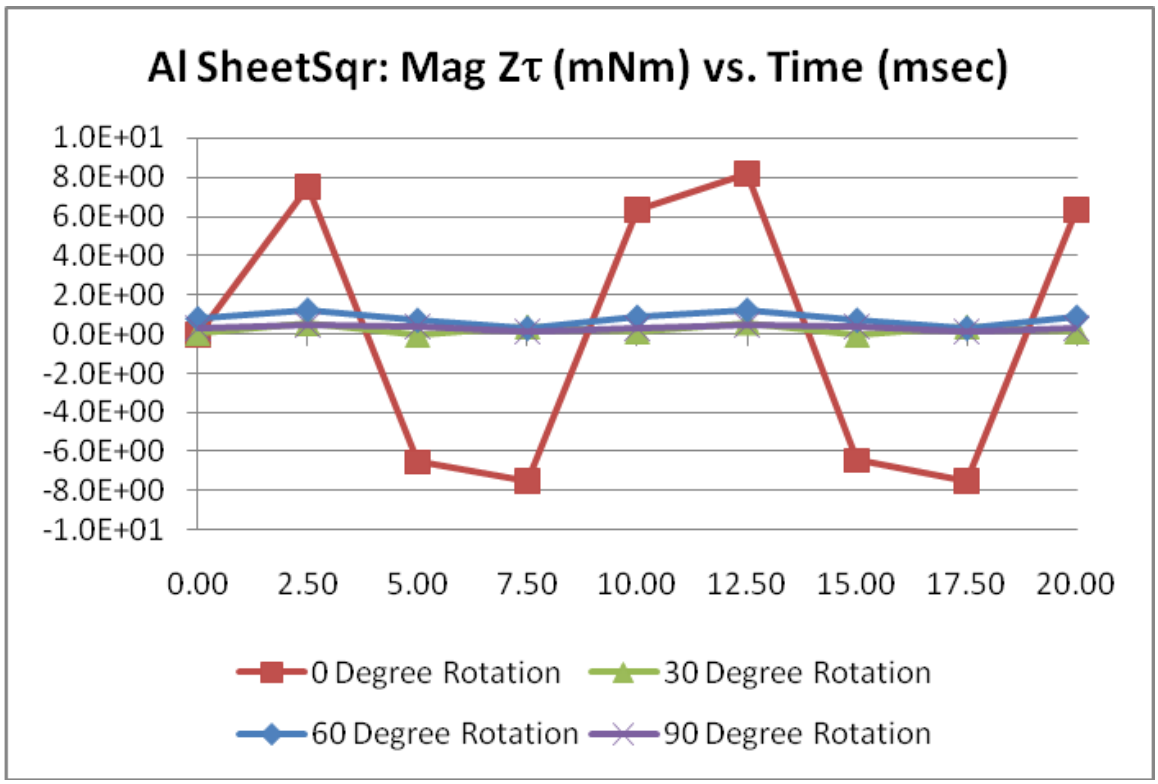

Figure 72. Round Perforated Aluminum Sheet – Z-Axis Torque vs. Time

Other Techniques

It is natural to assume that eddy currents formed in a conducting sheet will, at least in the ideal sense, circulate around the entire sheet. Therefore, any disruption in that circulation will distort the current path and make it less able to interact with an external magnetic field. Furthermore, the disruption may increase the current path and reduce the magnitude of the eddy current, further reducing its ability to interact with an external magnetic field.

Configuration 1

Assuming that the ideal eddy current conduction path utilizes the entire conducting volume of a conducting sheet, a disruption consisting of a single perforation should reduce the

eddy current by increasing the path length, changing the conduction path, and thus reduce the torque experienced on the sheet.

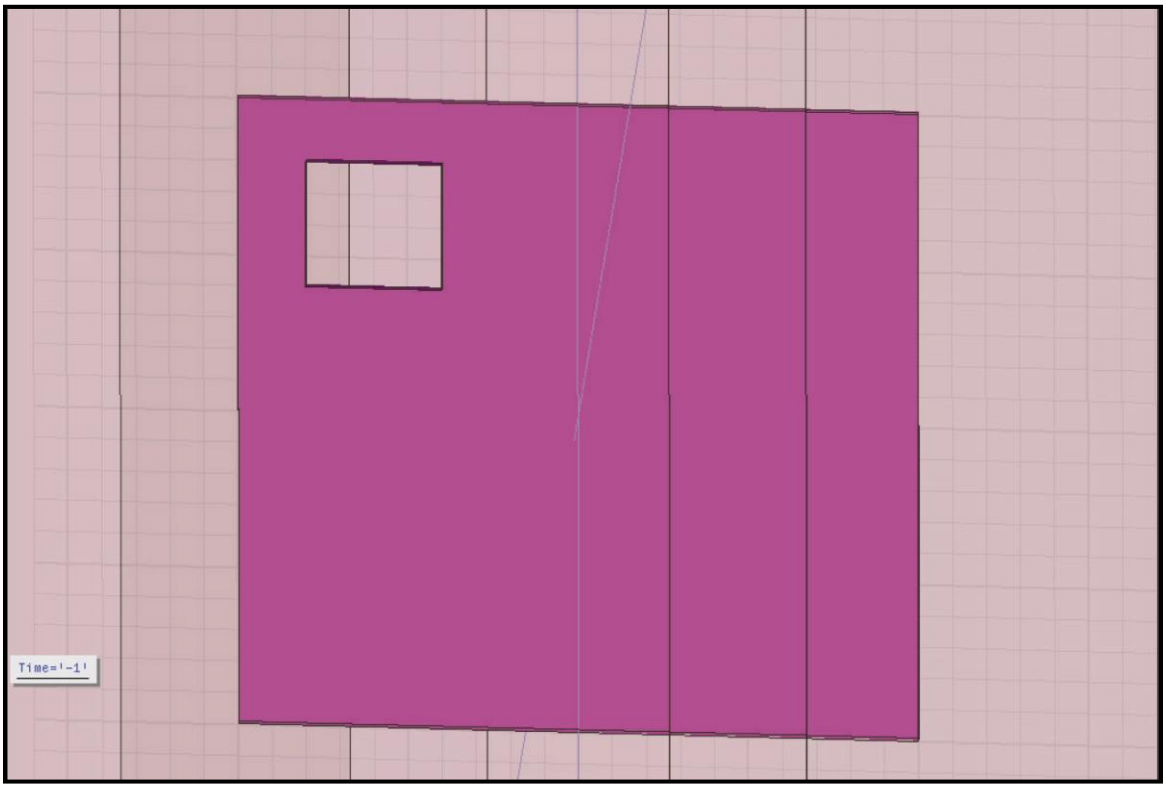

Figure 73. Aluminum Sheet – Sheet01

The sheet configuration shown in Figure 73, named Sheet01, is a 100 mm x 1 mm x 100 mm aluminum sheet with a 20 mm x 20 mm square cutout located 10 mm from each of two edges as shown.

Configuration 2

Another sheet configuration shown in Figure 74, named Sheet02, is also a 100 mm x 1 mm x 100 mm aluminum sheet with a 20 mm x 20 mm square cutout, but the cutout has been

located at 20 mm from each of two edges. The cutout was moved to determine if perhaps the eddy current path is more or less interrupted by the location of the cutout.

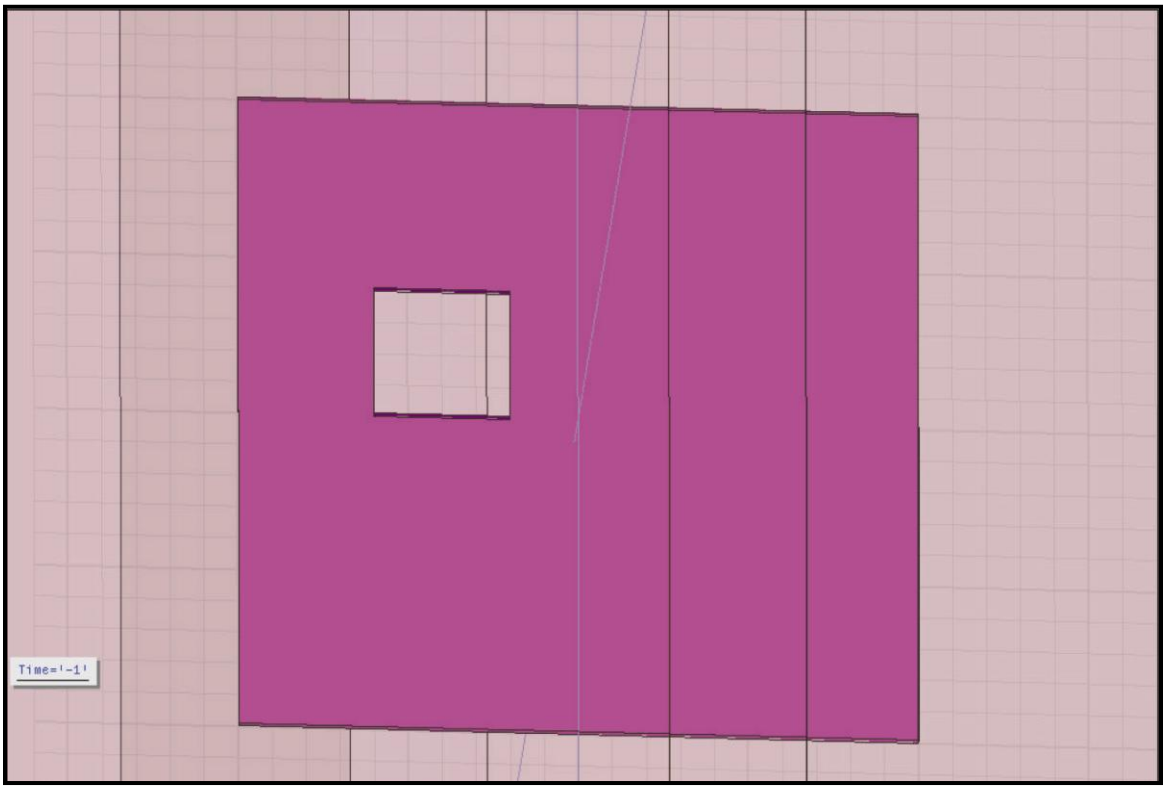

Figure 74. Aluminum Sheet – Sheet02

Configuration 3

The cutout pattern is extended to include two cutouts, as shown in Figure 75, both 20 mm x 20 mm, with one located 10 mm from the two edges as shown, and the second one located 10 mm from one edge, but separated from the first cutout by a gap of 10 mm. The sheet in Figure 75 is named Sheet03.

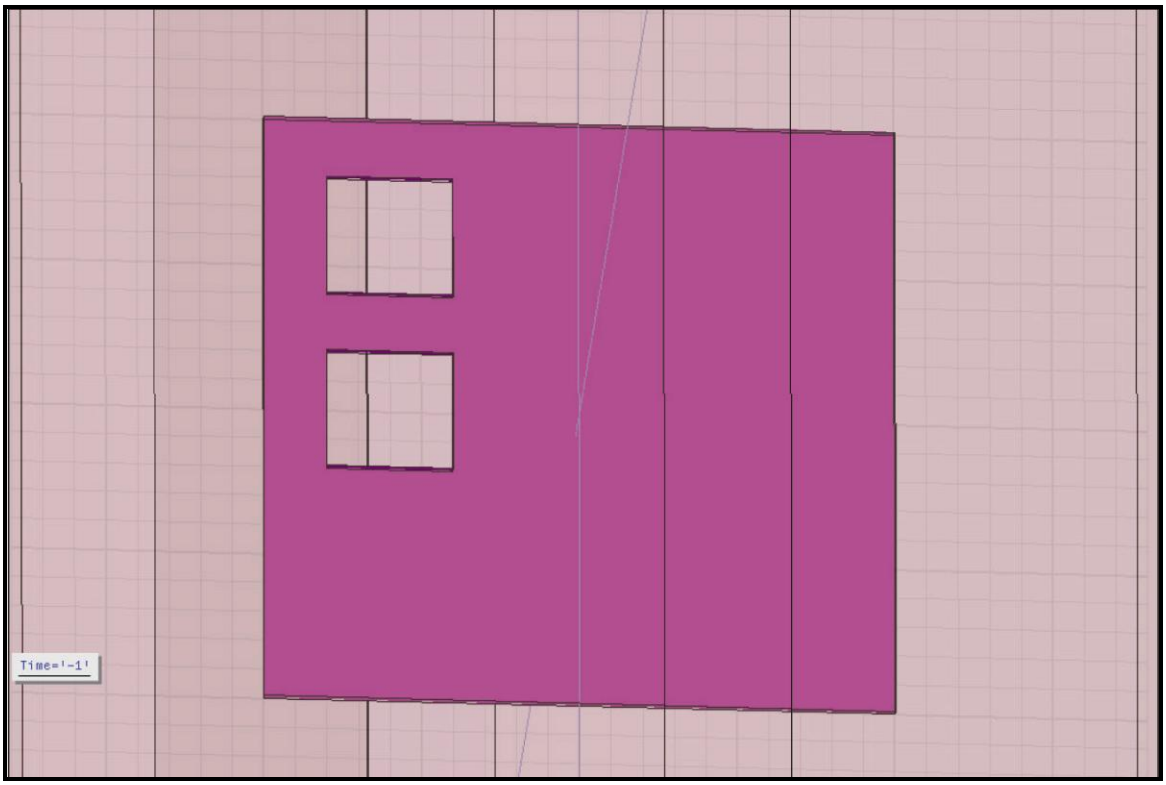

Figure 75. Aluminum Sheet – Sheet03

Configuration 4

The next pattern, named Sheet04, extends the pattern group by moving one of the cutouts to the far side of the sheet, 10 mm from the opposite edge from the first cutout. The cutout pattern is shown in Figure 76.

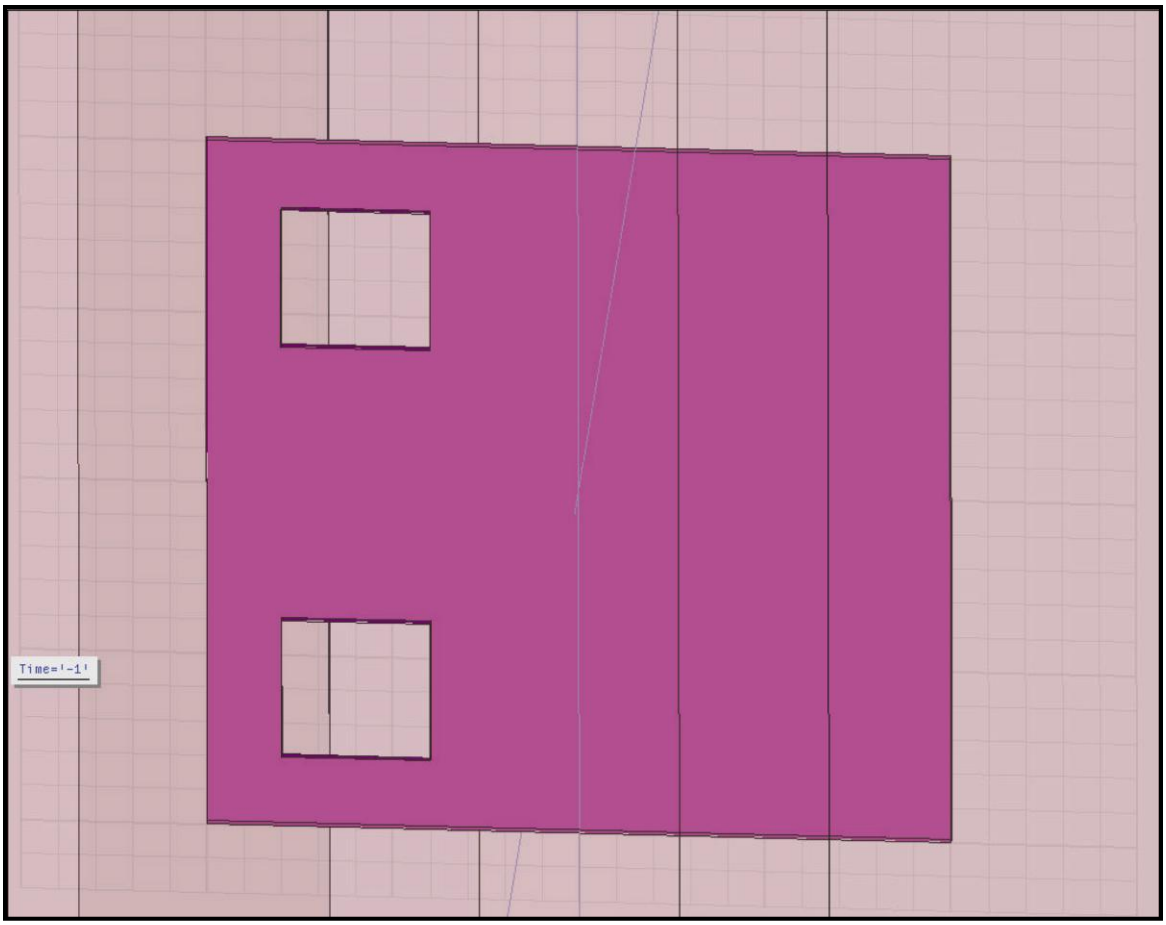

Figure 76. Aluminum Sheet – Sheet04

Configuration 5

Finally, Figure 77 shows a cutout pattern similar to that of the Twin Loop. In this case, the primary objective is not to measure current in the central leg of the pattern, but to more closely simulate a sheet of material that may have large dimension cutouts relative to the overall dimensions of the sheet, that will closely approximately an enclosure with external cutouts, or a belt buckle used as a mechanical strap to hold devices to a patient.

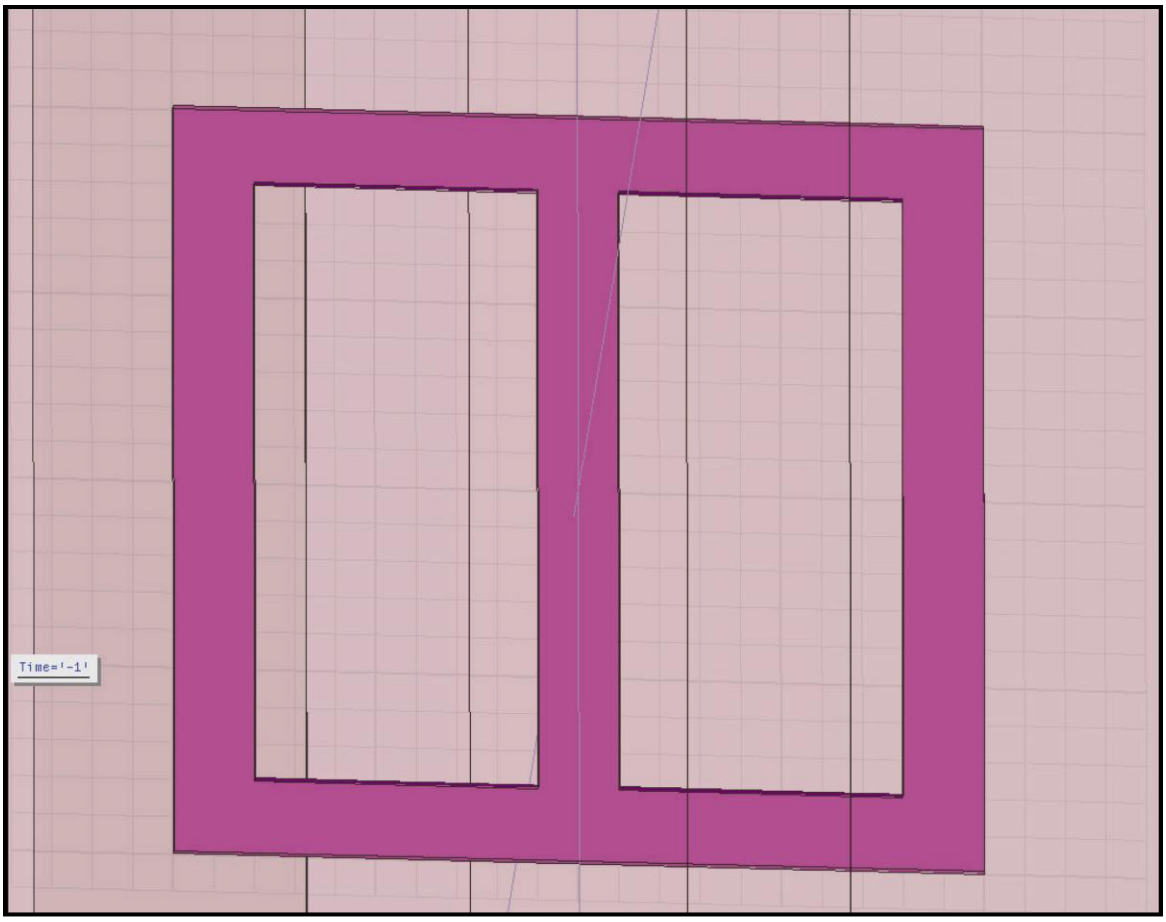

Figure 77. Aluminum Sheet – Sheet05

In the configuration named Sheet05, as shown in Figure 77, the cutouts are designed to leave a band of material 10 mm in width around the perimeter of a 100 mm x 1 mm x 100 mm aluminum sheet. A central band of material, also 10 mm in width runs down the exact center of the pattern.

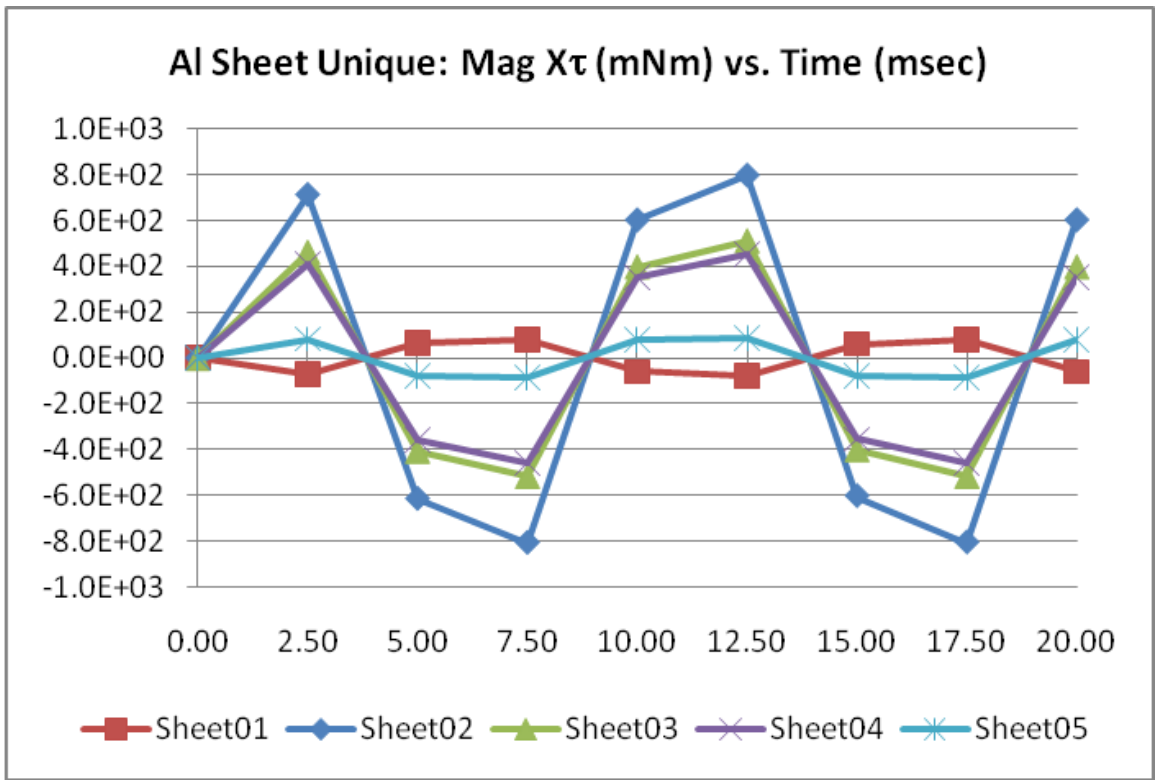

Figure 78. Perforated Aluminum Sheet – X-Axis Torque vs. Time

The graph of Figure 78 plots the x-axis torque experienced by each of the 5 sheets with various hole locations. The horizontal axis is a plot of time in milliseconds and the vertical axis is a plot of the magnitude of the x-axis torque measured in milli-Newton-meters. All sheets are oriented in the 0-degree rotation position. It is assumed that axial rotation will produce similar results as those in previous test volumes.

The plot of Sheet01 indicates that the eddy current has been reduced significantly from an uncut sheet. The peak value of the uncut sheet is approximately 1000 mNm (1Nm), to approximately 100 mNm (0.1Nm), a factor of 10. Additionally, a comparative phase reversal has occurred indicating the the induced eddy current contributor has changed direction.

The plot of Sheet02 indicates that the movement of the hole from the corner towards the middle of the sheet has demonstrated that the eddy currents tends to circulate along the exterior perimeter as demonstrated by the increased torque.

The plot of Sheet03 reinforces the edge based eddy current but also supports the indication that the continual loss of conducting material contributes to the reduction in eddy current magnitude, as is expected.

Sheet04 simply moves one of the cutouts and has little effect on the eddy current contributing to the torque.

However, the plot of Sheet05 is significantly reduced, due in a greater extent to the reduction in material as opposed to eddy current path lenghtening or path changes.

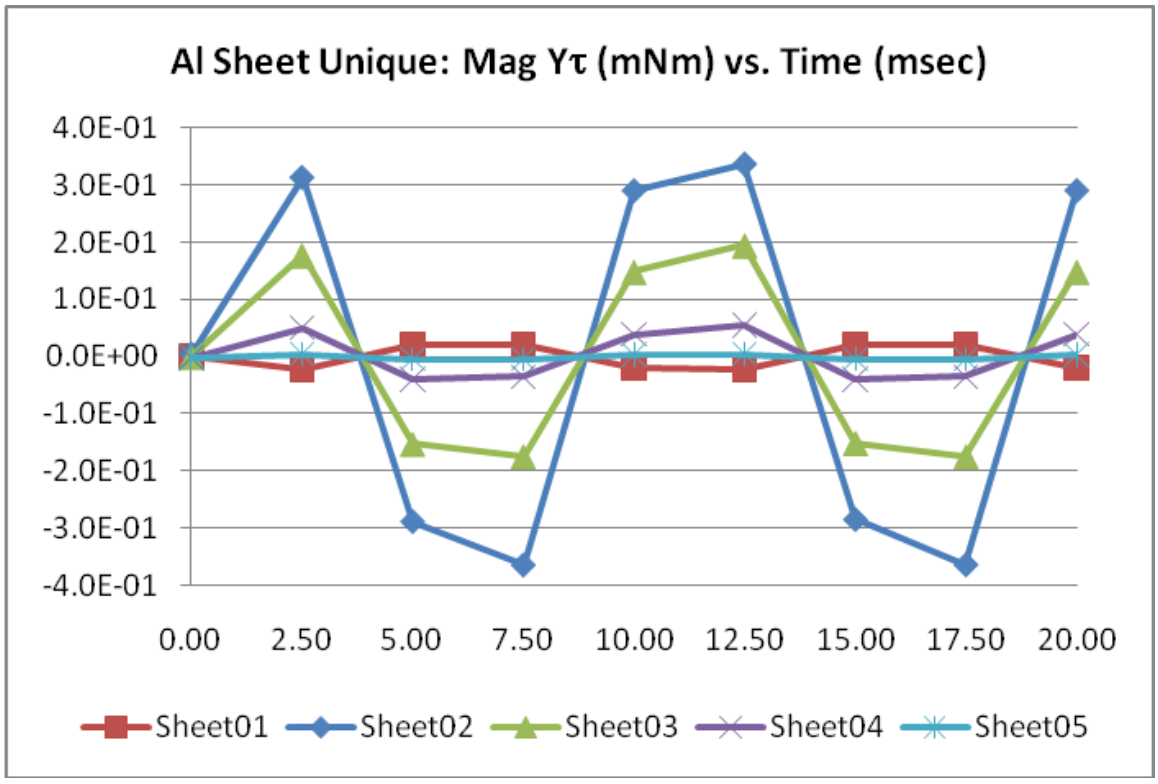

Figure 79. Perforated Aluminum Sheet – Y-Axis Torque vs. Time

As expected the y-axis torques are much less than those of the x-axis as shown in Figure 79.

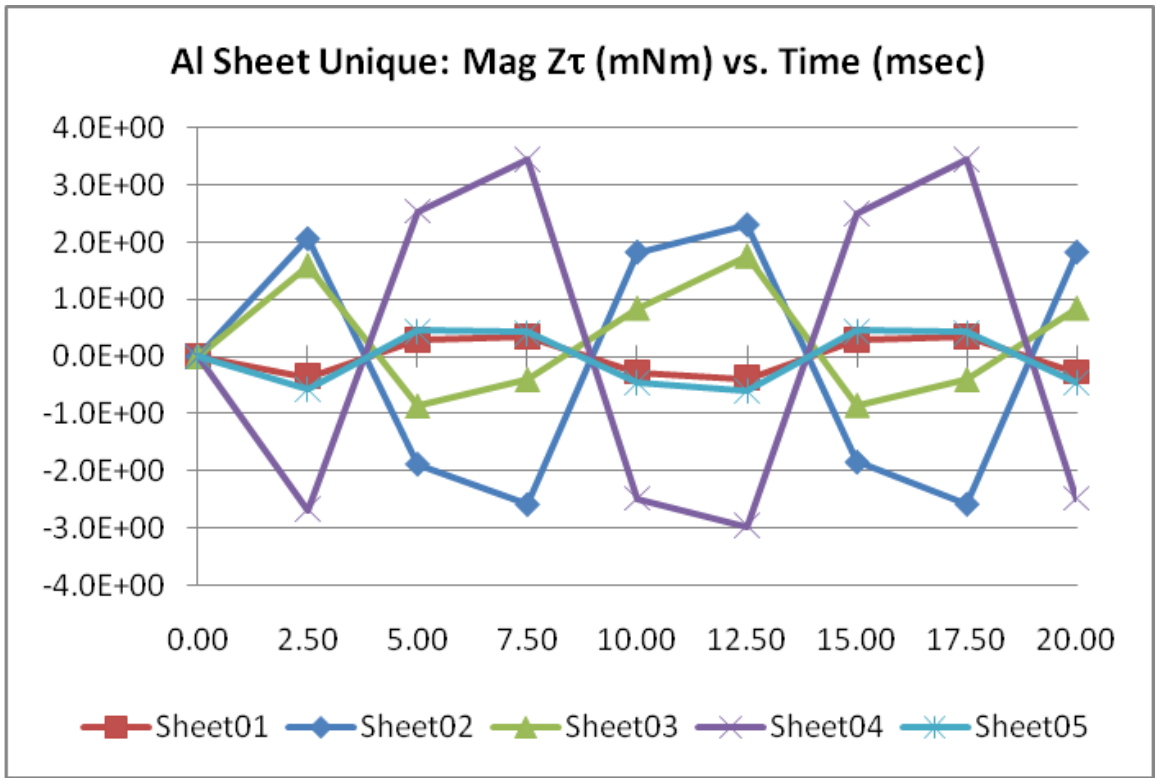

Figure 80. Perforated Aluminum Sheet – Z-Axis Torque vs. Time

In the case of materials with hole patterns, the z-axis torque (Figure 80) indicates that the eddy current flow in the sheet as opposed to the thickness dimension.

CHAPTER NINE: CONCLUSION

The data accumulated represents hundreds of man-hours tending to numerous simulations using a dual Pentium-IV based laptop running Ansoft's Maxwell 3D program. It is impossible to view this many simulations and not get a subjective opinion of the results.

After collecting many megabytes of data, extracting the meaningful pieces for presentation (without overwhelming the reader), plotting the data, and formatting the graphs for visual clarity, it is impossible not to validate the correct assumptions and refute the incorrect assumptions.

The major conclusions that can be drawn from this work are:

1. Eddy currents are established by changing magnetic fields.
2. Eddy currents will react most strongly with the strongest magnetic field – not necessarily with the field that created it in the first place.
3. Better conductors produce larger eddy currents.
4. Path disruptions decrease eddy currents in two ways – change in direction and increased path length.
5. Orientation contributes significantly to the eddy current effects.
6. Shape has less of a contribution to eddy currents than path length or disruption pattern.
7. Ferromagnetic materials create other effects that dwarf eddy current effects.

Although there are a number of graphs with data that may not perfectly line up with anticipated results, they are adequately explained with sufficient detail to be useful. Additional causes of unruly data may include improper setups of the Maxwell software and complexities too

small to be seen or recognized at the level of this thesis. Therefore, it is advised that the data presented here is used in conjunction with sound engineering design practices, adequate testing before deployment, and a small bit of skepticism.

The results of the work on this thesis leave many interesting areas for future work. The work on this thesis also creates many additional questions to be answered. Future work includes:

1. Simulation of the sagittal and axial gradient coils to obtain eddy current data with all possible inducing sources and compare with single source inducers (as is the case with this thesis).
2. Simulation of the RF coils to incorporate the effects of higher frequency induced eddy currents.
3. Simulation and addition of shim coils to create a more uniform bore field, eliminating fringe effects.
4. Addition of frequency domain components to the simulation extending the tactile frequency range into the audible frequency range and incorporating inertial components of material mass.
5. Extending the range of shapes to more complex and varied combinations, including actual configurations in use today.
6. More detailed mapping of eddy current paths in response to one, two, or three gradient coils as well as RF coils.
7. Developing alternative scanning methods that may further reduce or eliminate eddy currents and their effects, such as radial scanning.
8. Development of predictive and “rule-of-thumb” equations for use in equipment design.

9. Build objective hardware simulators that can be used to “insert” test volumes and determine the complete range of effects before the material is incorporated into a design.

APPENDIX

Maxwell 3D Design

This appendix describes the steps required to model and simulate the reference solenoid, the bore coil, the gradient coils, and the MRI simulator used in this thesis. The various test volumes and their modifications are also described.

Maxwell 3D is an electromagnetic field simulation tool used for the design of high performance electromechanical components. It uses the finite element method for solving static, frequency domain, and time varying electromagnetic fields. Use of Ansoft, Inc. documentation is essential to creation and analysis of the MRI simulator.[28, 29, 30, 31, 32, 33,34]

It is important to note that significant performance enhancements can be achieved by:

1. Creating field plots and data tables after the analysis is completed. The interaction between Maxwell 3D and Microsoft Windows creates a memory management problem that utilizes significant computer resources and temporary files. If field plots and data tables are established prior to initiation of the analysis, Maxwell 3D attempts to populate the data during the course of analysis, creating a memory sharing problem. Allowing Maxwell 3D to complete the analysis, then populate the field plots and data tables resolves this conflict and allows the data to be populated many times faster.
2. Create reasonable meshes to separate the item of interest into the smallest number of tetrahedral necessary to achieve results within the tolerance needed to extract meaningful results.
3. Incorporate boundary conditions and dummy volumes to focus Maxwell's interests to only those elements needed.
4. Do not run parametric analysis on complex shapes as this creates its own memory management problems that significantly reduce performance. Manually adjust individual parameters as needed.

Reference Solenoid

The reference solenoid is an arbitrary solenoid used to validate the mathematics of Maxwell 3D for B field generation.

Bore Coil

For this simulation, the precise dimensions of the magnet are unimportant, but the enclosed magnetic field is very important. In order to obtain a static magnetic field with a sufficiently large space and a relatively uniform field, a cylinder of approximately 100 cm in diameter and 200 cm in length was designed. The outer diameter of the bore magnet is set at 200 cm. This provides ample volume in which to insert test volumes of a size anticipated to be found in most electronic or mechanical devices inserted into an MRI's bore.

Project Setup

1. Open Maxwell 3D. A default project, *Project1*, should be loaded. If not, follow the next steps, otherwise, skip to step 3.
2. Click **File** > **New**. This will create a new file with the default name *Project1*. A project is a collection of one or more designs.
3. Click **Project** > **Insert Maxwell Design**. This will create a new design with the default name *MaxwellDesign1*.
4. Click **File** > **Save As**. The **Save As** dialog box appears and allows the project to be saved given a new name. Choose a name or use *BoreCoil* as the file name.
5. Right click on the **Maxwell Design** object in the **Project Management** window and rename the object *BoreCoil*. Click **Enter**.

Environment Setup

1. Click **Maxwell** > **Solution Type**. The Solution Type window will appear allowing the solution to chosen as Magnetostatic, Eddy Current, Transient, Electric, Electric – Electrostatic, and Electric – DC Conduction. Choose **Transient**. Although the bore field is a static field created by a uniform DC current in the bore conductor, the Magnetostatic solver is not capable of generating time-varying excitations. Although the Eddy Current solver seems

like a logical choice, it too is not capable of handling time-varying excitations. All solvers, however, are capable of applying the eddy current effects to selected objects, therefore, the transient solver is chosen to accommodate the time varying excitations of the gradient coils and the eddy current effects are selected for the test volumes as described later.

2. Click **3D Modeler** > **Units**. The default unit is the millimeter. This will be used throughout the design.

Create Model Geometry

The bore coil is modeled by creating two cylinders of material that are subtracted from each other to form a tube of material through which a DC current flows to create the MRI bore's static magnetic field. The exact strength of the field varies with different MRI machines. Here 1.5 T is used at the center of the bore field as the baseline.

Create Bore Magnet

1. Ensure the XY drawing plane is selected.
2. Click **Draw** > **Cylinder**. The cursor changes to a small black box indicating Drawing mode.
3. Select the center of the cylinder by clicking the (0,0,0) location in the **3D Modeler** window.
4. Click any distance along the X or Y axis to create the radius of the cylinder. The exact dimensions will be designated later and are not critical at this time.
5. Click any distance along the Z axis to create the cylinder length. The exact distances will be designated next. When the cylinder length is created, a **Properties** window will appear.
6. Edit the radius and height of the cylinder in the **Properties** window. They are Radius = 1000 mm and Height = 2000 mm. Click **OK**. The cylinder created will most likely extend well beyond the extents of the current 3D Modeler widow.
7. Click **View** > **Fit All** > **All Views** to resize the window to display the cylinder. The drawing should be as shown in Figure 81.

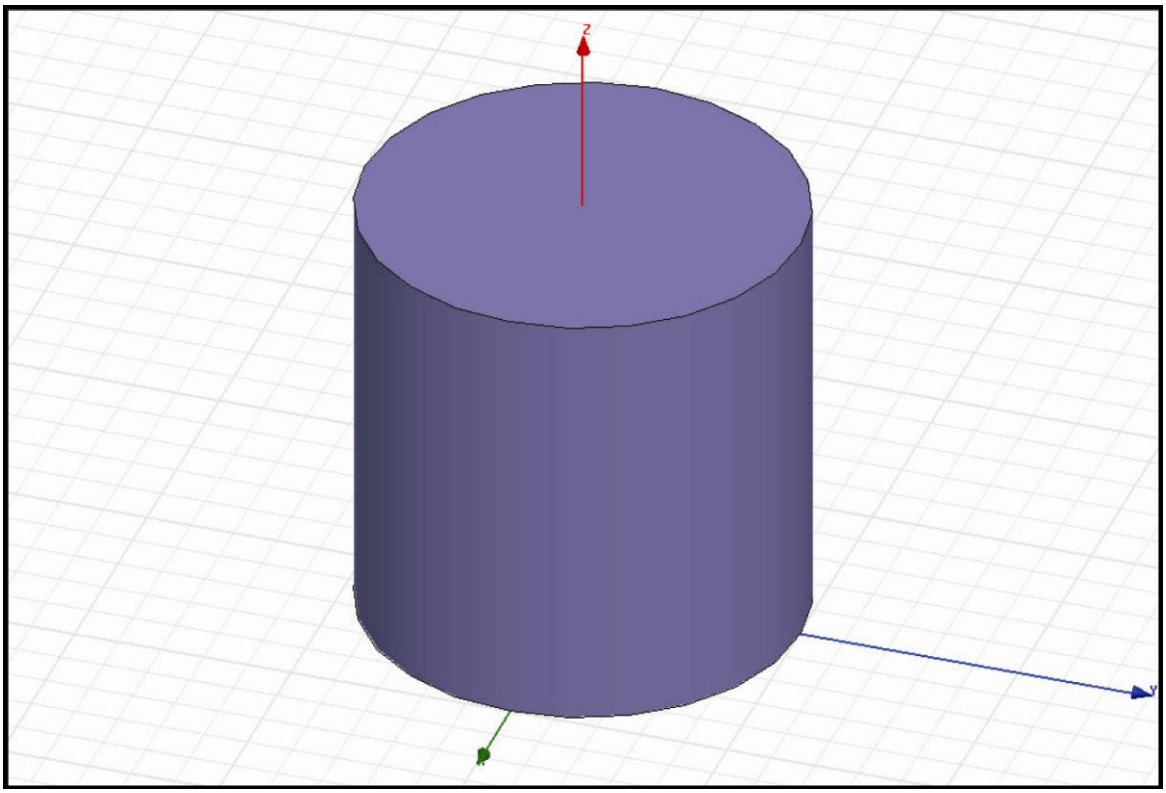

Figure 81. Cylinder

8. Click **Draw** > **Cylinder** to start the internal cylinder.
9. Select the center of the cylinder by clicking the (0,0,0) location in the **3D Modeler** window.
10. Click any distance along the X or Y axis to create the radius of the cylinder.
11. Click any distance along the Z axis to create the cylinder length.
12. Edit the radius and height of the cylinder in the **Properties** window. They are Radius = 500 mm and Height = 2000 mm. Click **OK**.
13. Click **View** > **Fit All** > **All Views** to resize the window to display the cylinder, if needed. The drawing should look similar to Figure 82.

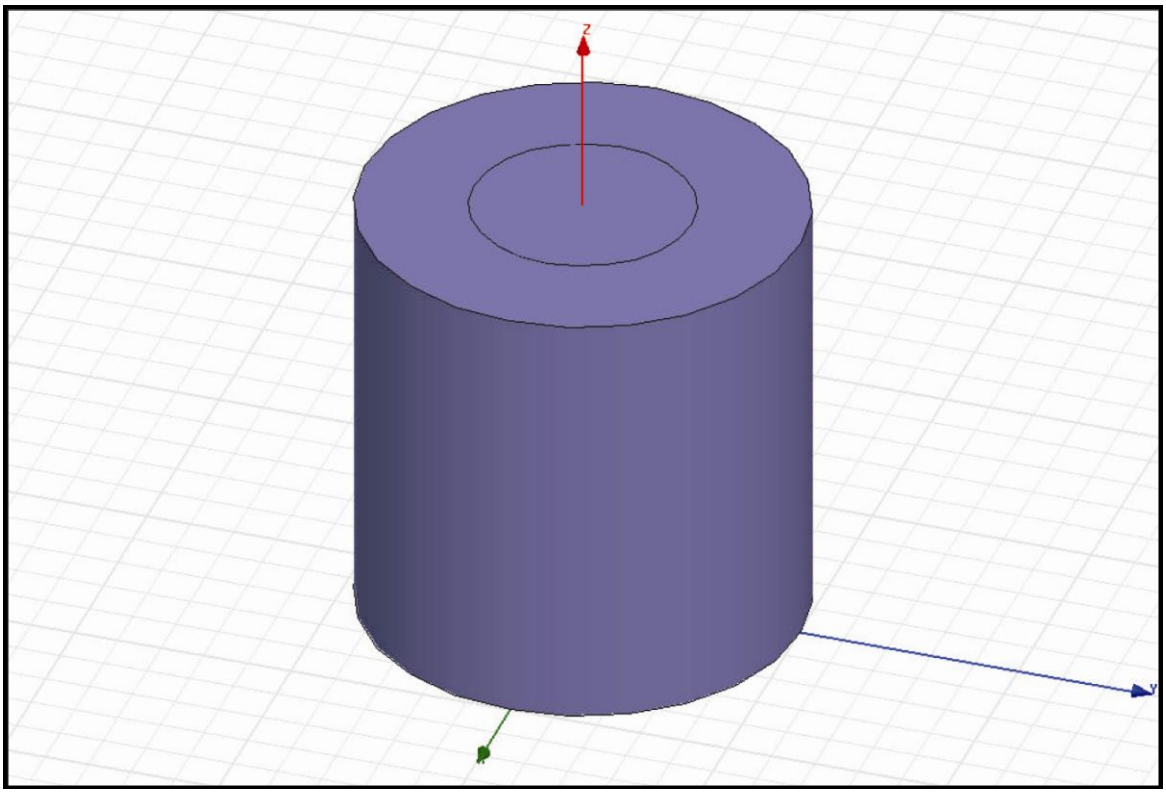

Figure 82. Twin Cylinders

14. In the History Tree window, select *Cylinder1*. Press and hold down Ctrl and select *Cylinder2*. Both cylinders should be highlighted in dark blue while the Maxwell window is active (grey when Maxwell is inactive).
15. Click **3D Modeler** > **Boolean** > **Subtract** to display the **Subtract** window. Two lists of parts are displayed. The **Blank Parts** window lists the items that will remain after the operation and the **Tool Parts** window lists the items that will be removed from the part. The result should look like the drawing in Figure 83.

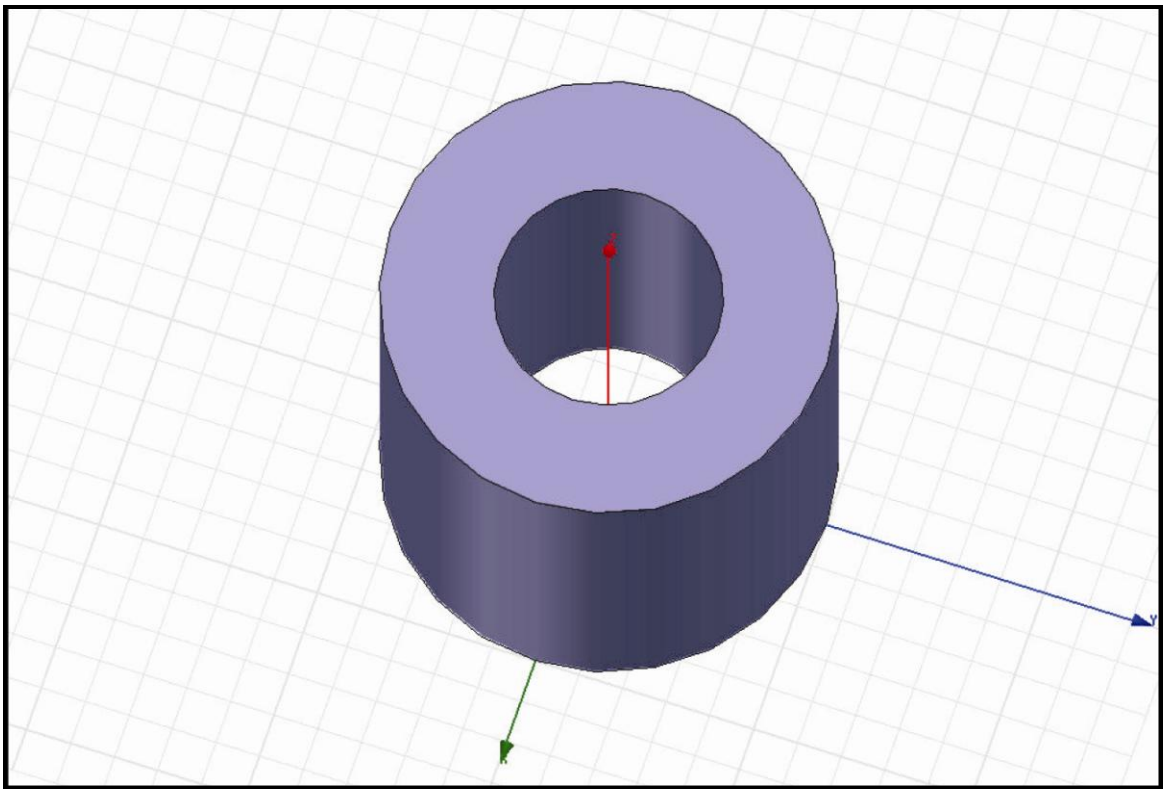

Figure 83. BoreCoil

16. Highlight *Cylinder1* and edit the name in the Project Manager window to *BoreCoil*.
17. Click the box under the Material – Value cell to display the **Select Definition** window.
18. Scroll up the window to select copper as the material comprising the *BoreCoil*.
19. Click **OK** to close the window.

Create Bore Magnet Terminals

Create the Bore Magnet terminals. This will be used to define the DC current which creates the static magnetic field.

1. In the History Tree window select the *BoreCoil* object.
2. Click **3D Modeler** > **Surface** > **Section** to display the Section window. The YZ plane is an appropriate plane to section the Bore Magnet. The XZ plane would work just as well, but the XY plane is not appropriate.
3. Click **OK** to close the window. This creates one section object consisting of two rectangular sections of the *BoreCoil* coil. The drawing should look like this:

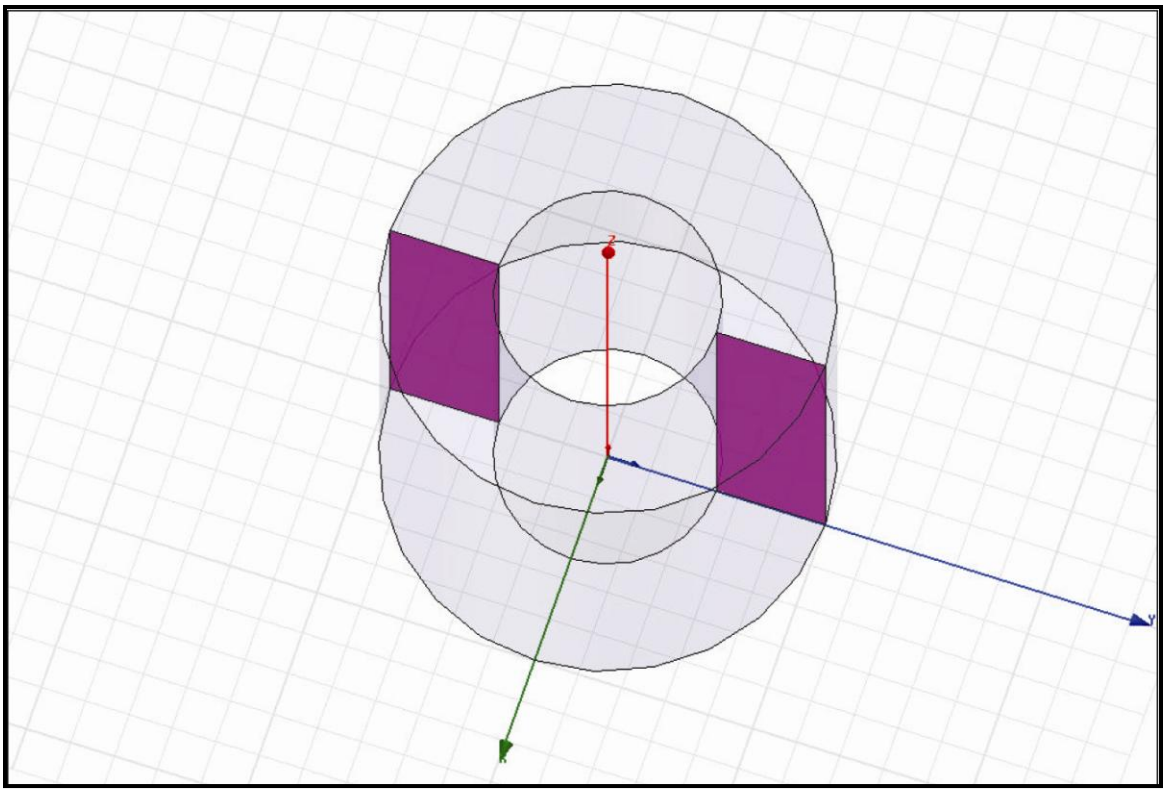

Figure 84. Sectioned BoreCoil

4. Click the *Section1* object in the **History Tree** window.
5. Click **3D Modeler** > **Boolean** > **Separate Bodies**. This will separate the two section sheets into *Section1* and *Section1_1*. When applying the current, Maxwell inserts the current into the entire sheet. If both sections remain part of the model, the two currents will be inserted simultaneously, effectively cancelling each other. Therefore, only one section is required so that the current circulates around the entire coil.
6. Click on *Section1_1* in the **History Tree** window to highlight it.
7. Place the mouse over the *Section1_1* object and right click to display the drop down menu.
8. Scroll down the menu and select **Edit** > **Delete** to remove the extraneous *Section1_1* object. Only the *Section1* sheet object should remain. The *BoreCoil* should now look like this:

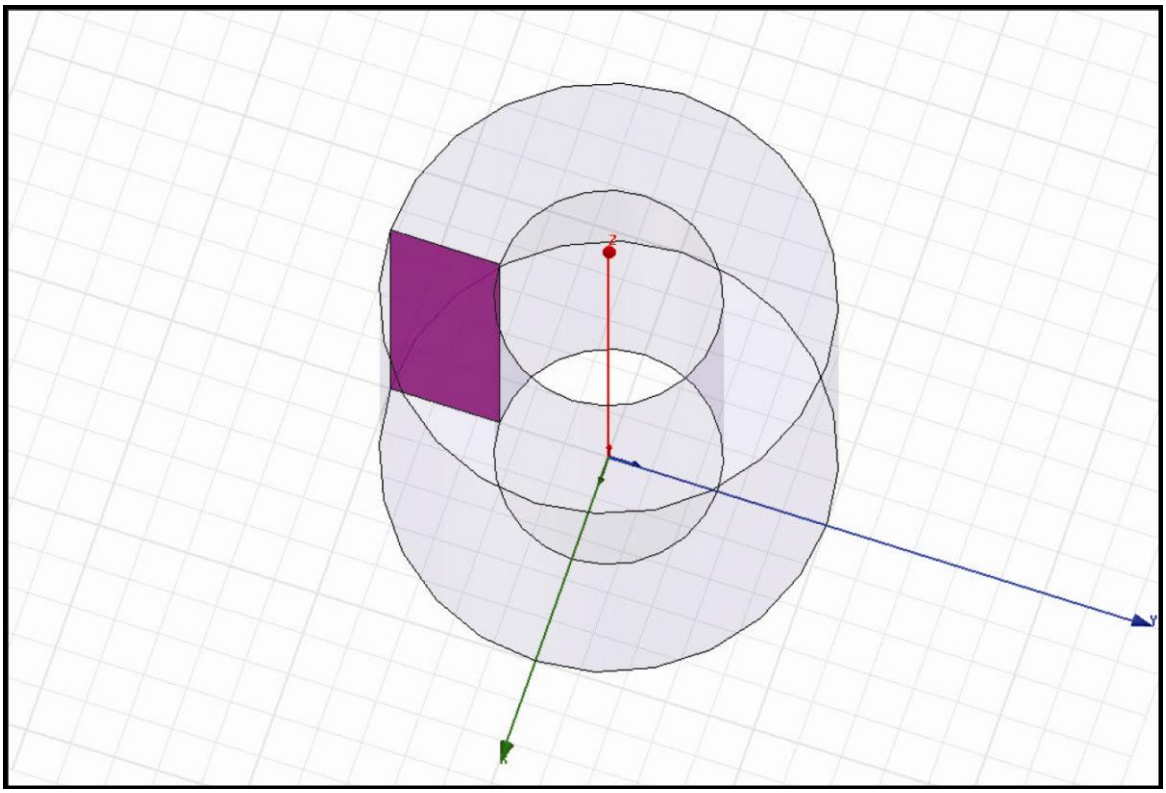

Figure 85. Single Section BoreCoil

Create the Background (Region)

The background region box defines the extents to which Maxwell 3D will partition the region into finite elements. The magnetic field of an MRI exists in a region of space filled with air. The background is designated to be air.

1. Click **Draw** > **Box**. Similar to the cylinder, the first, second and third dimensions of the box are selected with the mouse. The exact dimensions are not critical as the Properties box will be edited to describe the Background.
2. Edit the Position to be -2500, -2500, -4000. Xsize = 5000, Ysize = 5000, and Zsize = 5000 will define a box with dimensions of 5000 mm x 5000 mm x 5000 mm (16.4 ft. x 16.4 ft. x 16.4 ft.). These dimensions approximate the size of a typical MRI installation.
3. Click the **Attribute** tab in the **Project Manager** window.
4. Edit the name of the box to *bgnd* ("Background" is a reserved name in Maxwell 3D).
5. Click the box in the Material – Value cell to display the **Select Definition** window.
6. Scroll up the window to select "air" as the material in the *bgnd* box.
7. Click the "edit" box in the Color – Value cell to display the **Color** selection window. Edit as desired.

8. Click **OK** to close the **Color** window.
9. Click the box in the Transparent – Value cell to display the **Set Transparency** selection window.
10. Set the transparency to 95%.
11. Click **OK** to close the **Set Transparency** window. The drawing should now look like this:

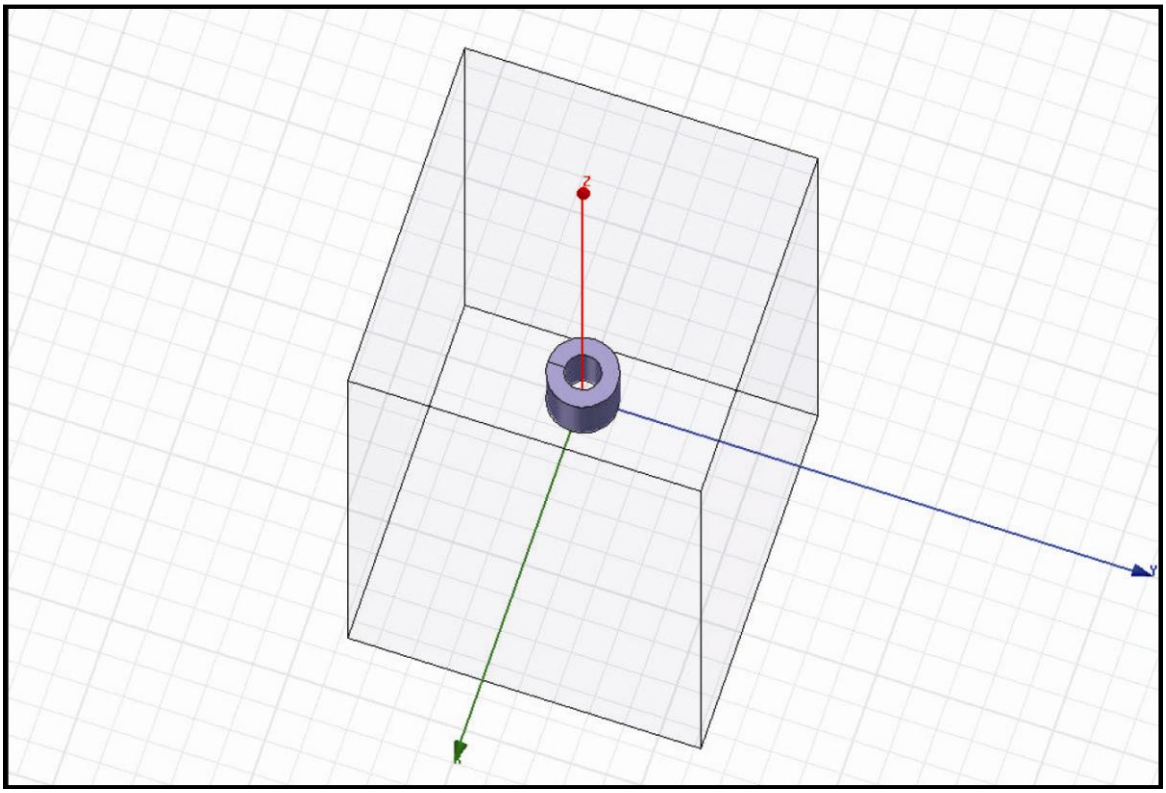

Figure 86. BoreCoil Environment

Assign Excitations

A DC current is required in the *BoreCoil* to create the static magnetic field.

1. Using the various rotation and translation tools in the menu bar, position the drawing so that the *BoreCoil* fills the design window.
2. Select *Section1* in the History Tree window.
3. Click **Maxwell** > **Excitations** > **Assign** > **Current** from the menu to display the **Current Excitation** window.
4. Edit the values in the window to name the current *BoreCurrent* with a value of 2,983,900 Amps. (This is really 2,983,900 Amps through 1 turn of the *BoreCoil*.)
5. Select **Stranded** as the Type and click the **Swap Direction** button until the vector indicates the positive X direction. By choosing **Stranded** for the *BoreCurrent* Type, Maxwell creates a

uniform distribution of current through the *BoreCoil* section area, simulating a multi-turn solenoid. This will create current flow that produces a magnetic field that is positive in the Z direction (right hand rule).

6. Click **OK** to close the window. The drawing should look like that shown in Figure 87.

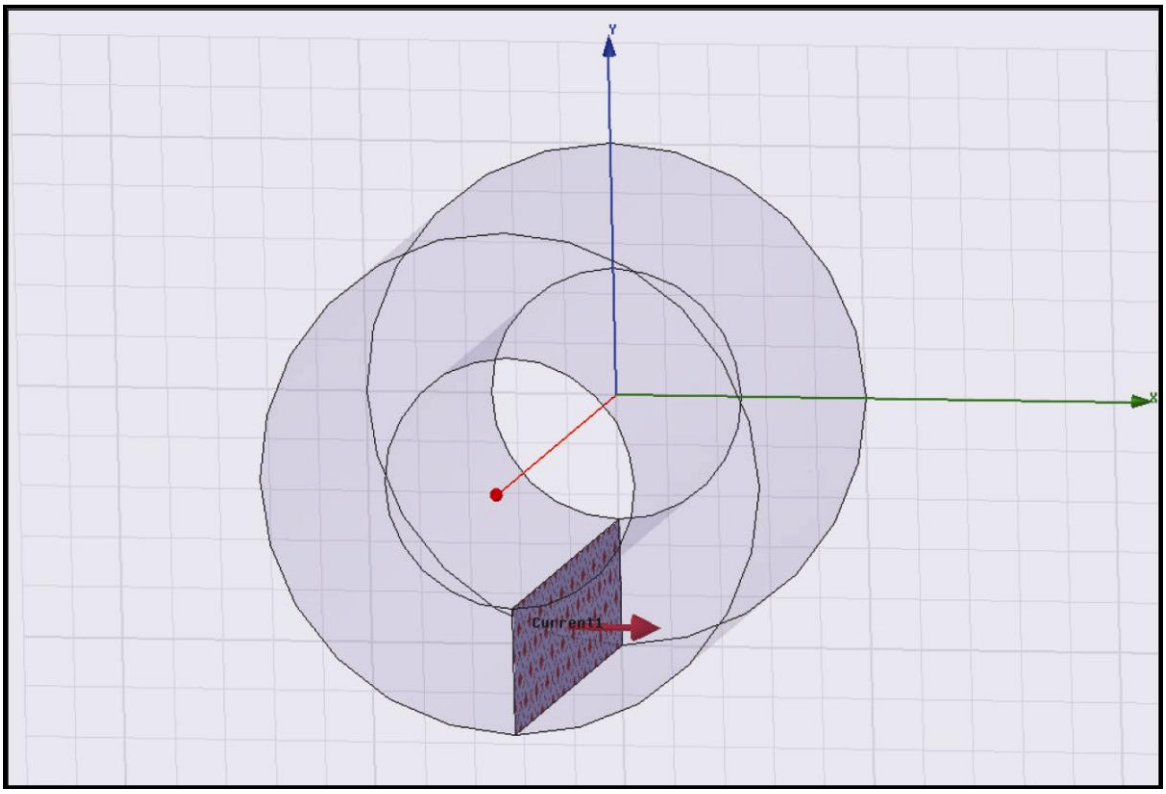

Figure 87. BoreCoil Current

Set Up the Analysis

1. Click on the "+" sign in front of the *BoreCoil* object in the **Project Management** window to expand the properties of the design object.
2. Right click on the **Analysis** object and select the **Add Solution Setup** menu item to open the **Solve Setup** window.
3. Click **OK**.
4. Select the Global:XZ plane in the **History Tree** window.
5. Right click on the Field Overlays object in the **Project Management** window.
6. Navigate the menu and select **Field Overlay** > **Fields** > **B** > **Mag_B** to display the **Create Field Plot** window.
7. Use the default settings and click **DONE** to close the window.
8. Right click on the **Analysis** object and click on **Analyze All**.

9. When Maxwell has completed the analysis, expand the **Field Overlays** object and click on the **Mag_B1** object to display the results. The resultant plot should look like this:

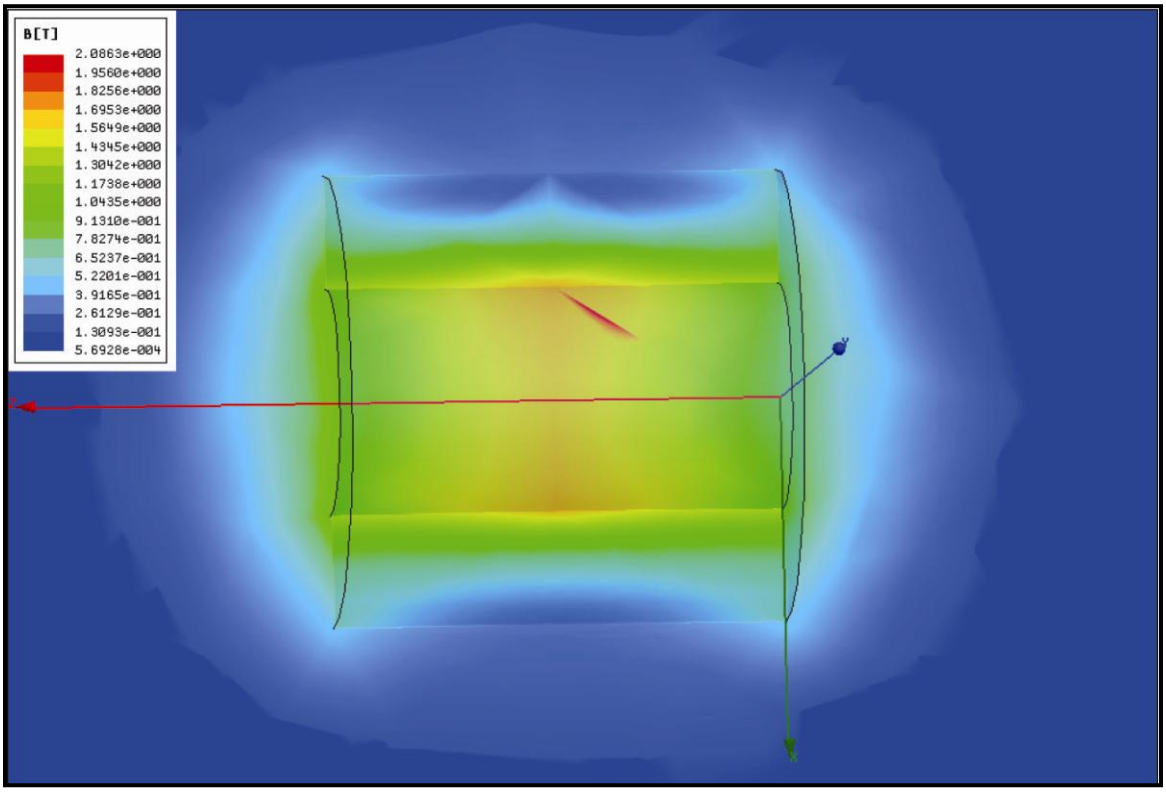

Figure 88. BoreCoil Field Plot

Set Up the Data Collection

1. Navigate the menu and select **Draw** > **Line** to begin the process of drawing a line through the volume where data is to be collected.
2. Maxwell will ask: A solution exists; do you want to create a non-model object? The answer to this is "Yes." Click the **Yes** button to continue.
3. Navigate down the "Lines" object to the **Create Line** item and edit the properties of the line. In this case the data collected along the line will be down the z-axis of the *BoreCoil*, so the endpoints of the line are 0,0,-500 and 0,0,1500, to give the line 500 mm of length above and below the *BoreCoil* central volume.

Gradient Coil

For this simulation, the dimensions of the gradient coil should match the bore magnet. The gradient magnet will consist of 4 “saddle” coils positioned in such a manner as to add to the strength of the magnetic field at the top and linearly decrease the field to the bottom.

Create Model Geometry

The gradient coil is modeled by creating two rectangles that are swept through an arc of 120 degrees and are subtracted from each other to form a saddle coil through which a DC current flows to create the gradient coil’s magnetic field. The effect on the bore field is to create a linear variation on the bore field of 1.0 Gauss per centimeter. This variation can only be simulated for a small volume at the epicenter of the MRI simulator since. With the addition of shim coils, the remaining gradient coils, and other more complex aspects of the MRI itself, a uniform gradient field across all desired axes can be developed, but is beyond the scope of this thesis and is left to future work.

Create the Gradient Magnet

1. The centerline of the *BoreCoil* is coincident with the Z axis, so we will develop the saddle coils to also have a centerline along the Z axis. In the drawing menu bar, there is a drop-down box indicating the currently displayed drawing plane. Drop the box and select the **YZ** plane.
2. Click **Draw** > **Rectangle**. The cursor changes to a small black box indicating Drawing mode.
3. Select a point on the YZ plane and drag a rectangle with the major length along the Z axis. When completed, the **Properties** window will appear.
4. Edit the Position to be 0,1000,2001. This defines the starting position of the rectangle. We are leaving a 1mm gap between the *BoreCoil* and the *SaddleCoil*.
5. Edit the YSize to be -100 and the ZSize to be 2000. The Y dimension will define the thickness of the coils to be 100mm and the length to be 2000mm. The current in the arcs of the *SaddleCoil* closest to the *BoreCoil* will create a magnetic field that contributes to the bore field. The arcs furthest away from the *BoreCoil* are sufficiently far away as to have little effect on the bore field. Similarly, a *SaddleCoil* at the opposite side of the *BoreCoil* will be excited with current that subtracts from the *BoreCoil* field. The magnetic field between the coils will vary to produce a linearly varying field in the volume of interest. Like the bore field, the gradient fields will not be sufficiently modeled to simulate a true MRI field with less than 5ppm variation across the entire bore, but will create the desired 1 Gauss per

centimeter across the volume of interest, approximately a 5-inch cube at the epicenter. The drawing should look like that shown in Figure 89.

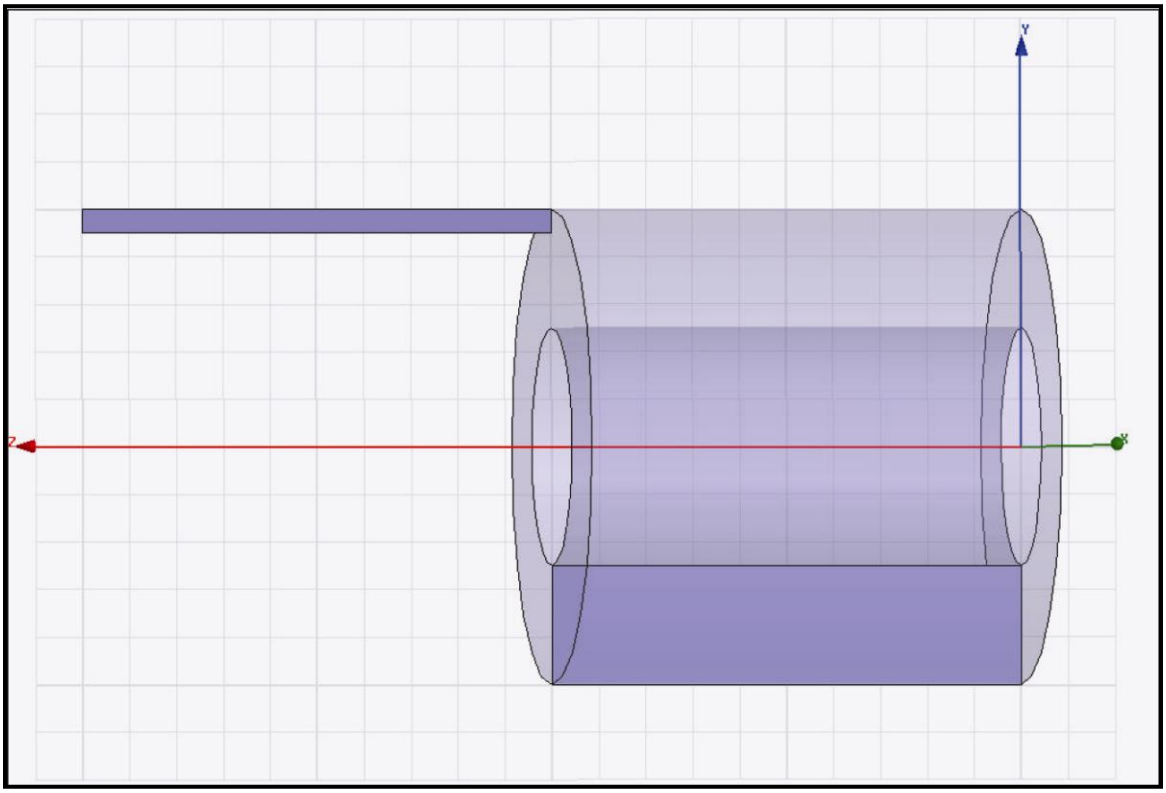

Figure 89. Gradient Coil Outer Rectangle

6. Click **View** > **Fit All** > **All Views** to resize the window to display the rectangle, if needed.
7. Click on the *Rectangle1* object in the **History Tree** window.
8. Click on **Draw** > **Sweep** > **Around Axis** to display the **Sweep Around Axis** window.
9. Click on the Z axis radio button in order to sweep the rectangle around the Z axis.
10. In the Angle of sweep, replace the value with 65 to sweep the rectangle 65 degrees clockwise from the Y axis.
11. The Properties window will display. Click **OK** to close. The drawing should look like this.

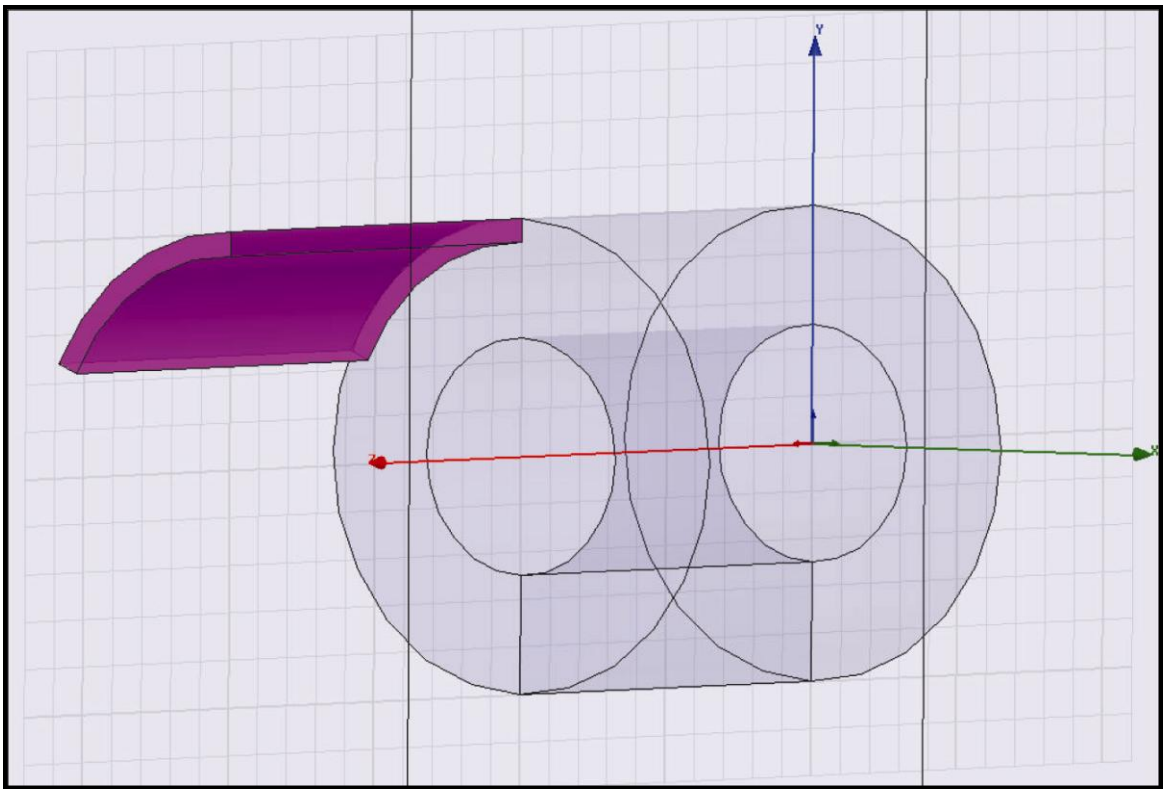

Figure 90. Gradient Coil Sweep

12. Click **Draw Rectangle** again and draw another rectangle right on top of the first rectangle. This will create *Rectangle2*.
13. Click on **Draw** > **Sweep** > **Around Axis** to display the **Sweep Around Axis** window.
14. Click on the Z axis radio button in order to sweep the rectangle around the Z axis.
15. In the Angle of sweep, replace the value with -65 to sweep the rectangle 65 degrees counterclockwise from the Y axis. The drawing will now look similar to this:

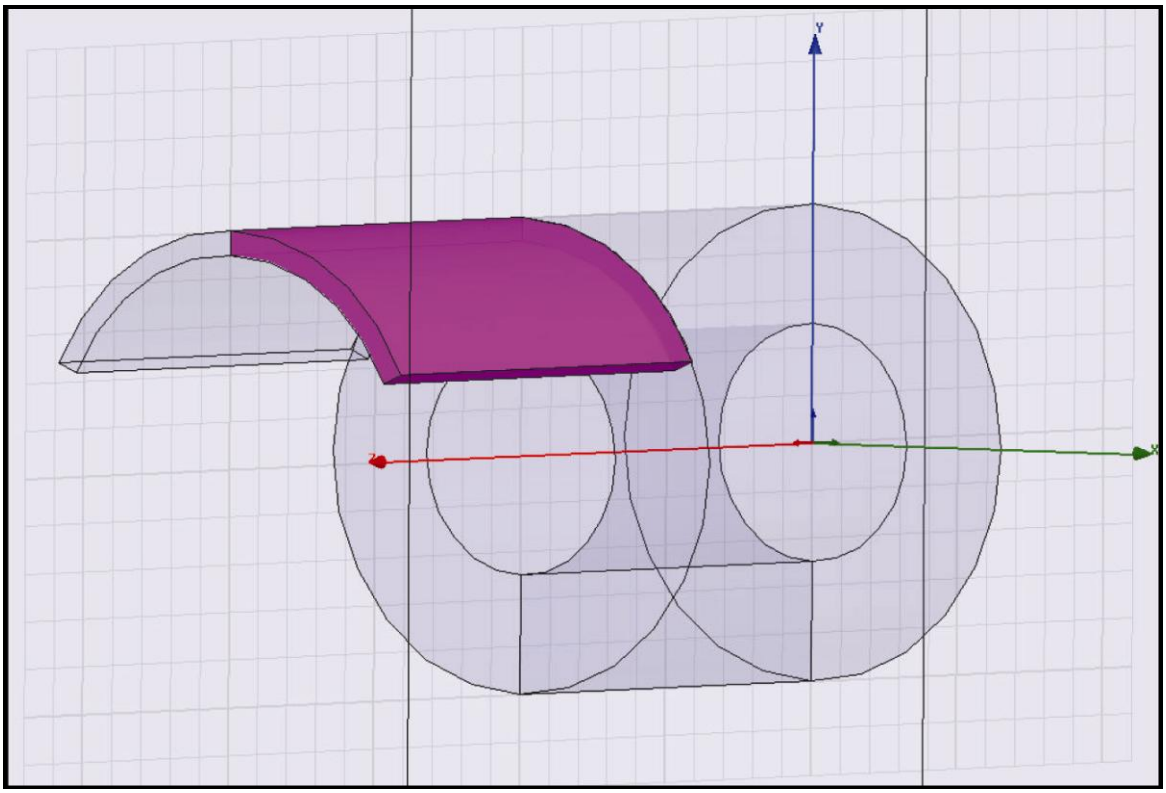

Figure 91. Gradient Coil Volume

16. Select *Rectangle1*. Select *Rectangle2* by holding down the Ctrl button while clicking on *Rectangle2*. Both rectangles should be highlighted in dark blue.
17. Select **3D Modeler** > **Boolean** > **Unite** to combine both swept rectangles into one curved plate.
18. It is important to use the same radius to create the second curved plate, so the first curved plate must be moved. Click *Rectangle1* in the **History Tree** window.
19. Click on the **Move** button in the drawing toolbar.
20. Select a starting point at 0,0,0 and an end point at 0,2000,0 to move the first curved plate 2000 mm away from the Z axis. (Any direction can be used, but the exact position must be retained as the volume must be returned exactly to its starting position.)
21. Click **Draw** > **Rectangle**. The cursor changes to a small black box indicating Drawing mode.
22. Select a point on the YZ plane further away from the Z axis giving plenty of room to create another curved plate and drag a rectangle with the major length along the Z axis. When completed, the Properties window will appear.
23. Edit the Position to be 0,1000,2101. This defines the starting position of the rectangle.
24. Edit the YSize to be -100 and the ZSize to be 1800. The Y dimension will define the thickness of the coils to be 100mm and the length to be 1800 mm. This will define the curved plate that is subtracted from the first plate to form the saddle coil. The drawing should now look like this:

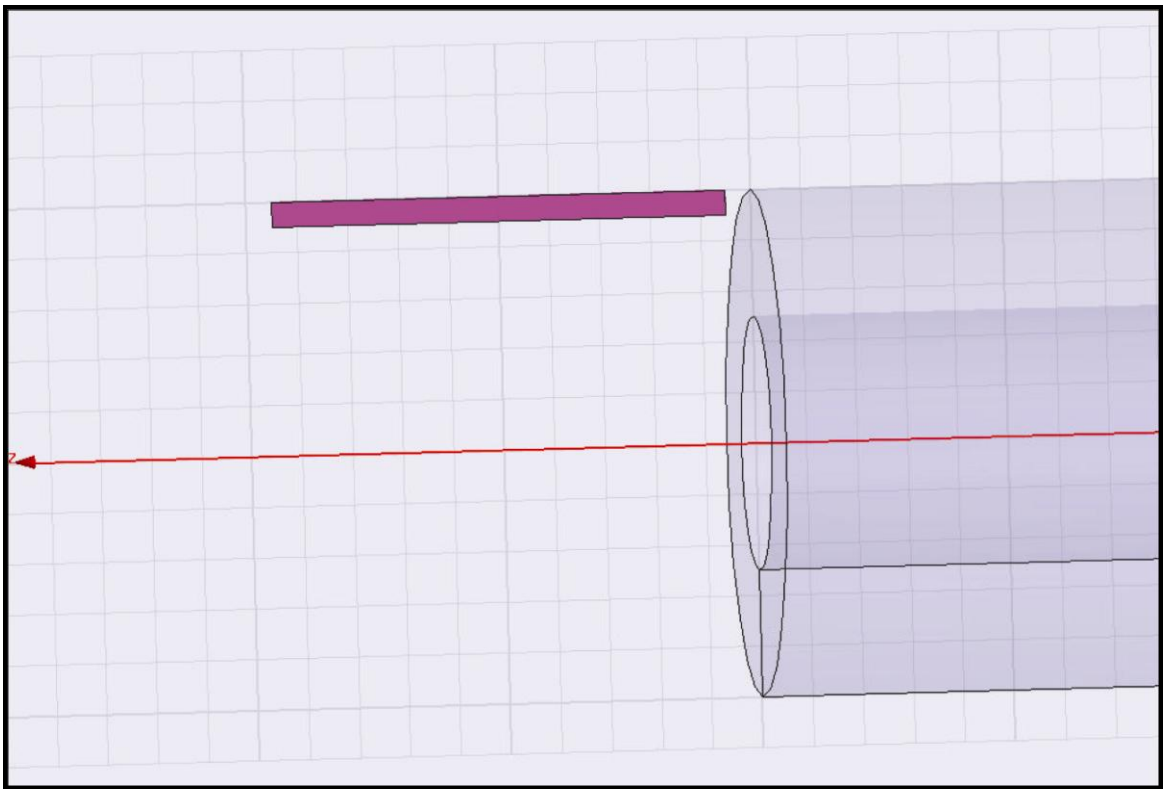

Figure 92. Second Gradient Coil Rectangle

25. Click **View** > **Fit All** > **All Views** to resize the window to display the rectangle.
26. Click on the *Rectangle3* object in the **History Tree** window.
27. Click on **Draw** > **Sweep** > **Around Axis** to display the **Sweep Around Axis** window.
28. Click on the Z axis radio button in order to sweep the rectangle around the Z axis.
29. In the Angle of sweep, replace the value with 60 to sweep the rectangle 60 degrees clockwise from the Y axis.
30. The Properties window will display. Click **OK** to close.
31. Click **Draw Rectangle** again and draw another rectangle right on top of the first rectangle. This will create *Rectangle4*.
32. Click on **Draw** > **Sweep** > **Around Axis** to display the **Sweep Around Axis** window.
33. Click on the Z axis radio button in order to sweep the rectangle around the Z axis.
34. In the Angle of sweep, replace the value with -60 to sweep the rectangle 60 degrees counterclockwise from the Y axis.
35. Select *Rectangle3*. Select *Rectangle4* by holding down the Ctrl button while clicking on *Rectangle4*. Both rectangles should be highlighted in dark blue.
36. Select **3D Modeler** > **Boolean** > **Unite** to combine both swept rectangles into one curved plate.
37. Move the first curved plate back on top of the second curved plate by selecting *Rectangle1*.
38. Click **Move**.

39. When the Properties window appears, ensure that the move is 0,-2000,0 to place the first curved plate on top of the second curved plate. This is what the result should look like:

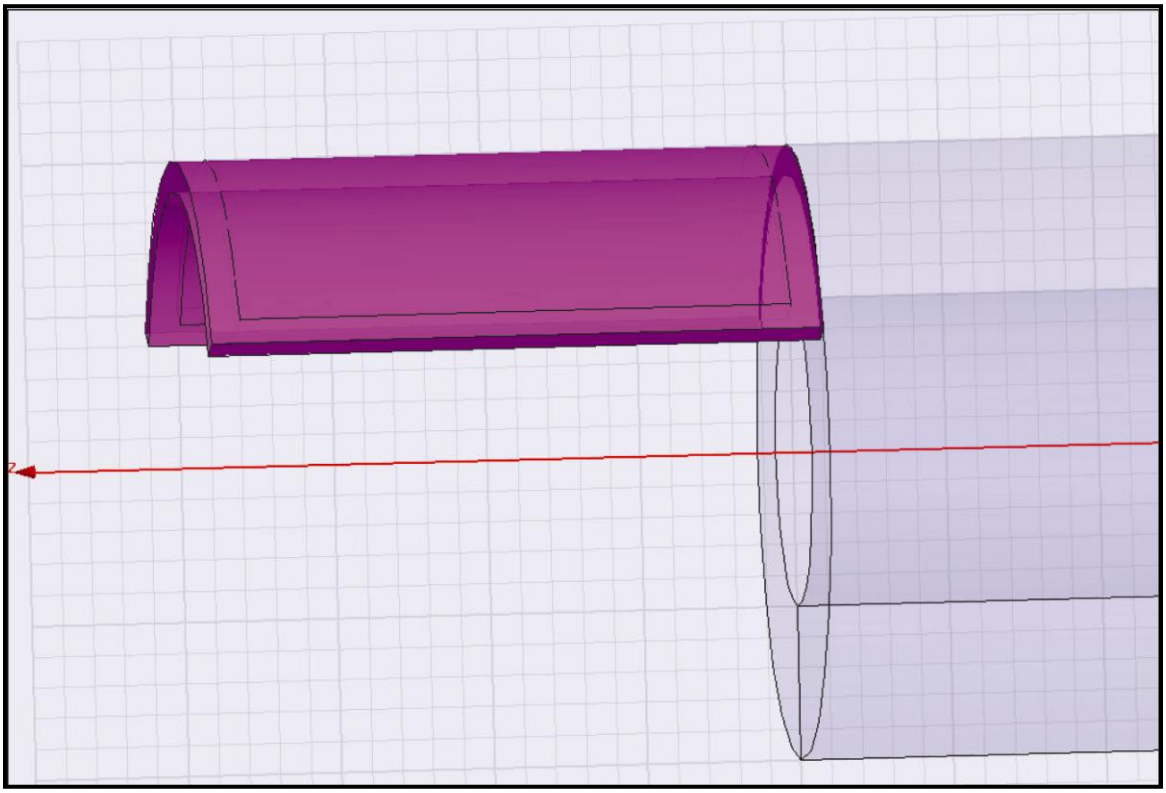

Figure 93. Superimposed Gradient Coil Volumes

40. Click *Rectangle1* and *Rectangle3* using the Ctrl key to simultaneously select them.
41. Select **3D Modeler** > **Boolean** > **Subtract** to display the Subtract window. Ensure that *Rectangle1* is in the Blank Parts area and *Rectangle3* is in the Tool area. Click **OK** to perform the subtraction and close the window. This completes on saddle coil. It should now look like this:

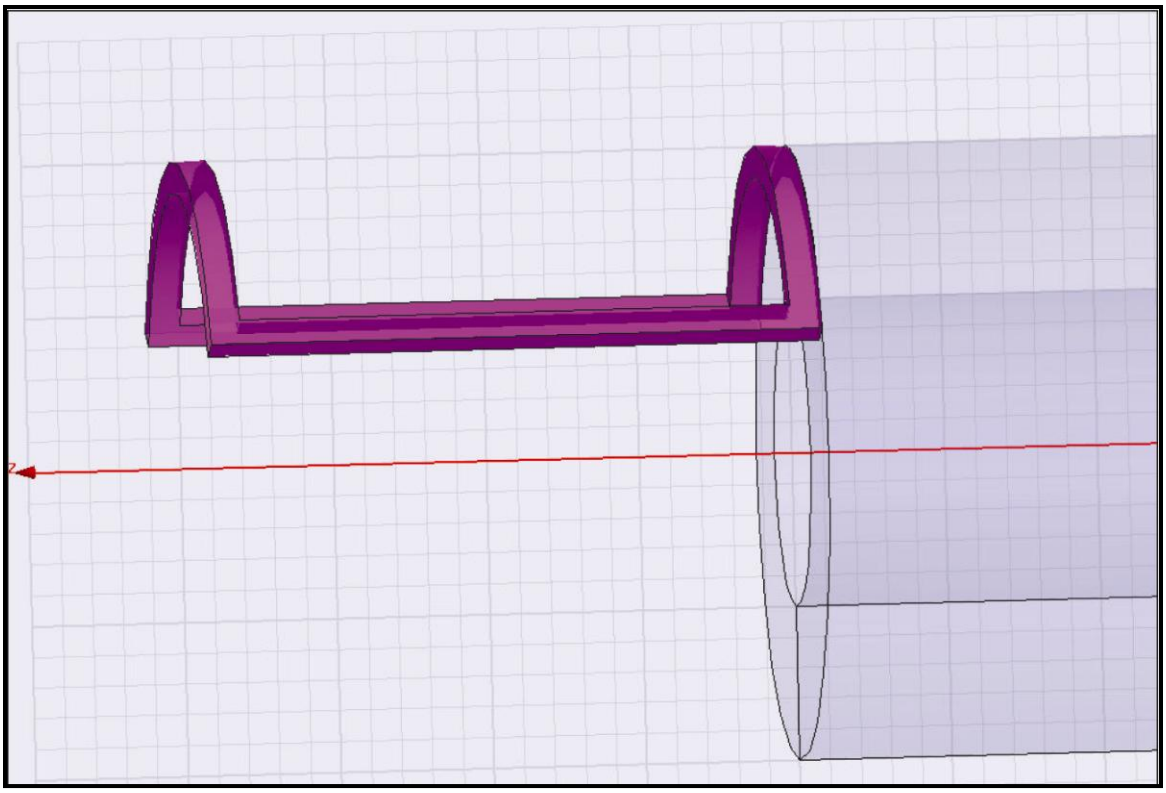

Figure 94. Completed Gradient Coil

42. Right Click on the *Rectangle1* object in the History Tree window and select **Properties**.
43. Rename the object to *SaddleCoil1*.
44. Ensure the *SaddleCoil1* object is highlighted by clicking on it in the **History Tree** window.
45. Click on the **Mirror Duplicate** button in the drawing menu bar. Click on the 0,0,0 point to start the mirror operation. Click along the negative Y axis to create the mirrored object. It will be named *SaddleCoil1_1*. The drawing should now look like this:

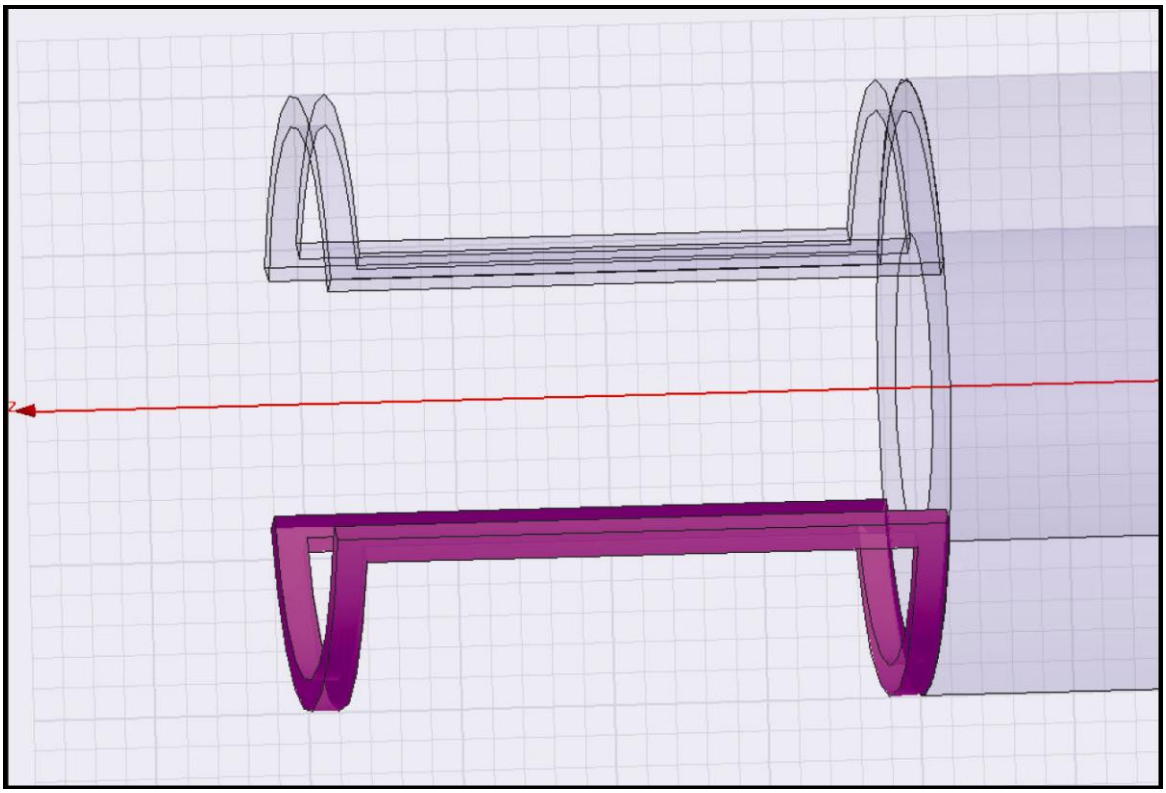

Figure 95. Mirrored Gradient Coils

46. Rename the created object to *SaddleCoil2*.
47. Select both *SaddleCoil1* and *SaddleCoil2* using the Ctrl key.
48. Click on the **Mirror Duplicate** button in the drawing menu bar.
49. Click along the Z axis to create *SaddleCoil1_1* and *SaddleCoil2_1* along the Z axis. This will position the second pair of coils 2001mm too far down the Z-axis. They will look like this:

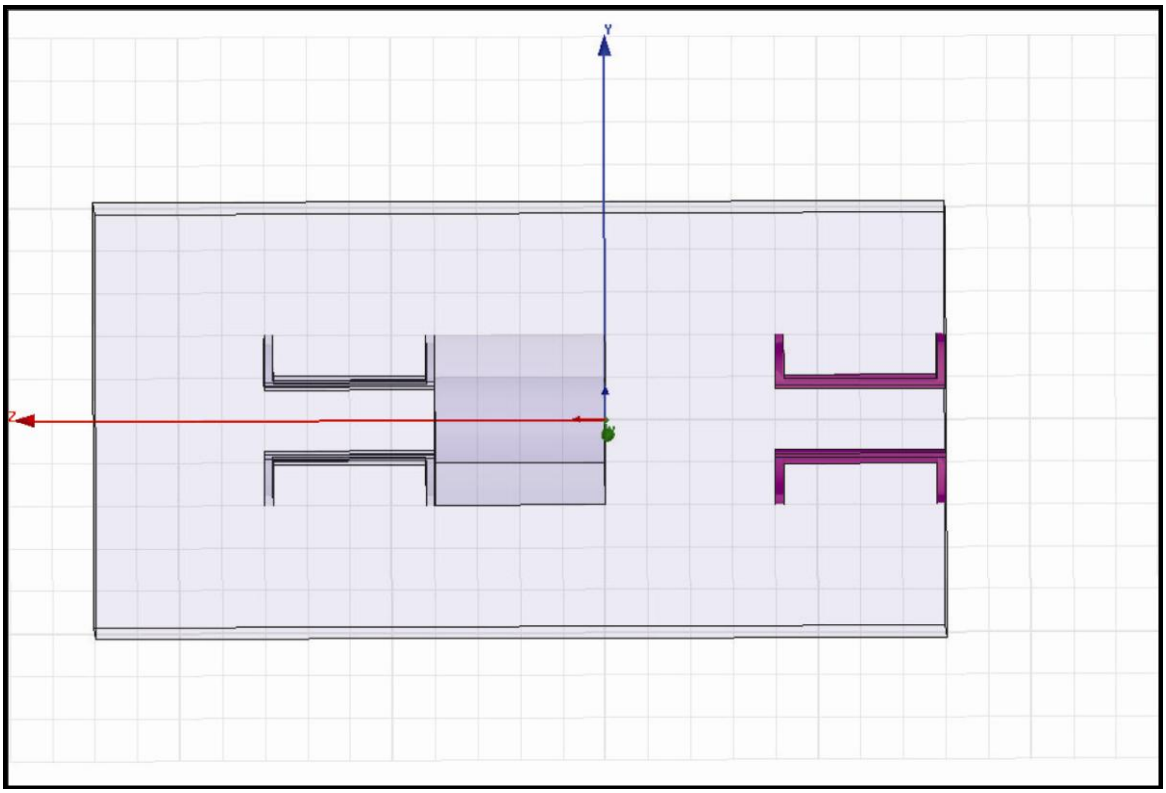

Figure 96. Gradient Coils

50. Highlight both coils in order to move them back into position.
51. Move the coils toward the bore exactly 2000mm towards the bore. This will place them 1mm away from the *BoreCoil*.
52. Rename *SaddleCoil1_1* to *SaddleCoil3* (The coil opposite of *SaddleCoil1*).
53. Rename *SaddleCoil2_1* to *SaddleCoil4*. They will now look like this.

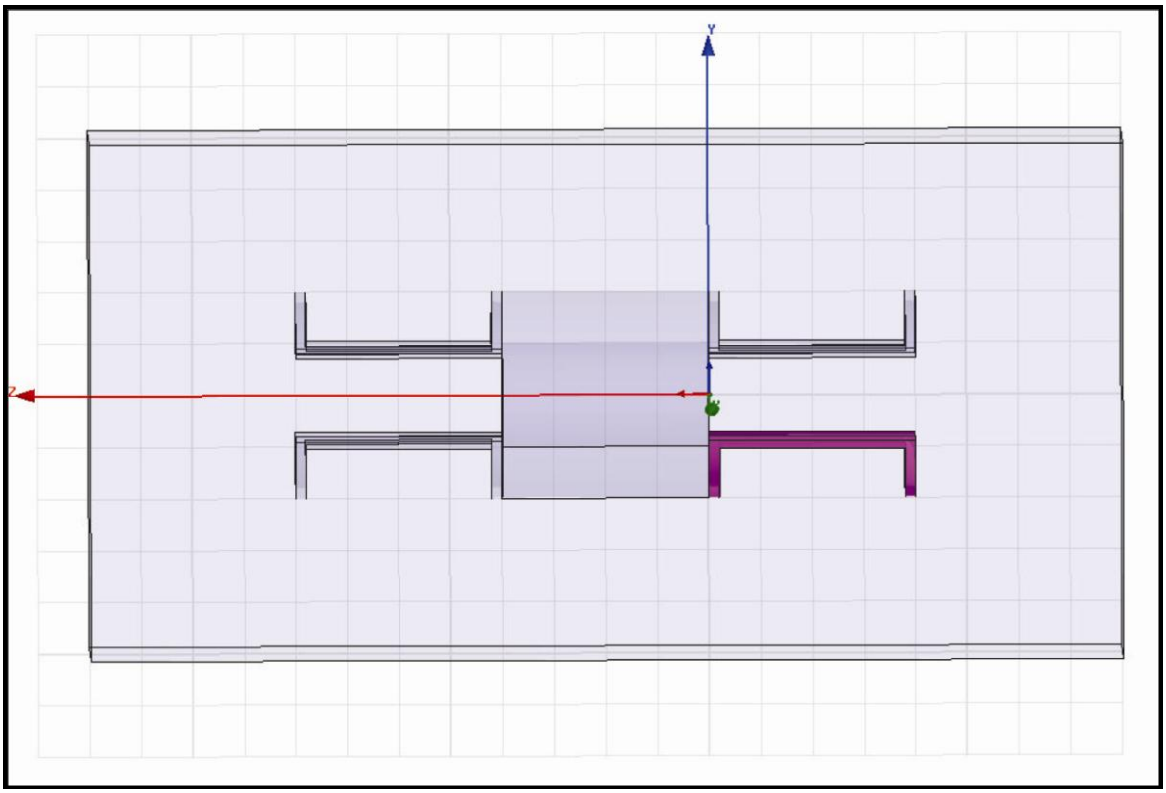

Figure 97. Completed Gradient Coils

54. Click the *vacuum* object under *Objects* in the **History Tree** window.
55. Right click and change the material to copper.
56. Scroll up the window to select copper as the material comprising the *BoreCoil*.
57. Click **OK** to close the window.

Create the Gradient Magnet Terminals

Create the Gradient Magnet terminals. This will be used to define the DC current which creates the static magnetic field.

1. In the **History Tree** window select all four saddle coils, *SaddleCoil1*, *SaddleCoil2*, *SaddleCoil3*, and *SaddleCoil4*.
2. Click **3D Modeler** > **Surface** > **Section** to display the Section window. The YZ plane is an appropriate plane to section the Gradient magnet.
3. Click **OK** to close the window. This creates four section objects consisting of two rectangular sections of the appropriate *SaddleCoil* objects.
4. Click the *Section1*, *Section2*, *Section3*, and *Section4*, objects in the **History Tree** window.

5. Click **3D Modeler** > **Boolean** > **Separate Bodies**. This will separate the section sheets into *Section1*, *Section1_1*, *Section2*, *Section2_1*, *Section3*, *Section3_1*, *Section4*, and *Section4_1*. When applying the current, Maxwell inserts the current into the entire sheet. If both sections remain part of the model, the two currents will be inserted simultaneously, effectively cancelling each other. Therefore, only one section is required so that the current circulates around the entire coil.
6. Click on *Section1*, *Section2*, *Section3*, and *Section4* in the **History Tree** window to highlight it.
7. Delete the highlighted sections.

Assign Excitations

An AC current is required in the *SaddleCoil* to create the time varying magnetic field.

1. Select *Section1_1* in the **History Tree** window.
2. Click **Maxwell** > **Excitations** > **Assign** > **Current** from the menu to display the **Current Excitation** window.
3. Edit the values in the window to name the current *Current1* with a value of 1 Amps. (This is simulated as 1,000,000 Amps through 1 turn of *SaddleCoil1*.)
4. Select **Stranded** as the Type and click the **Swap Direction** button until the vector indicates the positive X direction. The excitation should look like this:

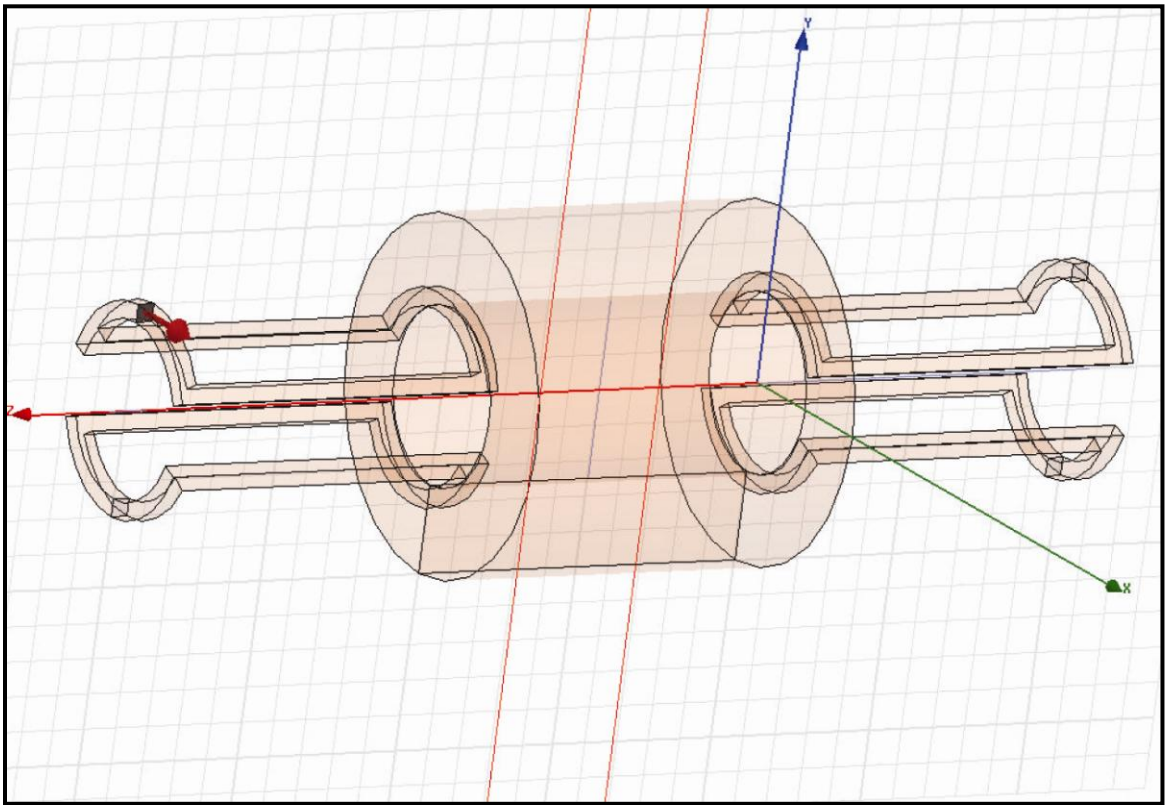

Figure 98. SaddleCoil1 Current

5. Click **OK** to close the window.
6. Select *Section2_1* in the **History Tree** window.
7. Click **Maxwell** > **Excitations** > **Assign** > **Current** from the menu to display the **Current Excitation** window.
8. Edit the values in the window to name the current *Current2* with a value of 1 Amps. (This is simulated as 1,000,000 Amps through 1 turn of *SaddleCoil2*.)
9. Select **Stranded** as the Type and click the **Swap Direction** button until the vector indicates the positive X direction. The excitation should look like this:

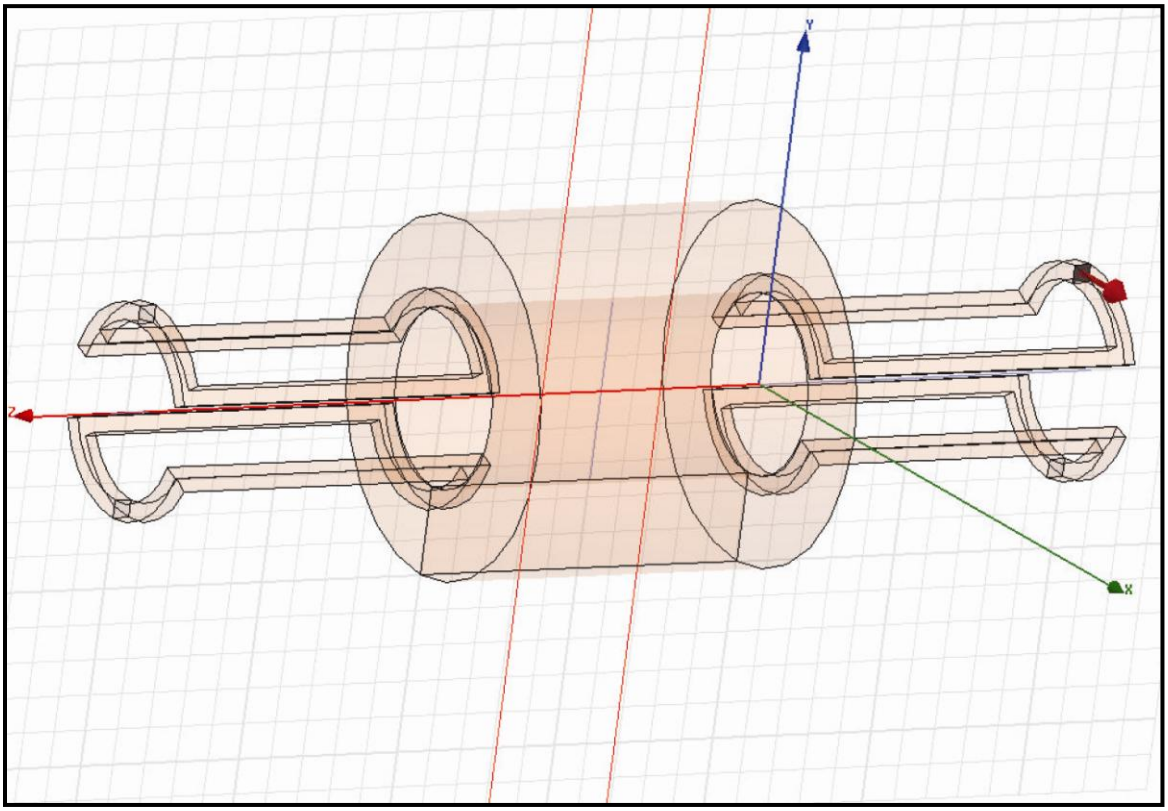

Figure 99. SaddleCoil2 Current

10. Click **OK** to close the window.
11. Select *Section3_1* in the **History Tree** window.
12. Click **Maxwell** > **Excitations** > **Assign** > **Current** from the menu to display the **Current Excitation** window.
13. Edit the values in the window to name the current *Current3* with a value of 1 Amps. (This is simulated as 1,000,000 Amps through 1 turn of *SaddleCoil3*.)

14. Select **Stranded** as the Type and click the **Swap Direction** button until the vector indicates the positive X direction. The excitation should look like this:

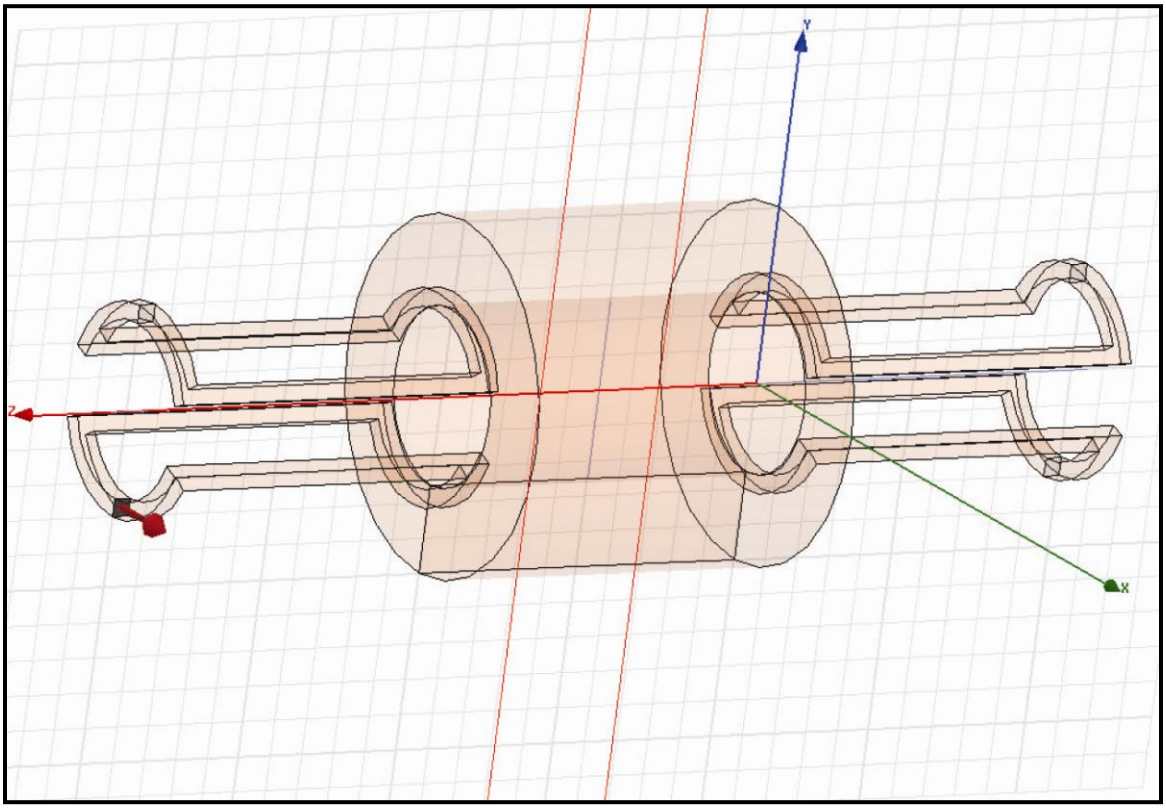

Figure 100. SaddleCoil3 Current

15. Click **OK** to close the window.
16. Select *Section4_1* in the **History Tree** window.
17. Click **Maxwell** > **Excitations** > **Assign** > **Current** from the menu to display the **Current Excitation** window.
18. Edit the values in the window to name the current *Current4* with a value of 1 Amps. (This is simulated as 1,000,000 Amps through 1 turn of *SaddleCoil4*.)
19. Select **Stranded** as the Type and click the **Swap Direction** button until the vector indicates the positive X direction. The excitation should look like this:

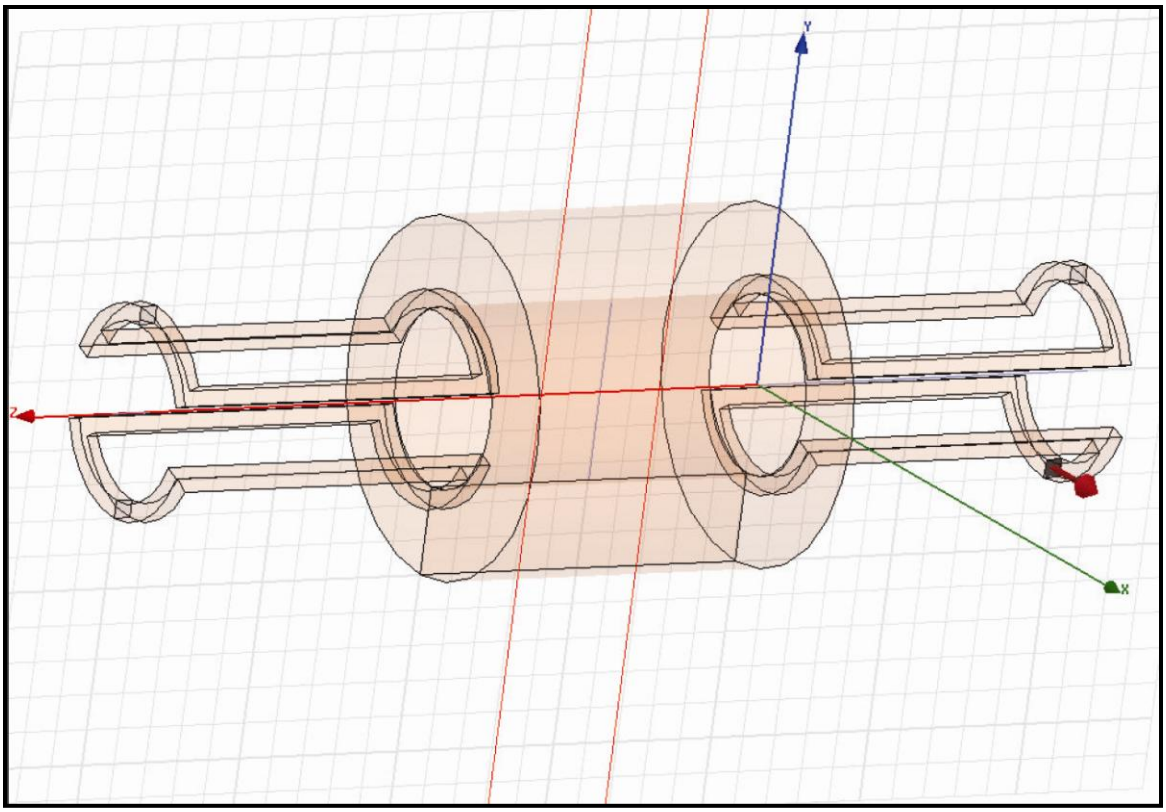

Figure 101. SaddleCoil4 Current

20. Click **OK** to close the window.

Field Calculator

The Field Calculator available in Maxwell 3D allows the user to perform a variety of tasks beyond the built-in functions of Maxwell 3D. These post-processing and plotting capabilities include vector operations, vector algebra, calculus, and can be fully scripted. The calculation steps used to determine the current through a surface are:

1. Click **Maxwell** > **Fields** > **Calculator** from the menu bar. This will launch the Field Calculator.
2. Under the **Input** column, click **Quantity** > **J**. This selects the current vector as a quantity to be operated upon.
3. Also under the **Input** column, click **Geometry** > **Volume** > **TwinLoop**. This doesn't really contribute to the overall calculation, but indicates where to restrict Maxwell's area of interest, namely to that of the TwinLoop volume. This allows Maxwell to eliminate

calculation of the J vector for all model elements outside the realm of the TwinLoop and significantly improves processing performance.

4. Under the **General** column, click **Domain**. This selection concludes the selection of the TwinLoop as the domain of interest.
5. Under the **Vector** column, click **Normal**. This adds the normal vector to the equation.
6. Finally, under the **Scalar** column, click the ∫ button to complete the surface integral calculation.
7. To complete the assignment of the equation, click the **Add** button and name the equation.
8. Click **Done** to exit from the Field Calculator.

REFERENCES

[1] Kroot, J. M. B. (2005). *Analysis of eddy currents in a gradient coil.* Eindhoven, Netherlands: Ponsen & Looijen.

[2] Kroot, J. M. B., van Eijndhoven, S. J. L., & van de Ven, A. A. F. (2007). *Eddy currents in a transverse MRI gradient coil.* Eindhoven, Netherlands: Eindhoven University of Technology.

[3] Kroot, J. M. B., van Eijndhoven, S. J. L., & van de Ven, A. A. F. (2007). *Eddy currents in a gradient coil, modeled as circular loops of strips.* Eindhoven, Netherlands: Eindhoven University of Technology.

[4] Reese, T. G., Heid, O., Weissfoff, R. M., & Wedeen, V. J. (2003). Reduction of eddy-current-induced distortion in diffusion MRI using a twice-refocused spin echo. *Magnetic Resonance in Medicine, 49,* 177-182.

[5] Ma, C., & Jiang, X. H. (2007) A new eddy-current compensation method in MRI. *Vol. 3., No. 6. PIERS Online.*

[6] Hoffmeister, B. (2007). *Electrical eddy currents in the human body: MRI scans and medical implants.* Retrieved 26 October 2007 from the University of Mississippi, Rhodes College, Department of Physics Web site: www.phy.olemiss.edu/Hoffmeister.ppt.

[7] Haacke, E. M., Brown, R. W., Thompson, M. R., & Venkatesan, R. (1999). *Magnetic resonance imaging physical principals and sequence design.* New York, NY: John Wiley & Sons, Inc.

[8] Crowell, B. (2005). *Simple nature* [Electronic version]. Retrieved 21 October 2007, from http://www.lightandmatter.com/area1sn.html

[9] Halliday, D. & Resnick, R. (1974). *Fundamentals of physics.* New York, NY: John Wiley & Sons, Inc.

[10] Maxwell 3D (Version 11.1.1) [Computer Software]. Pittsburgh, PA: Ansoft Corporation.

[11] Burke, H. E. (1986). *Handbook of magnetic phenomena.* New York, NY: Van Nostrand Reinhold Company, Inc.

[12] Chakeres, D. W. & Schmalbrock, P. (1992). *Fundamentals of magnetic resonance imaging.* Baltimore, MD: Williams & Wilkins.

[13] Hornak, J. P. (2007). *The basics of MRI* [Electronic version]. Retrieved 16 October 2007, from http://www.cis.rit.edu/htbooks/mri/index.html

[14] Crowell, B. (2005).

[15] Haacke et. al.

[16] Weast, R.C. (Ed.). (1976). Handbook of chemistry and physics (57th ed.). Cleveland, OH: CRC Press, Inc.

[17] Weast, R.C. (Ed.). (1976).

[18] Haacke et. al.

[19] Haacke et. al.

[20] Weast, R.C. (Ed.). (1976).

[21] Chakeres, D.W. (1992).

[22] Ibid.

[23] Halliday, D. & Resnick, R. (1974).

[24] Crowell, B. (2005).

[25] *User's Guide – Maxwell 3D.* (2005) Pittsburg, PA: Ansoft Corporation.

[26] Weast, R.C. (Ed.). (1976).

[27] Maxwell 3D (Version 11.1.1) [Computer Software].

[28] *Getting started with Maxwell: designing a rotational actuator.* (2005) Pittsburg, PA: Ansoft Corporation.

[29] *Getting started with Maxwell: transient problem.* (2005) Pittsburg, PA: Ansoft Corporation.

[30] *Getting started: a 2D magnetostatic problem.* (2005) Pittsburg, PA: Ansoft Corporation.

[31] *Getting started: a 2D magnetostatic problem.* (2005) Pittsburg, PA: Ansoft Corporation.

[32] *Getting started: a 2D transient linear motion problem.* (2005) Pittsburg, PA: Ansoft Corporation.

[33] *Getting started: a 2D parametric problem.* (2005) Pittsburg, PA: Ansoft Corporation.

[34] *An introduction to the Ansoft macro language.* (2005) Pittsburg, PA: Ansoft Corporation.